Ministry of Higher Education and Scientific Research

Hassiba Benbouali University of Chlef

Faculty of Technology

Department of Mechanical Engineering

THESIS

Presented for obtaining the diploma of

DOCTORATE

Major: Mechanical engineering

Specialty: Mechanical construction

By:

Mohamed TELDJOUN

Title:

Mechanical and tribological behavior of reinforced polymers

Defended on December 16th 2024, in front of the committee members:

Mohamed Hadj Miloud	MCA	Hassiba Benbouali University of Chlef	President
Madjid Meriem Benziane	Professor	Hassiba Benbouali University of Chlef	Examiner
Ibrahim Zidane	Professor	Hassiba Benbouali University of Chlef	Examiner
Zakarya Madaoui	MCA	Yahia Fares University of Medea	Examiner
Hamou Zahoul	Professor	Hassiba Benbouali University of Chlef	Invited
Mohammed MENDAS	Professor	Hassiba Benbouali University of Chlef	Supervisor
Salah MEZLINI	Professor	National School of Engineers of Monastir-Tunisia	Co-Supervisor

ملخص:

تبحث هذه الأطروحة في تطوير وتوصيف مركبات البولي بروبيلين (PP) المملوءة بحشوات قابلة للتحلل الحيوي، مع التركيز على سلوكها الترييبولوجي وخصائصها الميكانيكية. تهدف الدراسة إلى تلبية الحاجة المتزايدة للمواد المستدامة في التطبيقات المختلفة. دفعت المخاوف البيئية المتزايدة والحاجة إلى المواد المستدامة البحث نحو الحشوات القابلة للتحلل الحيوي للبوليمرات. ومع ذلك، فإن تأثير هذه الحشوات على الخصائص الميكانيكية والترييبولوجية لمركبات البوليمر غير مفهوم بشكل جيد.

يتضمن البحث تحضير مركبات PP المملوءة بمسحوق التلك وقشور اللوز. تم تصنيع مركبات PP-talc باستخدام قولبة الحقن مع محتوى التلك المتغير (0-50%)، وتم التحقيق في سلوكها الترييبولوجي من خلال اختبارات الانزلاق المتبادل في ظروف جافة ودرجة حرارة الغرفة. بالإضافة إلى ذلك، تم تحضير مركبات PP المملوءة بقشور اللوز بمحتويات حشو مختلفة (0، 5، 10، و 15%) باستخدام الخلط الساخن والضغط. تم فحص الخصائص الميكانيكية والترييبولوجية لهذه المركبات بدقة.

تم التحقيق في السلوك الترييبولوجي لمركبات PP-talc بشكل أكبر باستخدام اختبارات الخدش الميكروي والانزلاق المتبادل تحت ظروف بيئية مختلفة. تم تقييم وتحليل معامل الاحتكاك (COF) ومعدل التآكل (Wr) عند مستويات ثابتة مختلفة من الاحتكاك (5000، 10000، و 15000 دورة). قدمت تحليلات المجهر الإلكتروني الماسح (SEM) لمسارات التآكل رؤى حول أنماط الضرر الناجم عن التآكل بناءً على محتوى التلك. بالنسبة لمركبات PP المملوءة بقشور اللوز، تم التحقيق في تأثير الحشوات الحيوية على الخصائص الميكانيكية والترييبولوجية من خلال اختبارات صلابةShore D ، واختبارات الشد، ودراسات جهاز الاحتكاك القرصي. تم تحليل النتائج ومناقشتها فيما يتعلق بمحتوى الحشو وحجمه.

تظهر الدراسة أن الحشوات القابلة للتحلل الحيوي يمكن أن تؤثر بشكل كبير على الخصائص الميكانيكية والترييبولوجية لمركبات .PP توفر النتائج رؤى قيمة لتطوير مواد مستدامة ذات تطبيقات محتملة في مختلف الصناعات.

الكلمات المفتاحية: البوليمر، المركب، علم الاحتكاك، القابلية التحلل، الحشو.

Abstract:

This thesis investigates the development and characterization of polypropylene (PP) composites filled with biodegradable fillers, focusing on their tribological behavior and mechanical properties. The study aims to address the growing need for sustainable materials in various applications. The increasing environmental concerns and the need for sustainable materials have driven the research towards biodegradable fillers for polymers. However, the impact of these fillers on the mechanical and tribological properties of polymer composites is not well understood.

The research involves the preparation of PP composites filled with talc powder and almond shell fillers. The PP-talc composites were fabricated using injection molding with varying talc content (0-50%), and their tribological behavior was investigated through reciprocating sliding tests under dry conditions at room temperature. Additionally, PP-almond shell biocomposites were prepared with different filler contents (0, 5, 10, and 15%) using hot mixing and compression molding. The mechanical and tribological properties of these composites were thoroughly examined. The tribological behavior of PP-talc composites was further investigated using microscratch and reciprocating sliding tests under various environmental conditions. The coefficient of friction (COF) and wear rate (Wr) were evaluated and analyzed at different friction steady-state levels (5000, 10000, and 15000 cycles). Scanning Electron Microscopy (SEM) analyses of wear tracks provided insights into wear-induced damage patterns based on talc content. For the PP-almond shell fillers biocomposites, the effects of biofillers on mechanical and tribological properties were investigated through Shore D hardness tests, tensile tests, and pin-on-disk tribometer studies. The results were analyzed and discussed in relation to filler content and size.

The study demonstrates that biodegradable fillers can significantly influence the mechanical and tribological properties of PP composites. The findings provide valuable insights into the development of sustainable materials with potential applications in various industries.

Keywords: Polymer, Composite, Tribology, Biodegradable, Fillers.

Résumé:

Cette thèse étudie le développement et la caractérisation des composites de polypropylène (PP) remplis de charges biodégradables, en se concentrant sur leur comportement tribologique et leurs propriétés mécaniques. L'étude vise à répondre au besoin croissant de matériaux durables dans diverses applications. Les préoccupations environnementales croissantes et la nécessité de matériaux durables ont conduit la recherche vers des charges biodégradables pour les polymères. Cependant, l'impact de ces charges sur les propriétés mécaniques et tribologiques des composites polymères n'est pas bien compris.

La recherche implique la préparation de composites PP remplis de poudre de talc et de coquilles d'amande. Les composites PP-talc ont été fabriqués par moulage par injection avec une teneur en talc variable (0-50%), et leur comportement tribologique a été étudié par des tests de glissement réciproque dans des conditions sèches à température ambiante. De plus, des biocomposites PP-coquilles d'amande ont été préparés avec différentes teneurs en charges (0, 5, 10 et 15%) en utilisant le mélange à chaud et le moulage par compression. Les propriétés mécaniques et tribologiques de ces composites ont été minutieusement examinées.

Le comportement tribologique des composites PP-talc a été étudié plus en détail à l'aide de tests de micro-rayure et de glissement réciproque dans diverses conditions environnementales. Le coefficient de frottement (COF) et le taux d'usure (Wr) ont été évalués et analysés à différents niveaux de frottement stable (5000, 10000 et 15000 cycles). Les analyses de microscopie électronique à balayage (SEM) des traces d'usure ont fourni des informations sur les motifs de dommages causés par l'usure en fonction de la teneur en talc. Pour les biocomposites PP-coquilles d'amande, les effets des charges biodégradables sur les propriétés mécaniques et tribologiques ont été étudiés à l'aide de tests de dureté Shore D, de tests de traction et d'études de tribomètre à disque. Les résultats ont été analysés et discutés en fonction de la teneur et de la taille des charges.

L'étude démontre que les charges biodégradables peuvent influencer de manière significative les propriétés mécaniques et tribologiques des composites PP. Les résultats fournissent des informations précieuses pour le développement de matériaux durables avec des applications potentielles dans diverses industries.

Mots clés : Polymère, Composite, Tribologie, Biodégradable, Charges.

Contents

Abstracts: Arabic, English, French

Content

Figures list

Tables list

Abbreviation

General introduction……..…...……...…....1

Chapite1: Tribology of polymers filled with natural fillers: Literature review……...….6

1.1. Introduction……..……..7
1.2. Polymer Tribology……..…....7
1.3. Biodegradable fillers for polymer composites……...……...……....9
1.3.1. Biodegradable fillers Classification……...……..…….....9
1.3.1.1. Minerals..…….…...……...……...……...10
1.3.1.2. Animals……..…….…...……...……...……...11
1.3.1.3. Cellulose/lignocellulose…….……...……...……..….13
1.3.1.4. Biopolymers…….……..……...…….....……14
1.3.2. Advantages and challenges of biodegradable fillers……...…….....…..15
1.3.2.1. Improved polymers properties……...……...……..….15
1.3.2.2. Reduced environmental impact and waste generation……...…….....19
1.3.3. Different treatments of biofillers ……...…….....20
1.3.4. Polymer biodegradable fillers composites fabrication…….....……...…...22
1.4. Tribological Behavior of Filled Polymer Composites with Biodegradable Fillers…...24
1.4.1. Animal fillers……..……...……...…….....24
1.4.2. Waste agriculture biodegradables fillers……...……...…….....25
1.4.3. Wood based filler reinforced biocomposites……...……..29
1.5. Applications of biodegradables fillers based polymers……...……...…35
1.5.1. Automotive, aerospace, and other applications……...……...……..…….35
1.5.2. Biomedical applications……...……...……...……...……37
1.5.3. Environmental and economic impact of biocomposites……...…….……37
1.6. Conclusion…….....38
References……...…….....39

Chapter 2: Experimental procedure for Polypropylene composite: Talc Powder and Almond Shells Particles fillers……...…….....…….....45

2.1. Introduction……...……...……...……...…….....46
2.2. Polypropylene Talc composite: Tribological caracterization methods……...……46
2.2.1. PP-Talc composite material……...……...….……...46

2.2.2. Tribological test…….....…47
2.2.2.1. Scratch test under temperature effect…….....47
2.2.2.2. Microscratch test…….....55
2.2.2.3. Reciprocating sliding test ……..……...……...…….....56
2.2.2.4. Wear measurement…….……...……...……...…...57
2.2.2.5. Worn surfaces examination……...……...…….58
2.3. Polypropylene-Almond Shells Particles: Biocomposite preparation……..…….58
2.3.1. Matrix materials and Almond shells collection ……...……..….....58
2.3.2. PP-Almond shells fillers biocomposite elaboration ……...……...….....59
2.3.2.1. Almond shells fillers preparation……..….60
2.3.2.2. PP-ASF biocomposite preparation…….....62
2.3.3. PP-ASF biocomposite: Mechanical test……...……...….....63
2.3.4. PP-ASF biocomposite: Tribological tests……..…….....64
2.4. Conclusion……...……...……..…….....65
References…….…….…….....66

Chapter 3: Reciprocating sliding behavior of PP-talc composite…….....68

3.1. Introduction……...……...……...……...……...…69
3.2. Tribological properties of PP-talc composite……..70
3.2.1. Scratch test……...70
3.2.1.1. Friction coefficient vs. normal loads under different temperature degrees……..…70
3.2.2. PP talc reciprocating sliding…….……...……...……71
3.2.2.1. Coefficient of friction (COF) ……...……...……...……71
3.2.2.2. Wear rate……...……...……...……...……...73
3.2.2.3 Worn surfaces examination……...……...……...……...……75
3.2.2.4. Discussions……...……...……...…77
3.3. Conclusion ……...……...……...……...……...79
References…….…….…….....80

Chapter 4: Mechanical and tribological properties of PP Almond shells biocomposite……...84

4.1. Introduction……...……...……...…….....85
4.2. Mechanical properties…….……...……...……..……..86
4.2.1. Shore D hardness……...……...……...…….....86
4.2.2. Tensile test properties……...……...……...…….....87
4.3. Tribological properties……...……...……...……..……...88
4.3.1. Friction coefficient (COF) ……...……...……...88
4.3.2. Wear coefficient (W_c) ……...……...……...…….....90
4.3.3. Wear mechanisms……...……...……...……..…92
4.3.4. Discussion...……...……... ...……..……94
4.4. Conclusion……...……...……...……...…….....96

References…….…….…….....97
General conclusion and perspectives……..……..…….....99

Figures list

Chapter 1

Figure 1. 1. Classification of natural fibers [14]. ……....9
Figure 1.2. Stress–strain curves of PP–talc composite for different talc proportions at room temperature [24]. ……..16
Figure 1.3. SEM images of a) PP-SA1, b) PP-SA3, c) PP-SA5 and d) PP-SA7 composites [25] ……...16
Figure 1.4. (a) Pure ASP and (b) Pure LLDPE. Microstructure of LLDPE reinforced with different wt% of ASP: (c) 5%, (d) 10%, (e) 20%, (f) 30%, and (g and h) 40% [28] …..……18
Figure 1.5. Tensile-modulus [31] ……..……... 19
Figure 1.6. Tensile-strength [31]……..……..19
Figure 1.7. PP cherry seed composites samples, b) Block-on-ring tribological system [51]……26
Figure 1.8. a) The average trends for the COF calculated for a 250 N load, b) The average trends for the COF calculated for a 500 N load [51] ……..……..……...26
Figure 1.9. Signs of wear and residual oil observed after friction tests on the surfaces of the samples [51] ..……27
Figure 1.10. Wear loss vs applied normal load [52] ……..……...28
Figure 1.11. COF vs. applied normal load [52] ……..…….28
Figure 1.12. Interface temperature of different CLP filler based composites [52] ……...29
Figure 1.13. Fabrication of WF filled PP matrix by Ibrahim et al [56] ……..……30
Figure 1.14. (A) The effect of WF content on the coefficient of friction under different abrasive surfaces. (B) The change in wear area at different WF content under different abrasive surfaces [56] ……..….31
Figure 1.15. Microscopic micrographs for the wear surface of WF/PP composites tested using different abrasive surfaces [56] ……....31
Figure 1.16. Steady state coefficient of friction [31] ……...32
Figure 1.17. Wear coefficients [31] ……..…32
Figure 1.18. SEM images of unrecycled polypropylene wear scars [31] ……..…33
Figure 1.19. Example of 10 wt % filler-content recycled polypropylene [31] ……..…34
Figure 1.20. Schematically presented wear behavior for unrecycled (WPC) and recycled (RWPC) composites with wood-filler content: a) below 20 wt % and b) above 20 wt % [31] ……...34
Figure 1.21. Some interior automotive parts made from bio-fiber composites [57] ……36
Figure 1.22. The airplane components made from natural fillers [57] ……...…..36

Chapter 2

Figure 2.1. PP-talc specimens. ……..……....47
Figure 2.2. The microscratch installation with the heating device……..……...….48

Figure 2.3. Schematic and dimensions of the heating device and its components……48
Figure 2.4. Heat temperature rise vs. time……49
Figure 2.5. Control circuit and its schema……..50
Figure 2.6. Temperature stability vs. Time at: (a) 40, (b) 60 and (c) 80 °C……...53
Figure 2.7. Tangential and normal loads vs. sliding distance at different temperatures for imposed normal load 10 N and 15 N……..……54
Figure 2.8. Scheme of the indenter-specimen contact geometry in microscratch test…..……..55
Figure 2.9. Reciprocating sliding tester and slider-specimen contact details. ……....57
Figure 2.10. Wear track profile measurement…..……...…...58
Figure 2.11. a) PP talc specimens coated with a gold layer and b) Q250 EDX Thermo Fisher Scanning Electron Microscopy (SEM)……...…58
Figure 2.12. a) Almond tree (2023 summer season, Ain Defla zone, Algeria) and b) Almond shells……...…59
Figure 2.13. ASF Morphology, (a) D1 and (b) D2…….……60
Figure 2.14. Particles size distributions of D1 and D2…..……...61
Figure 2.15. Thermogravimetric analysis of ASF (a) TG and (b) DTG for D1 and D2…..…62
Figure 2.16. The biocomposite preparation process……..62
Figure 2.17. a) Brbender plastograph, b) The used molds and c) Laboratory presses hydraulic……....63
Figure 2.18. a) Bareiss durometer and b) PP-ASF specimens……..……....…64
Figure 2.19. Tensile test specimens…….…64
Figure 2.20. Tribological test settings…….…..65

Chapter 3

Figure 3.1. Friction coefficient vs. normal loads under different temperature degrees……..…70
Figure 3.2. COF evolution vs. number of cycles and talc proportions……...…71
Figure 3.3. Track surface profile at 15000 cycles (a) and wear rate at 5000, 10000, and 15000 cycles vs. talc proportion (b) ……74
Figure 3.4. SEM micrographs of the worn surfaces vs. talc proportions or 15000 cycles…….…76
Figure 3.5. Material transfer on the slider after 15000 cycles vs. talc proportion…….…78

Chapter 4

Figure 4.1. PP-ASF specimens Shore D hardness……86
Figure 4.2. PP-ASF specimen's tensile properties……87
Figure 4.3. Friction coefficient vs. test duration……....89
Figure 4.4. Steady state average COF_m. ……...90
Figure 4.5. Wear coefficient, W_c vs the size and proportion of particle at the end of wear tests.91
Figure 4.6. Wear depth *vs.* sliding distance……..….92
Figure 4.7. PP-ASF wear tracks micrographs and Optical 3D, a) PP, b) PP-D1-5, c) PP-D1-10, d) PP-D1-15, e) PP-D2-5, f) PP-D2-10 and g) PP-D2-15…...……..…….93

Tables list

Chapter 1

Table 1.1. Tensile modulus and strength and elongation and stress at break of the PP-SA composites [25] ……17
Table 1.2. Some of the significant studies on the manufacturing of natural fibers reinforced polymers composites (NFRPCs) [44] ……23
Table 1.3. Some application of bio fibers in automotive industry [57] ……36

Chapter 2

Table 2.1. Electrical parameters used for the temperature stability study……...51
Table 2.2. Temperature errors ΔT/T in %.....53
Table 2.3. Structural characteristics of obtained specimens……63

Chapter 3

Chapter 4

Abbreviation

CO_2: Carbon dioxide

GDP: Gross Domestic Product

SEM: Scanning Electronic Microscopy

wt.%: Weight proportion

CC: Calcium carbonate

CFF: chicken feather fibers

PP/SA: Polypropylene/silica aerogel

PP: Polypropylene

PP-talc: Polypropylene composite material filled with talc

ASF: Almond shells fillers

PP-ASF: Polypropylene composite material filled with Almond shells fillers

Ft: Tangential force

Fn: Normal force

COF: Coefficient of friction

μ_a: Adhesive friction component

μ_l: Plowing friction component

W_r: Wear rate

W_c: Wear coefficient

COF_m: Average coefficient of friction

WD: Wear depth

General introduction

Tribology is the study of interacting surfaces in motion, encompassing friction, lubrication, and wear. This interdisciplinary field involves physics, chemistry, materials science, and engineering [1]. The term gained prominence after the 1966 "Jost Report," which highlighted the significant financial impact of friction, wear, and corrosion on the UK (united kingdom) economy [2]. Despite extensive research, friction and wear still significantly affect global energy used and CO_2 emissions. In 2017, Kenneth Holmberg and Ali Erdemir evaluated their worldwide economic impact, focusing on transportation, manufacturing, power generation, and residential sectors [3]. Their conclusion ware approximately 23% of the world's total energy consumption comes from tribological contacts. 20% of this is used to overcome friction, while 3% is used to replace worn parts and equipment due to wear and related failures. By utilizing new surface technologies, materials, and lubrication methods to reduce friction and wear in vehicles, machinery, and other equipment worldwide, energy losses from friction and wear could potentially be reduced by 40% in the long term (15 years) and by 18% in the short term (8 years). These savings would amount to 1.4% of global GDP (Gross Domestic Product) annually and 8.7% of total global energy consumption in the long term. The largest short-term energy savings are expected in the transportation (25%) and power generation (20%) sectors, while the potential savings in manufacturing and residential sectors are estimated to be around 10%. In the longer term, the savings would be 55%, 40%, 25%, and 20%, respectively, in these sectors. Implementing advanced tribological technologies could also reduce global carbon dioxide emissions by up to 1460 metric tons of CO_2 equivalent in the short term, with cost savings of 450,000 million Euros. In the long term, the reduction could be as high as 3140 metric tons of CO_2 equivalent, with cost savings of 970,000 million Euros [3].

Polymer components are increasingly replacing metals in various applications, particularly in automotive weight reduction, due to their advantages such as being readily formed with minimal waste, being lighter, cheaper, corrosion-resistant, quieter, and requiring less maintenance [4]. Therefore, more attention is now needed for metal-polymer and polymer-polymer tribological contacts. Polymer tribology is more complex and less well-understood compared to metal tribology. Whereas there are well-established 'Laws of Friction' for metal and ceramic contacts, polymer-metal contacts generally do not follow these laws. This is due to factors such as the relative softness of polymers, their lower thermal conductivities leading to higher heat generation in contacts, and their significantly lower melting points. If these issues are not properly addressed, polymer applications in rolling, sliding, or bearing components may

face problems [4]. The conclusions drawn may not automatically transfer to more severe wear conditions, such as heavy abrasion or erosion. Nevertheless, the range of available polymers suitable for varied operating conditions of strength, temperature, environmental resistance, friction, and wear is extensive [4].

The tribological behavior of polymer composites filled with biodegradable fillers presents a complex interplay of material properties that are critical to the performance and longevity of these systems. The incorporation of biodegradable fillers into polymers aims to enhance sustainability and reduce environmental impact. However, this integration poses challenges in maintaining the mechanical strength, thermal stability, and wear resistance of the composite material. Biodegradable fillers, often derived from natural sources such as cellulose, starch, or proteins, can introduce variability in the composite due to their inherent biological origin. The disparity in thermal properties between the polymer matrix and the fillers can lead to differential thermal expansion, causing internal stresses and potential delamination at the interface. Furthermore, the wear mechanisms in such composites are influenced by the morphology and distribution of the fillers. Uneven dispersion can create localized regions of weakness, exacerbating wear. The filler's shape and size also play a pivotal role; for instance, spherical fillers may enhance lubricity, while fibrous fillers could improve load distribution but might also act as stress concentrators. To address these issues, surface modification of fillers and the use of coupling agents are strategies employed to improve interfacial adhesion and compatibility. Additionally, the optimization of filler content is crucial to balance the trade-offs between biodegradability and mechanical performance. The tribological behavior of polymers filled with biodegradable fillers is a multifaceted problem that necessitates a holistic approach to material design and engineering. It requires careful consideration of the interactions between the polymer matrix and the fillers, as well as the processing methods and operating conditions under which the composite will be utilized.

The aims of this thesis were the investigation of mechanical and tribological properties of polymer filled with biodegradable fillers, investigate the effect of the biodegradable fillers properties as its size, shape, proportion. Investigate also the effect of several possible testing condition as temperature, tribological loads, non-repetitive and repetitive sliding condition and number of sliding cycles. For these aims, in this thesis, tow Polypropylene composites were tested. PP-talc composite were examined through microscratch test under the effect of temperature and via reciprocating sliding test with low, medium and high number of sliding

test. In addition, PP Almond shell fillers was fabricated with several filler sizes and loading, then its tribological behavior was determined via pin on disk tribometer.

This thesis contains four chapters:

The first chapter presents a literature review on the polymers and its tribology, the biodegradables fillers for polymers, its nature and its classification. The preparation of polymer composite based on biodegradable fillers and its tribological behavior. Finally its application was presented.

The second chapter describes the experimental procedure for the development and characterization of a polypropylene (PP) composite material filled with talc powder and PP composite material filled with Almond shells fillers. The PP talc composite was fabricated using injection molding, with the talc content varying from 0 to 50%. To investigate the tribological behavior of the PP-talc composites, a reciprocating sliding test was conducted under dry condition and room temperature. In addition the PP Almond shells fillers biocomposite was elaboration with 0, 5, 10 and 15% via hot mixing and moulding compression. The mechanical and tribological testing were clearly described.

The third chapter presents an investigation of the tribological behavior of talc-filled polypropylene (PP-talc) via microscratch and reciprocating sliding tests. The PP talc composite was tested under possible environmental temperatures and with four normal load for the microscratch, the COF was evaluated, analyzed and discussed. For the reciprocating sliding, both the normal load and sliding speed were maintained constant until reaching 15000 cycles. Furthermore, both COF and W_r tribological parameters were determined and compared at three levels of friction steady-state: low, average, and high number of cycles: 5000, 10000, and 15000, respectively. The Scanning Electronic Microscopy (SEM) analyses of wear tracks after 15000 cycles were also realized to examine the wear-induced damage forms in the function of the talc proportion. Thus, the determined tribological parameter findings were also discussed by virtue of observed damage-caused patterns.

Finally, in last chapter, Almond shell agro-waste material has been utilized to produce ASF as filler then are incorporated into PP homopolymer matrix for preparing biodegradable and sustainable Polypropylene-Almond shell fillers (PP-ASF) based biocomposite. Two ASF size ranges, diameter 1 (D1) and diameter 2 (D2) of 600 µm ≤ D1 ≤ 900 µm and 400 µm ≤ D2 ≤ 600 µm. To lighten certain ambiguity of the effect of biofillers on mechanical and tribological

properties, Shore D hardness and mechanical properties via tensile tests were determined. Additionally using a pin-on-disk tribometer, a tribological study treating the effect of ASF size and proportion in the PP composites was conducted. The Shore D hardness, tensile properties, friction coefficient, wear rate, penetration depth, and friction damage results were analyzed and discussed regarding the filler content and its size.

References

[1] Hutchings, Ian, and Philip Shipway. Tribology: friction and wear of engineering materials. Butterworth-heinemann, 2017.

[2] H.P. Jost, Lubrication (Tribology) - a Report on the Present Position and Industry's Needs, Department of Education and Science, H.M. Stationary Office, London, UK, 1966. http://www.skf.com/binary/68-33957/SKFfilament-wound-bushings.pdf.

[3] K. Holmberg, A. Erdemir, Influence of tribology on global energy consumption, costs and emissions, Friction 5 (2017) 263e284.

[4] M. Fox, Polymer Tribology, vol. 135, Lube Magazine, 2016, pp. 32e37.

Chapite1: Tribology of polymers filled with natural fillers: Literature review

1.1. Introduction

The study of tribology in polymers has gained significant attention due to the unique properties and applications of these materials in various industries. Polymers are favored for their natural elasticity, shock absorption capabilities, low friction coefficients, and wear resistance, making them ideal for components such as bearings and seals. However, the tribological behavior of polymers differs markedly from that of metals, primarily due to their viscoelastic nature, which leads to time-dependent properties. Additionally, polymers can absorb external lubricants, altering their characteristics and impacting performance.

The complexity of polymer tribology arises from factors such as interfacial interactions, operating conditions, and environmental influences, which diverge from traditional metal tribology. Historical research in this field dates back to 1949, yet the continued exploration of polymer composites-especially those filled with biodegradable materials-highlights the evolving understanding of friction and wear mechanisms. This literature review aims to synthesize current knowledge on the tribological performance of polymers filled with biodegradable fillers, examining the influences of various additives on mechanical properties and environmental sustainability. This examination aims to provide insights into the promising applications of these materials across industries, including automotive and aerospace, while addressing the challenges that remain in the field of polymer tribology.

1.2. Polymer Tribology

Polymers are being increasingly used in tribological applications, such as bearings and seals, due to their advantageous properties [1]. These include their natural elasticity, ability to accommodate shock loading, low friction coefficients, and wear resistance [2]. However, the tribology of polymers differs significantly from the tribology of metals for several reasons. Unlike metals, polymers exhibit viscoelastic behavior, meaning their properties are highly dependent on time [3]. This viscoelasticity is a fundamental difference between polymer and metal tribology. Additionally, external liquid lubricants that work well for other materials like metals can be easily absorbed by polymers. This absorption can alter the properties of the polymer and affect its tribological performance. Further complexity arises because polymers are easily influenced by the operating conditions and the surrounding environment [4]. This makes polymer tribology more challenging compared to metal tribology. Nonetheless, polymer tribology is a fascinating area because polymers can be modified, both on the surface and in the

bulk, through various chemical and physical means to suit a particular application. This ability to control the friction and wear properties of polymers makes them attractive and promising materials for tribologists. As a result, there are now various tribological systems composed of polymers, metals, and ceramic materials in sliding or rolling contacts, taking advantage of the tailorable tribological properties of polymers.

Traditional tribology, along with the experimental methods originally developed for metals, may not be directly applicable to the study of polymer tribology. This is because polymer tribology is influenced by different interfacial and operational conditions, such as the formation of transfer films, thermal heat generation, and contact pressure. The earliest known reference on tribology studies of polymers dates back to 1949, with the work of Shooter and Thomas [5]. The successful introduction of bulk polymers in bearing applications led to the use of polymer composites, where their tribological and mechanical properties were modified by incorporating filler additives. Since then, thousands of studies have been conducted by hundreds of researchers, all aimed at understanding the fundamental mechanisms of friction and wear in polymers and polymer composites. This growing body of research highlights the unique challenges and complexities associated with polymer tribology, which differ from the traditional tribology of metals.

Numerous studies have highlighted that friction force and wear rates in tribological systems depend on factors such as surface roughness, relative motion, material type, temperature, normal force, stick-slip behavior, humidity, lubrication, and vibration [6]. Additionally, the tribological performance of polymer composites is influenced by parameters like molecular structure, processing, treatment, properties, viscoelastic behavior, and surface texture [7]. Researchers, including Watanabe, Tanaka, and Bahadur, have emphasized the impact of normal load, sliding speed, and temperature on the tribological behavior of polyamide, high-density polyethylene (HDPE), and their composites [8]. Applied load and sliding speed significantly affect wear behavior in polymer composites, with load having a greater influence than speed [9]. While some authors have observed a decrease in the friction coefficient of polymers and composites rubbing against metals with increasing load, others have reported different views [10]. Stuart et al found that the friction coefficient increases with load [11]. Overall, the coefficient of friction tends to decrease linearly with increasing applied pressure across various material combinations. Notably, the applied load exerts a stronger influence on sliding wear in polymer composites than sliding velocity [12].

1.3. Biodegradable fillers for polymer composites

Biodegradable materials have gained significant attention due to their potential to address environmental concerns associated with conventional petroleum-based plastics. In particular, biodegradable polymer composites, which combine biodegradable fillers with polymers, offer a promising avenue for sustainable materials development. Over the past several decades, conventional petroleum-based polymers have seen widespread use in various sectors, including automotive, marine, aerospace, food packaging, and construction. However, their negative impact on the environment, health risks, and contribution to solid waste pollution have raised concerns. Approximately 140 million tons of petroleum-based polymers are manufactured globally, leading to significant environmental challenges [13]. Researchers and engineers are increasingly interested in polymer biodegradation as a solution to these issues.

1.3.1. Biodegradable fillers Classification

Biodegradables fillers can be categorized based on their origins: plants, animals, or minerals. Plant fillers primarily consist of cellulose, while animal fillers are composed of proteins. Plant fillers include bast fibers, leaf or hard fibers, seed fillers, fruit fillers, wood fillers, cereal straw, and other grass fibers. Figure 1.1 present the biodegradable natural fibers classification by T. Gurunathan et al [14].

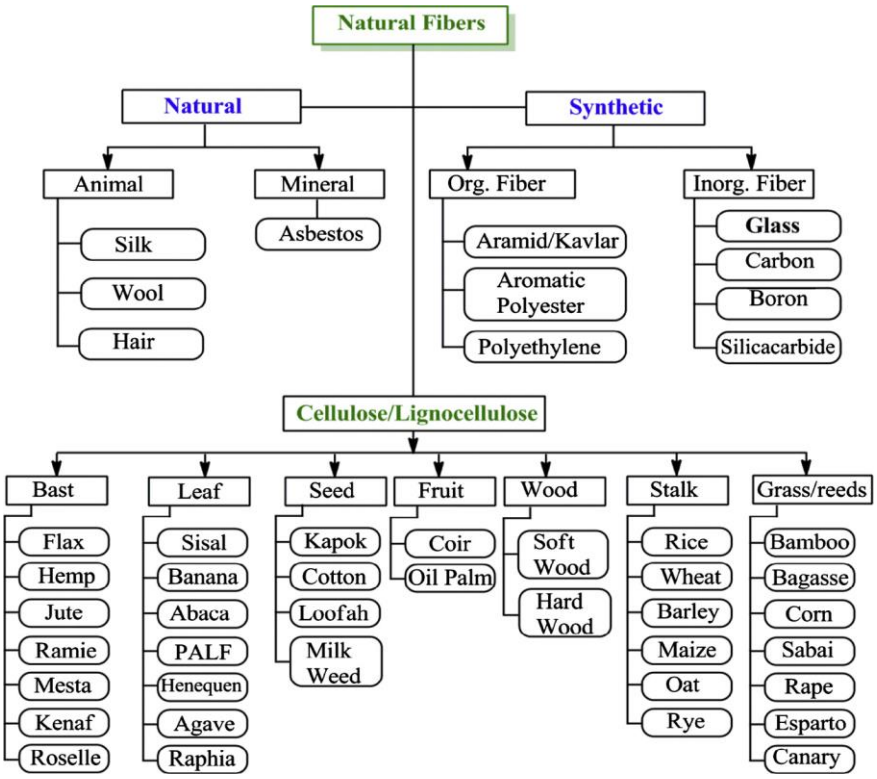

Figure 1.1. Classification of natural fibers [14].

In addition of the mentioned classes of biodegradables fillers, there are biopolymers that can be blended with other polymers which make biopolymer composites. Biopolymers are polymeric materials derived from bio-based resources. They have become the preferred choice for polymer blends due to several key factors such as its Biodegradability**,** Renewability, Economy and Availability. One commonly exploited biopolymer for blending is cellulose, which can be combined with other polymers to create innovative materials.

1.3.1.1. Minerals

A mineral is typically a crystalline substance that occurs naturally and possesses a specific chemical formula. In nature, minerals are often discovered as either individual rocks or ores, ranging from simple mineral forms to intricate combinations. Numerous minerals meet the criteria necessary for polymer-related uses due to their plentiful supply, affordability, transparency, chemical inactivity, and ease of shaping into desired particle sizes and forms. These minerals are transformed into fillers through mining and subsequent processes including grinding, purifying, sorting, heating, surface modification, and moisture removal.

Calcium Carbonate, CaCO3

Calcium carbonate (CC) is a natural filler material favored for its beneficial properties, extensively used in plastics like PVC and polypropylene, and often treated with fatty acids to improve its functionality. Calcite, the most common crystalline form of calcium carbonate, has a specific gravity of 2.7, a Mohs hardness of 3, and distinct refractive indices. CC is sourced from chalk, limestone, or marble, with each type impacting the filler's traits. Chalk, formed from marine organisms, is the softest and requires less energy to mill. Limestone, hardened chalk, and marble, the hardest, both demand more milling energy due to their denser crystal structures. Chalk-based fillers are known as whiting.

Clay

Clay minerals, derived from granite decomposition, are layered aluminosilicates Kaolinite Al_2O_3 $2SiO_2$ $2H_2O$, the main clay used in polymers, particularly elastomers, has a specific gravity of 2.6 and a Mohs hardness of 2.5 to 3. Its layered structure, with alternating alumina and silica, affects its categorization as hard or soft in elastomer reinforcement. Kaolinite's hexagonal, plate-like shape is crucial for enhancing polymer properties like viscosity and strength, outperforming spherical fillers like calcium carbonate. The performance of clay fillers

is greatly influenced by their aspect ratio, which varies with extraction and processing techniques.

Talc, $Mg_3 (Si_4O_{10}) (OH)_2$

Talc refers to a soft mineral and related minerals with similar properties. It consists of magnesium hydroxide layers sandwiched between silica layers, making it the softest known mineral with a Mohs hardness of 1. Talc's specific gravity is 2.8, and it has refractive indices of 1.54 and 1.59. Its properties vary with the deposit source and processing, displaying lamellar to massive structures. In the polymer industry, finely milled, platy talc with a high aspect ratio is valued, especially as a semi-reinforcing filler in polypropylene. The mineral's effectiveness is influenced by its shape, color, and purity, with its surface showing minimal reactivity except when used with specific additives like maleated PP.

Wollastonite

Wollastonite, a type of calcium silicate, is known for its acicular, white crystals, with a specific gravity of 2.9 and a Mohs hardness of 4.5. It has a refractive index range of 1.63 to 1.67. Pure, economically viable deposits are uncommon, making it more used in regions like the U.S. It’s valued in polymers for its needle-like shape and low water absorption, serving as an alternative to glass fiber. Wollastonite’s delicate structure requires careful handling to preserve its reinforcing acicularity. In the polymer industry, it’s used in polypropylene, polyamides, and thermosetting polymers, benefiting from surface treatments like silanes to enhance its properties.

1.3.1.2. Animals

Animal fibers like silk, wool, fur, and feathers contribute to creating biodegradable and environmentally friendly blends that help reduce significant solid waste. Wool is sourced from a variety of animals including sheep, alpaca, bison, cashmere goats, muskoxen, among others, with each type of fiber having multiple origins. Silk, fur, and feathers are also widely utilized materials. Studies have explored the role of animal fibers in reinforcing composite materials, revealing that wool is extensively used in textiles for diverse applications. Meanwhile, chicken feathers, often discarded by slaughterhouses, have potential as reinforcement when combined with different polymers to create various composite materials [15, 16].

Chicken Fibers

The poultry industry, predominantly chicken farming, generates four billion pounds of waste annually in the United States. Globally, the slaughter of 20 billion chickens leads to the production of the same amount of feather waste [17]. These feathers contribute to environmental pollution and are linked to various diseases in humans, including chlorosis, mycoplasmosis, and fowl cholera. Consequently, research into using chicken feather fibers (CFF) as primary elements in composite materials has been active for over twenty years. Efforts are underway to repurpose this waste into valuable products, leveraging the feathers' unique qualities such as their low density and excellent insulation properties.

Silk

In the wild, silk fibroin has evolved to thrive in complex environments, including damp or underwater areas, and to adhere to diverse surfaces. Silk fibroin, particularly from the Bombyx mori species, has been employed in numerous applications for a long time. Nature presents a range of silk fibroin compositions. Silkworms produce protein fibers that rely on two key proteins: fibroin and sericin [18]. Spider silk, a natural polymer fiber, is renowned for its exceptional tensile strength and durability, along with unique thermal, optical, and biocompatible characteristics. Its fundamental structure is made up of amino acids arranged in specific sequences of glycine, alanine, serine, valine, and tyrosine, which are essential for its robustness and elasticity [19]. A vast number of insects and the majority of butterfly larvae (around 140,000 Lepidoptera species) create silk during their metamorphosis [20].

Wool

Keratins exhibit a complex molecular and structural design akin to that of biological composite structures, which integrate diverse components within a single material to enhance its functional suitability [21]. Wool fibers are notably diverse in both composition and form, essentially constituting a biomaterial reliant on multiple components. A wool fiber comprises three distinct layers: the cuticle forms the outermost protective layer, followed by the cortex in the middle, and the medulla at the core [22]. Keratin proteins are resistant to dissolution in water, organic solvents, dilute acids, and bases, as well as to degradation in typical solvents. This resilience is attributed to the dense arrangement of α-helices and β-sheets within the polypeptide structure of wool keratin [23].

1.3.1.3. Cellulose/lignocellulose

Cellulose and lignocellulose fibers are plant-based materials that are integral to various applications due to their renewable nature and biodegradability. Cellulose fibers, extracted primarily from wood and plant materials, are known for their strength and versatility. Lignocellulose, a composite of cellulose, hemicellulose, and lignin, is found in the cell walls of plants. It provides structural support and is used in the production of biofuels, bioplastics, and as reinforcement in composite materials. These fibers are valued for their sustainability and are being increasingly utilized in eco-friendly products and technologies.

Date Palm

Cultivated widely for its fruit, the plant includes around 19 species with over 5000 varieties cultivated worldwide. Among the Phoenix genus, these trees stand as the tallest, reaching heights of approximately 23 meters. After the annual fruit harvest, a significant amount of date palm rachis and leaves are collected in various countries. Rich in cellulosic fiber, these by-products serve as a reinforcing agent within polymer matrices, including both thermoplastics and thermosets, and find applications in the automotive sector too.

Bamboo

Bamboo is often referred to as natural glass fiber due to its fibers' longitudinal arrangement. Abundantly found in dense forests, particularly in China, bamboo is favored as a reinforcing material in polymer matrices, attributed to its affordability, high tensile strength, lightness, and rigidity. Historically, it has been employed in the construction of structures such as houses, bridges, and boats.

Cotton

Cotton, a member of the Hibisceae sub-tribe within the Malvaceae family, is the predominant fiber used in textile manufacturing. It thrives in the warm climates of China, India, and the USA. The most favored varieties are Upland cotton and Pima cotton. During harvest, cotton leaves are gathered and compressed into large modules comparable in size to trucks. These are then transported to a cotton gin, where the cotton is processed to remove impurities like sticks, burrs, and seeds from the fibers. This process is a staple in the textile industry, and current research is focused on adapting these composite materials for broader industrial use.

Wood

Wood, sourced from various shrubs and trees, is a complex, moisture-absorbing, cellular, and directionally diverse solid. It consists mainly of cellulose (40%-50%) and hemicellulose (15%-25%), which are bonded by lignin (15%-30%). Typically, wood is categorized into softwood, like pine, or hardwood, such as oak. Softwoods primarily contain one type of wood cell, the tracheid, giving them a more consistent structure compared to hardwoods. Softwoods lack vessels, or pores, while hardwoods contain these vessels to varying degrees.

Fruit waste

Fruit peels, stones, and shells like Olive Pit, Almond Shell, Peach Stone, Pistachio Shell, Avocado Stone, Apricot Stone, Argan Shell and Walnut Shell are increasingly recognized as biodegradable fillers for polymers, offering an eco-friendly alternative to traditional, non-renewable fillers. These organic materials, which are often by-products of the food industry, can be processed into fine particles and incorporated into polymer matrices to enhance properties such as strength, stiffness, and biodegradability. Their use not only helps in reducing the reliance on synthetic fillers but also contributes to waste minimization and the development of sustainable materials in various industries.

1.3.1.4. Biopolymers

Polymers featuring backbones that break down in the presence of water can biodegrade under specific circumstances. Such polymers, designed for this capability, encompass a variety of types, including polyesters, polyamides, polyurethanes, polyureas, poly(amide-enamine)s, and polyanhydrides. These materials are engineered to decompose through hydrolysis when exposed to certain environmental conditions.

Aliphatic polyesters

Biodegradable polymers have gained interest for their diversity and synthesis ease. They involve a wide range of monomers, with polycondensation of bifunctional monomers leading to lower-weight polymers. Aliphatic polyesters fall into two categories: polyhydroxyalkanoates, made from hydroxyacids HO-R-COOH, like poly (glycolic acid) and poly (lactic acid), and poly (alkene dicarboxylate)s, created by polycondensing diols with dicarboxylic acids, exemplified by poly(butylene succinate) and poly(ethylene succinate).

Polycarbonate

Poly(trimethylene carbonate) (PTMC) is synthesized via ring-opening polymerization but has limited mechanical properties, leading to a preference for copolymers. Poly(propylene carbonate) (PPC) is made by copolymerizing propylene oxide with CO_2, known for compatibility and impact resistance, yet needing improved thermal stability and biodegradability, often addressed by blending. Poly(ethylene carbonate) (PEC) melts at 100-110 °C, and its blend with poly(tetramethylene succinate) (PTMS) enhances degradability, surpassing that of polyolefins.

Polycaprolactone

Through the ring-opening polymerization of ε-caprolactone, facilitated by a tin octoate catalyst, a semi-crystalline linear polymer is produced. This polymer, known as PCL, dissolves in numerous solvents. It has a notably low glass transition temperature, approximately -60 °C, and melts between 60 and 65 °C. At ambient temperatures, PCL maintains a semi-rigid state. It exhibits a modulus comparable to that of both low-density and high-density polyethylene, possesses modest tensile strength at 23 MPa, and can stretch significantly, with an elongation at break exceeding 700%. Due to its low glass transition temperature, PCL is commonly employed as a compatibilizer or as a flexible segment within polyurethane formulations.

1.3.2. Advantages and challenges of biodegradable fillers

1.3.2.1. Improved polymers properties

The addition of mineral fillers such as talc, calcium carbonate, kaolin, and mica to biodegradable polymers like PBS, PHBH, PBSA, and PBAT can enhance mechanical properties, making them tougher and more rigid without compromising biodegradability. Bouakkaz et al [24], studied the mechanical properties of polypropylene-talc composites with 5, 10, 40 and 50 wt% of talc with an average particle size of 1 mm. Figure 1.2 shows that adding 5% talc to PP reduces its ultimate strain by 17%, and increasing talc to 50% cuts elongation at break by 57%. While talc also lowers PP's tensile strength, this effect is less than on elongation. Talc's stiffness and uneven distribution in PP cause these reductions, decreasing ductility but increasing the material's stiffness due to a higher elastic modulus.

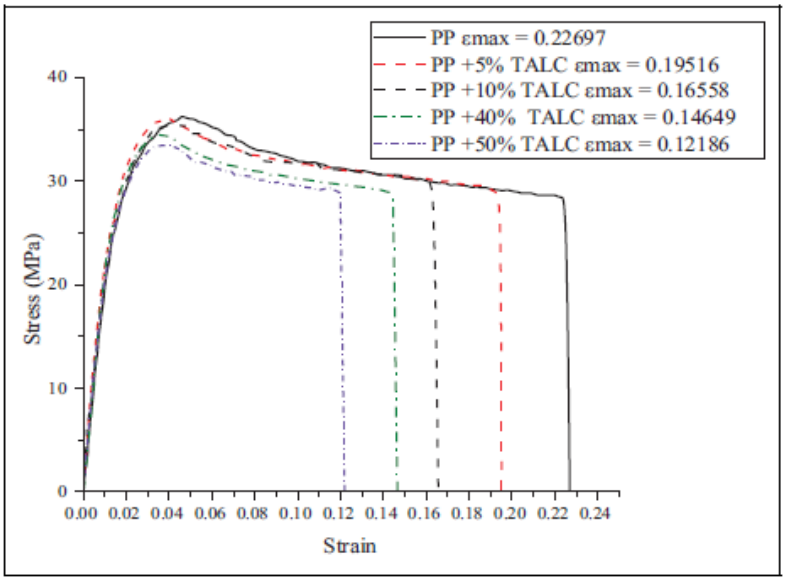

Figure 1.2. Stress-strain curves of PP-talc composite for different talc proportions at room temperature [24].

Zolfaghari et al [25] treat the mechanical properties of polypropylene/silica aerogel composites. The composites of PP/SA with 1, 3, 5 or 7 wt.% of SA (named as PP-SA0, PP-SA1, PPSA3, PP-SA5 and PP-SA7, respectively). Dispersion studies of PP with Silica Aerogel (SA) showed even distribution at 1% SA, slight unevenness at 3% SA, and clumping at 5% and 7% SA due to aerogels' large surface area and high surface energy. Despite increased clumping with higher SA content, the dispersion was acceptable up to 7% SA (Figure 1.3).

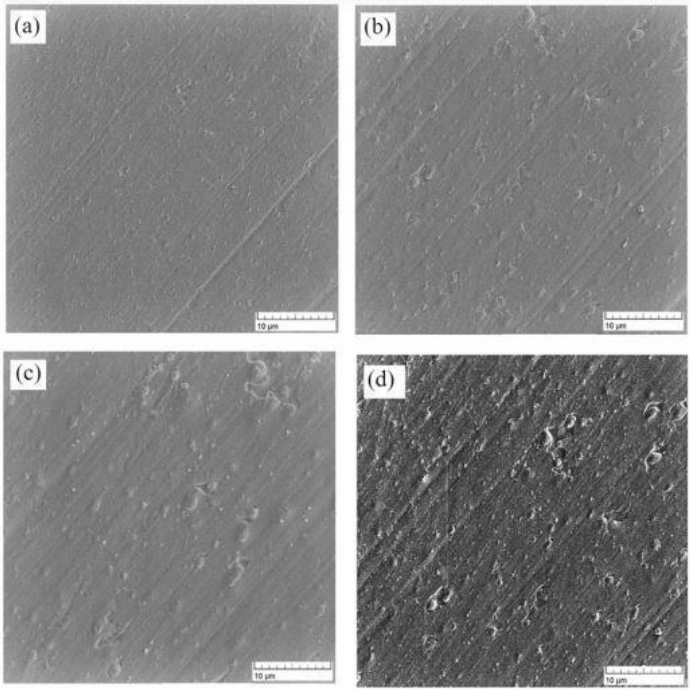

Figure 1.3. SEM images of a) PP-SA1, b) PP-SA3, c) PP-SA5 and d) PP-SA7 composites [25].

The mechanical properties gated by tensile tests presented in Table 1, Increasing Silica Aerogel (SA) in composites up to 7% weight improved the material's modulus due to the aerogel's high modulus. However, higher SA content generally reduced tensile strength, except for a slight increase at 1% SA. The aerogel's structure improved tensile modulus but caused particle clustering, negatively impacting strength and elasticity. SA's size and surface area promoted strong bonding with the PP matrix, enhancing tensile modulus.

Table 1.1. Tensile modulus and strength and elongation and stress at break of the PP-SA composites [25].

Sample	**PP-SA0**	**PP-SA1**	**PP-SA3**	**PP-SA5**	**PP-SA7**
Modulus (GPa)	2.35	2.4	2.7	2.9	4.07
Strength (MPa)	28.4	29.3	28.17	22.53	22.18
Elongation at break (%)	34.18	11.75	7.91	4.11	3.19
Stress at break (%)	23.55	21.86	21.13	18.14	15.39

Natural fibers used as fillers in biodegradable thermoplastics can mildly improve stiffness and strength, particularly in less common polymers like polyolefins, though they may not benefit more common materials like ABS and PLA [26]. Essabir et al [27] prepared a modified PP with a compatibilizer composite filled with Almond shells particles of 14 µm average size with 5, 10, 15, 20, 25 and 30 wt.%. The composite's morphology shows well-distributed particles within the PP matrix, without clumping, indicating strong particle-polymer interaction. The extrusion screw design and a coupling agent, which forms ester bonds, are key to this dispersion and improved particle wettability. In the contrast of what Boujelben et al [28] found with unmodified LLDPE filled with the same particles with 300 µm of size, the particles used as filler are evenly distributed within the LLDPE matrix without forming clusters. At lower concentrations (below 20 wt%), ASP particles are well-dispersed in the matrix (Figure 1.4), but at 30 wt% and 40 wt%, they tend to clump, forming voids and weak bonds. Compatibilizer enhance dispersion in PP composites with almond shell fillers up to 30 wt%, while LLDPE manages up to 20 wt%. Proper filler content is crucial for optimizing natural filler benefits in polymers. While they all agreed that almond fillings increase the elastic modulus of the composite while reducing ultimate strength and elongation at break.

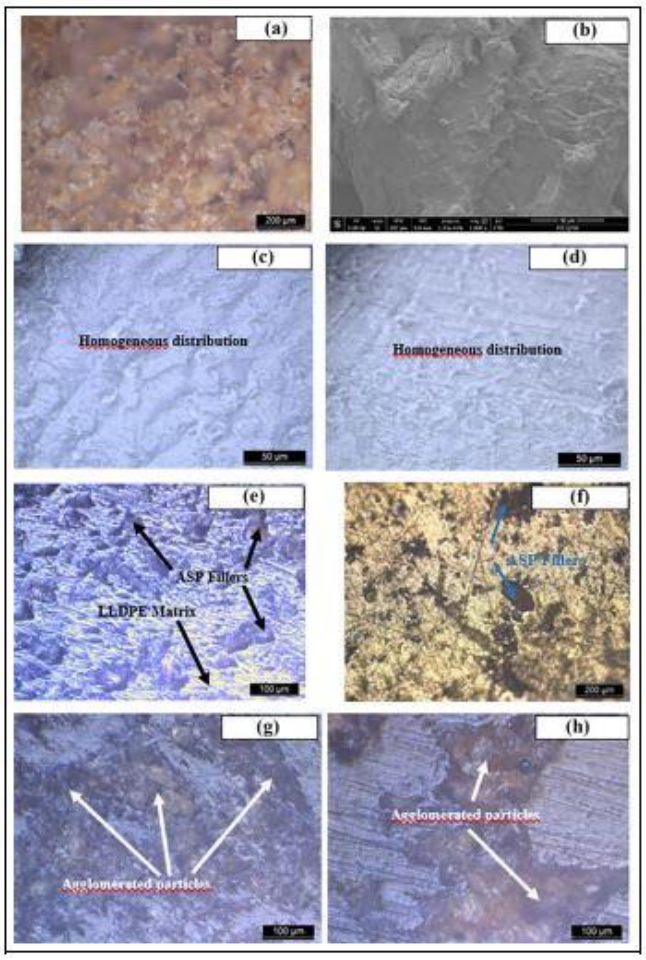

Figure 1.4. (a) Pure ASP and (b) Pure LLDPE. Microstructure of LLDPE reinforced with different wt% of ASP: (c) 5%, (d) 10%, (e) 20%, (f) 30%, and (g and h) 40% [28].

Lignocellulosic fillers like cotton, cellulose, and hydrolyzed-cellulose can enhance the Young's modulus of polycaprolactone-based composites, with cellulose providing the best mechanical properties due to better dispersion and interface interaction [29]. Using lignocellulose-rich biowaste like pecan nutshells in PLA, especially when combined with chemical modifications and physical treatments, can enhance thermal stability, crystallinity, and mechanical properties, while also promoting faster biodegradation [30].

P. Jan et al [31] prepared a green wood-based unrecycled and recycled polypropylene composites and determine the mechanical properties of the composite. Figure 1.5 illustrates the tensile modulus for various materials containing different proportions of wood. Both unrecycled and recycled polypropylene composites experienced an increase in modulus with added wood-filler, with unrecycled seeing a 95% rise and recycled a 140% rise at 40 wt% filler. The initial modulus advantage of unrecycled over recycled polypropylene narrowed from 26% to 8% with more wood-filler. Tensile strength decreased as wood-filler content grew, by 17%

in unrecycled and 10% in recycled, with unrecycled maintaining a 20-23% higher tensile strength than recycled. Figure 1.6 depicts the tensile strength, revealing a decrease in strain with more wood fillers for both types of polymers. While recycled polymers typically had higher strains than unrecycled ones, this difference lessened with more wood content, and at 40 wt % wood fibers, the trend reversed.

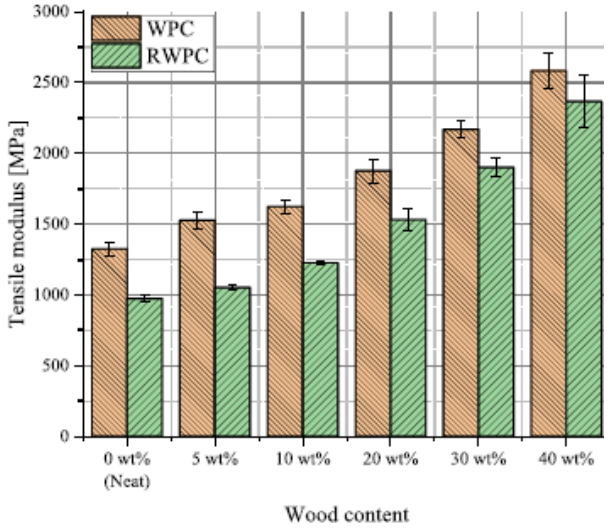

Figure 1.5. Tensile-modulus [31].

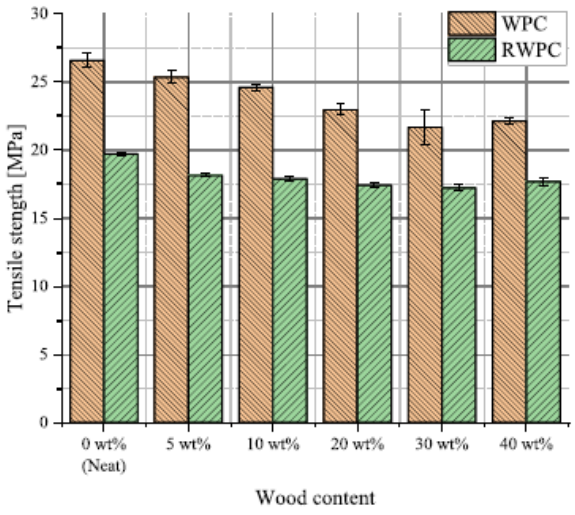

Figure 1.6. Tensile-strength [31].

The integration of biodegradable fillers into polymers generally enhances mechanical properties such as stiffness, strength, and thermal stability, also leads to an increase in hardness. Mineral fillers, natural fibers, and organic fillers each offer unique benefits, with the choice of filler and polymer matrix significantly influencing the overall performance. The enhancement in the mechanical properties and hardness is attributed to the reinforcing properties of the fillers, which improve the mechanical strength and rigidity of the polymer composites.

1.3.2.2. Reduced environmental impact and waste generation

Several studies suggest that the biodegradable fillers can reduce environmental impact and waste generation by conserving energy, reducing emissions, diverting waste from landfills, and utilizing renewable, biodegradable materials. Biodegradable fillers like calcium carbonate in PLA-based bottles significantly reduce environmental impacts compared to non-filled PLA bottles, particularly in terms of energy conservation and emission reduction [32]. Biodegradable food packaging materials, such as those made from thermoplastic starch (TPS) and polyhydroxyalkanoate (PHA), can offer positive greenhouse gas (GHG) outcomes if they effectively reduce food wastage [33]. Biodegradable Polymers, including those with natural fillers like wood flour, show promising degradation profiles under composting conditions,

contributing to waste reduction [34]. Biodegradable plastic blends, such as PLA blended with polycaprolactone (PCL), can degrade in home composting environments, although the degradation rates vary significantly across different environments [35]. Bioplastics derived from sustainable sources, such as microalgal residues, can be converted into biodegradable films, providing an eco-friendly alternative to conventional plastics [36]. Effective post-consumer management and further design improvements are necessary to ensure that

1.3.3. Different treatments of biofillers

A significant limitation of natural fibers within composite materials is their inherent tendency to absorb water, owing to their hydrophilic characteristics. This leads to suboptimal bonding between the fiber and the matrix, resulting in weaker mechanical performance of the composites. To overcome this, it's essential to chemically alter the fibers to reduce their water-absorbing properties.

Chemical treatments

Silane treatment

Treating sugar palm fibers with a mix of silane and NaOH creates silanol groups that bond with the fibers' -OH groups, enhancing the fiber-matrix interface and the composite's strength. The mechanical properties of silane-treated composites improve with varying immersion times, forming a hydrophobic silane layer that sticks to the matrix via van der Waals forces.

Acetylation treatment

The formation of the acetyl group on the surface of fibers serves to reduce their hydrophilic tendencies, thereby stabilizing the composites. This modification improves the bonding affinity between the fiber and matrix, leading to the creation of a robust bond that significantly enhances the composite's characteristics. The reaction of the acetyl group with the fibers' -OH groups imparts a hydrophobic quality to the fiber surface.

Stearic acid treatment

The application of stearic acid to fibers results in a reaction between the fiber's hydroxyl group and the stearic acid, which is intended to render the fiber surface less water-attracting, thus

enhancing compatibility. This treatment method is known to maintain the inherent strength of the fiber without substantial alteration.

Peroxide Treatment

This method is typically used on cellulose fibers to enhance the mechanical attributes of composites. The breakdown of peroxide generates free radicals that interact with the hydroxyl groups present in both the cellulose fiber and the matrix. This step is carried out subsequent to the fibers' alkalization. Fibers that have undergone alkaline treatment are immersed in a 6% solution of either benzoyl peroxide or dicumyl peroxide dissolved in acetone for approximately 30 minutes.

Benzoylation Treatment

In this approach, fibers undergo an initial NaOH treatment, then a subsequent ~15-minute benzoyl chloride (C_6H_5COCl) application. Following isolation, the fibers are briefly treated with ethanol for about 1 minute, washed with distilled water, and finally dried in an oven at 80°C for 24 hours. This process not only enhances the thermal stability of the fibers compared to their untreated counterparts but also diminishes their affinity for water. Moreover, it fortifies the bond between the fiber and matrix, thereby bolstering the composite's overall strength.

Physical treatments

This technique has a minimal impact on the fibers' chemical structure. It encompasses fiber stretching, calendaring, as well as corona, thermal, and plasma treatments, along with the mechanical interfacing of polymers. A stronger mechanical connection between the fiber and matrix typically leads to increased interface strength. Yarning methods are employed to produce fine strands of natural fibers. It is reported that such physical methods alter the natural fibers' surface, affecting only the outermost layer of the cell wall without changing the fibers' moisture-absorbing properties. While physical treatments can improve toughness, stretchability, and flexibility, overly aggressive treatments can cause damage to the fibers.

Mercerization

Mercerization, also known as alkaline treatment, involves immersing vegetable fibers in a strong base solution, typically sodium hydroxide (NaOH), which is highly concentrated. This process causes significant swelling and alters the fibers' fine structure, size, shape, and

mechanical characteristics. NaOH is favored for its ability to bleach or cleanse plant fiber surfaces, transforming native cellulose I into cellulose III. This change is accompanied by depolymerization and the creation of shorter crystallites. By adjusting the parameters of the mercerization process, fundamental properties of the fibers, like tensile strength and stretchability at the point of rupture, can be modified.

Corona

Corona discharge and cold plasma treatments are employed to activate surface oxidation. These treatments alter the surface energy of cellulose fibers and can increase the presence of aldehyde groups, particularly in wood fibers. Utilizing various gases allows for diverse surface modifications, including the introduction of surface crosslinking, adjustments to surface energy levels, and the generation of reactive free radicals and functional groups.

1.3.4. Polymer biodegradable fillers composites fabrication

Biodegradable filler-based polymer composites are crafted using diverse manufacturing techniques. These composites are valued for their acoustic, mechanical, and shape-changing abilities, along with their light weight, reduced ecological footprint, and improved disposal options. Unlike synthetic fillers, they require careful selection due to their unique microstructures and compositional characteristics, which differ among bio filler types. Understanding their reaction to heat, moisture, complex carbohydrate structures, inherent imperfections, and natural variation is essential for optimal performance. The size, complexity, and mechanical properties of the composites can be influenced by the chosen processing method.

Key parameters in biocomposite production include temperature, pressure, and duration. Biocomposites are generally created using methods similar to those for plastics or other composites. For cost efficiency and simplicity, hand lay-up and spray lay-up are commonly used in biocomposite production. Injection molding is frequently used for mass production of biocomposites. This process involves feeding pellets into a machine via a hopper, and for natural fiber composites, a hopper dryer is recommended to keep the pellets dry during injection. Compared to products made through compression molding, traditional injection molding processes tend to have lesser mechanical performance because they can only incorporate short fibers with low aspect ratios, while compression molding can handle long or continuous fibers. Beyond standard injection molding, specialized variants have been

developed, such as micro-injection molding for small components [37]. Pultrusion is a technique for creating biocomposites by soaking continuous fibers in a polymer matrix and then pulling them through a heated die. The pultrusion process has been applied to produce continuous composites with flax fiber-reinforced polypropylene to study their mechanical behavior [38]. Combining pultrusion with reaction injection molding (RIM) has also been explored to develop the reactive pultrusion process [39]. Solution casting is another straightforward biocomposite fabrication method, typically conducted at low temperatures to yield films with uniformity and clarity. While solvent casting can be used for creating nano-reinforced biocomposites, its slow speed, use of toxic solvents, and the cost of solvent recovery restrict its use to small-scale laboratory settings [40]. Electro-hydrodynamic methods like electrospinning have gained attention in the biomedical sector due to the submicron size of the produced fibers, which leads to a large surface-to-volume ratio and high porosity with interconnected spaces [41]. The spinnability of natural and biodegradable polymers allows for a dual process that combines electrospinning of a polymer solution with electrospraying of nanoparticle dispersions, resulting in nanoparticle-coated polymeric fibers suitable for drug delivery and tissue engineering [42]. Electrospinning stands out as the most effective technique for replicating the extracellular matrix's collagen nanofibers using biodegradable polymers or biocomposites for tissue repair [43]. Some of the significant studies on the manufacturing of natural fibers reinforced polymers composites (NFRPCs) are presented in Table 2.

Table 1.2. Some of the significant studies on the manufacturing of natural fibers reinforced polymers composites (NFRPCs) [44]

Composites	Manufacturing process	Remarks
Kenaf fiber-reinforced PLA composite	Compression molding	Linear incremental behavior was obtained for tensile and flexural strength up to 50% reinforcement. There was no effect of heat up to 160 °C on kenaf fiber.
Kenaf fiber-reinforced epoxy composite	Vacuum-assisted resin transfer molding	With the reinforcement of fiber, friction and wear performance of composite improved. Fiber reinforcement has a significant effect during the wear test as compared to sliding velocities and normal load.
Jute/betel nut fiber-reinforced polypropylene composite	Compression molding	Mechanical properties increased after reinforcing 10% bettle nut into jute/polypropylene composite as compared to neat polymer.

Kenaf powder reinforced recycled HDPE/natural rubber composite	Compression molding	The elastic modulus of the composite increased with fiber reinforcement. Tensile strength and strain decreased. By adding MAPE, tensile strength increased. Water uptake by composite increased by adding MAPE.
UHMWPE/HDPE blended kenaf/basalt composite	Compression molding	The tensile strength of the UHMWPE/HDPE blend increased on fiber reinforcement. Insignificant improvement in flexural and impact strength was observed after fiber Reinforcement.
Starch-grafted-polypropylene/kenaf fiber composite	Compression molding	Mechanical properties enhanced after kenaf fiber reinforcement.
Sisal Fiber reinforced polyester composites	Hand lay-up technique	Composite having kenaf fiber in anisotropic position had better properties than the fiber in a perpendicular or isotropic direction.
Sisal/cotton reinforced epoxy composite	Hand lay-up technique	40 wt% reinforced composite showed better mechanical properties as compared to 10%, 20%, 30%, and 50%.
Jute/kenaf/E-glass woven fabric epoxy composite	Vacuum-assisted resin transfer molding	Better tensile strength was observed in kenaf/glass composite as compared to jute/glass composite. The stacking of high strength fiber showed high mechanical strength.
Kenaf fiber-reinforced foam	Compression molding	Better interfacial bonding was observed after the treatment of kenaf fiber before composite manufacturing. The durability of treated fiber composite was more.
Kenaf fiber-reinforced natural rubber/ polyurethane composite	Compression molding	Composite with the maximum percentage of natural rubber showed better physical properties. Composite with the highest polyurethane showed the highest damping properties.
Glass fiber reinforced nylon 66/ polystyrene and LDPE composite	Microwave-assisted heating	Welding of thermoplastic-based composites performed. This process has the potential to replace thermosetting resins with advanced thermoplastic composites.

1.4. Tribological Behavior of Filled Polymer Composites with Biodegradable Fillers

1.4.1. Animal fillers

Yunhai Ma [45] examined how wool fiber affects the wear and friction characteristics when used as a reinforcement in friction materials. Fabrics reinforced with 3% by weight of wool fiber demonstrated a consistent friction coefficient and reduced wear rate. As temperatures increased, the friction coefficient's reliability improved. However, Rockwell hardness

decreased and impact force increased with higher wool fiber content. The study concluded that wool fiber-reinforced fabrics are effective for both elastic and abrasive applications. I OOladele [46] explored the influence of fiber content on the abrasion resistance of polyester composites reinforced with treated cow hair fiber. The best abrasion resistance was found at a cow hair fiber (CHF) content of 4% by weight. T Narendiranath Babu [47] assessed the tribological performance and Brinell hardness of composites made from Angora, Kenaf, and Ramie fibers mixed in specific ratios with Epoxy LY556 resin and Hardener HY951. It was observed that composites with Kenaf fibers displayed better tribological properties than those with Angora or Ramie fibers.

1.4.2. Waste agriculture biodegradables fillers

Studies have shown the influence of rice husk on the sliding wear characteristics of polymer composites. Rout and Satapathy created a composite with rice husk in an epoxy matrix to study its dry sliding wear behavior [48]. They found that wear behavior was affected by factors like the amount of filler, sliding speed, and load. Notably, a 20% weight concentration of rice husk significantly reduced wear on the composite's surface [48]. Other agricultural wastes, such as wheat husk, also serve as reinforcements, with rice husk composites showing lower wear resistance and coefficient of friction compared to those reinforced with wheat husk or coir fibers [49]. Ibrahim et al investigated the sliding wear behavior of date seed powder in polyester biocomposites, finding that a 25% weight filler content significantly lowered the coefficient of friction and wear rate at moderate speeds and loads. However, increasing the filler content above 15%, along with higher loads and speeds, decreased wear resistance [50].

Wojciechowski et al [51], were used cherry seed filler with polypropylene for strengthen it for tribological applications. Cherry seed filler with various proportions (5 %, 10 % and 15 %) and granulation ($d < 400$ μm, $400 < d < 630$ μm, and $630 < d < 800$ μm) was used for preparing the composite samples shaped dimensions 15×10×4 mm (Figure 1.7. a)). The composite were tested on block-on-ring tribological system (Figure 1.7. b)). Dry friction conditions were used, the used rings possessing an outer diameter measuring 45 mm and a width of 12 mm were fabricated using AISI 1045 steel, 200 rpm rotation velocity was used and 250 and 500 N normal loads were used.

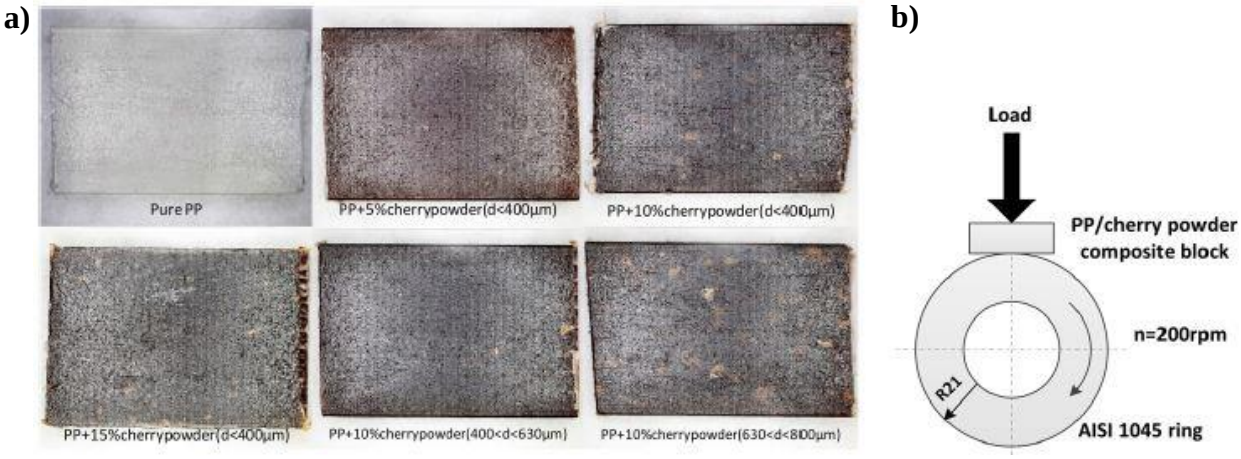

Figure 1.7. PP cherry seed composites samples, b) Block-on-ring tribological system [51].

The COF is presented in Figure 1.8, Under a 250 N load, polypropylene (PP) with 10% cherry seed powder (630-800 micrometers) reached a stable COF faster and maintained lower COF values than pure PP.

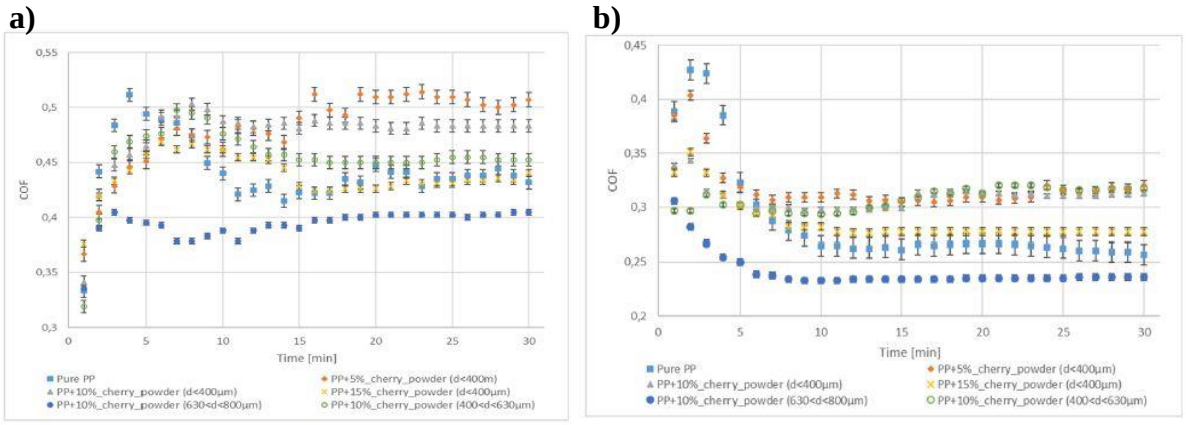

Figure 1.8. a) The average trends for the COF calculated for a 250 N load, b) The average trends for the COF calculated for a 500 N load [51].

Other mixtures had higher COF values, except for the 15% and 10% (400-630 micrometers) variants, which were similar to pure PP. At a 500 N load, all COF values stabilized quicker and were lower than at 250 N.

The relatively low yield strength of polymers leads to quicker plasticization and adherence to the metal counterpart under higher loads, as well as a more efficient expulsion of residual oil from the cherry seed filler (Figure 1.9). Adding cherry seed powder to polypropylene (PP) significantly reduces friction, with a 10% addition showing a 50% drop in COF. Higher filler content leads to steadier friction levels, while larger particle sizes (630-800 micrometers) minimize initial friction increases, especially under higher loads.

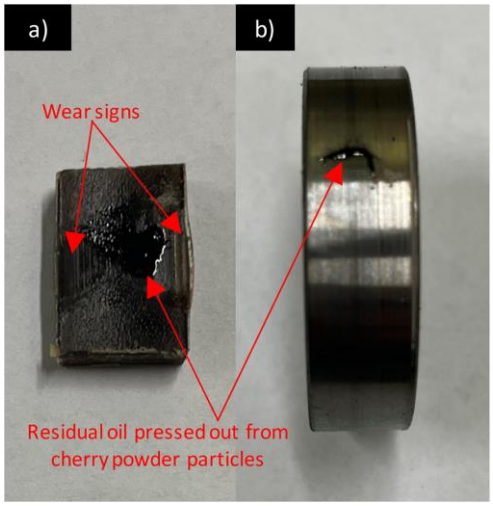

Figure 1.9. Signs of wear and residual oil observed after friction tests on the surfaces of the samples [51].

Cherry seed powder enhances the tribological properties of polypropylene (PP) composites. Low-content PP composites show abrasive wear, while higher contents shift to adhesive wear, lessened by larger particles due to fatty acids acting as lubricants. The best performance is seen with the largest particles (PP+10%, 630-800 μm), improving friction and wear resistance. Medium and high filler contents perform similarly to pure PP, beneficially incorporating waste without property degradation. However, the smallest fillers worsen tribological properties. The fatty acids from cherry seeds are key to better friction and wear outcomes [51].

Sharma et al [52], were prepared citrus limetta particles (CLP) with epoxy and studding it under tribological loading. CLP particles were produced in three distinct granular categories: fine (100–250 μm), medium (350–500 μm), and coarse (650–800 μm). These untreated particles comprise 20.8% cellulose, 17.2% hemi-cellulose, 8.9% lignin, 14.2% pectin, 3% ash, and 4.32% wax, based on dry weight percentage. Subsequently, composites incorporating 15% by weight of CLP fillers across these size ranges were fabricated using a casting process in a glass mold. Pins measuring 45 × 10 × 10 mm were then extracted according to ASTM G-99 standards from the solidified epoxy composite sheets. The wear testing was conducted using a Pin on Disc apparatus and a friction monitoring device. The tests were performed under dry sliding conditions with normal loads set at 30 N, 40 N, and 50 N. The experiments varied the sliding speeds to 3m/s, 4m/s, and 5m/s, following a circular trajectory, all at ambient room temperature. Each test maintained a consistent track radius of 60 mm and a total sliding distance of 5000 meters.

All samples showed increased wear loss with higher normal loads (Figure 1.10). Neat epoxy (NE) experienced significant wear loss under stress, which was reduced by up to 44.06% with the addition of CLP fillers, particularly CP1. This filler was most effective, showing a 68.57% reduction in wear loss at lower loads. While higher speeds increased wear, CLP fillers, especially CP1, counteracted this. Smaller CLP particles in CP1 enhanced wear resistance by improving bonding and reducing voids, whereas larger particles in CP3 were less effective due to potential deboning from increased friction.

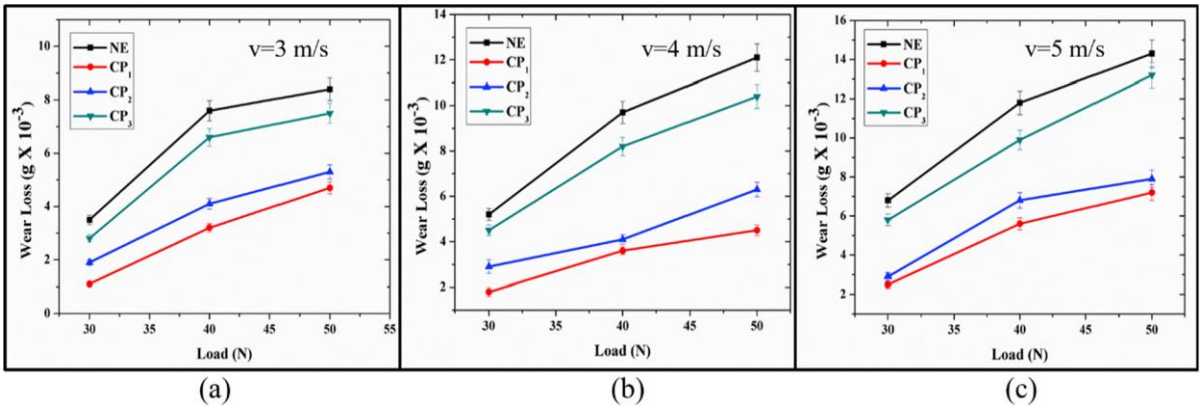

Figure 1.10. Wear loss vs applied normal load [52].

The coefficient of friction (COF) was determined by dividing the frictional force by the applied normal load, as detailed in figure 1.11. The study shows that neat epoxy (NE) had a higher coefficient of friction (COF), which was reduced by adding CLP fillers, particularly smaller particles. This reduction was consistent under various loads and speeds. Higher loads increased COF due to more contact pressure and heat, but CLP fillers, especially CP1 and CP2, effectively lowered COF. Larger CLP particles caused more friction, but overall, CLP fillers produced less debris and lower COF than synthetic fillers, potentially forming a lubricating film at lower speeds and higher temperatures, further reducing COF [52].

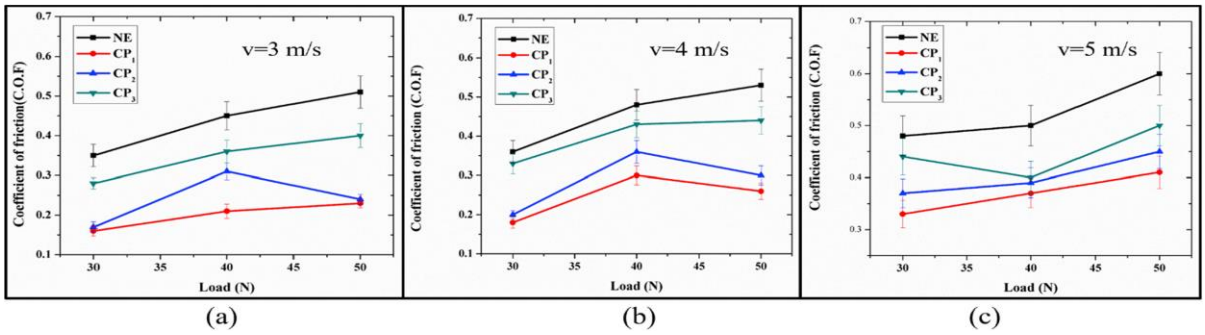

Figure 1.11. COF vs. applied normal load [52].

Friction at the contact surface generates heat, raising the temperature at the interface, as confirmed by IR thermometer readings. The highest temperatures were recorded at the furthest sliding distance of 5000 meters, as shown in Figure 1.12. As normal loads increase, so does the interface temperature, confirming that frictional force rises with load. Neat epoxy (NE) showed the highest interface temperature, while composites with CLP fillers, particularly CP1, had lower temperatures. CLP particles, once detached and surfaced during sliding, cool the interface more than NE, as evidenced by SEM images and lower average temperatures in composites with CLP fillers [52].

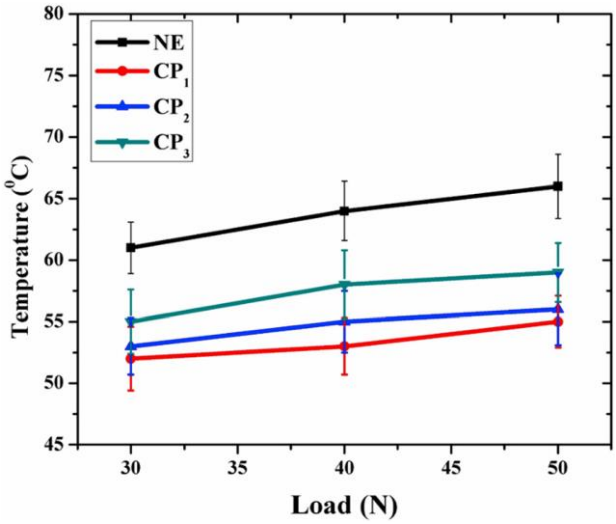

Figure 1.12. Interface temperature of different CLP filler based composites [52].

Sharma et al were conclude that Adding CLP fillers to the epoxy matrix significantly enhances the wear resistance of the resulting epoxy composites. Both wear loss and the coefficient of friction tend to rise with larger CLP filler particles and higher normal loads. CP1's notably low coefficient of friction suggests superior wear resistance, while CP3 shows increased friction and wear loss in comparison. It's clear that neat epoxy (NE) benefits from the integration of CLP fillers in terms of wear performance. Furthermore, incorporating 15% of CLP food waste as filler in epoxy not only improves wear properties but also represents a sustainable approach that could meaningfully reduce plastic consumption [52].

1.4.3. Wood based filler reinforced biocomposites

Mishra's research [88] indicated that composites with 150 μm teak wood dust exhibited superior wear resistance and mechanical properties. Kumar et al. [53] observed that adding mango, sheesham, mahogany, and babool dust to a polypropylene matrix reduced wear resistance as filler content increased. Composites with babool and sheesham dust had better mechanical

properties, whereas those with mango and mahogany were more wear-resistant [54]. Wood fillers' hydrophilic nature often leads to poor bonding and filler clumping in hydrophobic polymers, limiting mechanical performance [55]. To address this, techniques like adding crosslinking agents, modifying fillers and polymers, and using gamma radiation are employed for better filler distribution and dispersion.

Ibrahim et al [56] were fabricated wood flour WF filled PP matrix by a simple injection molding process in presence of MA-PP as a coupling agent figure 1.13.

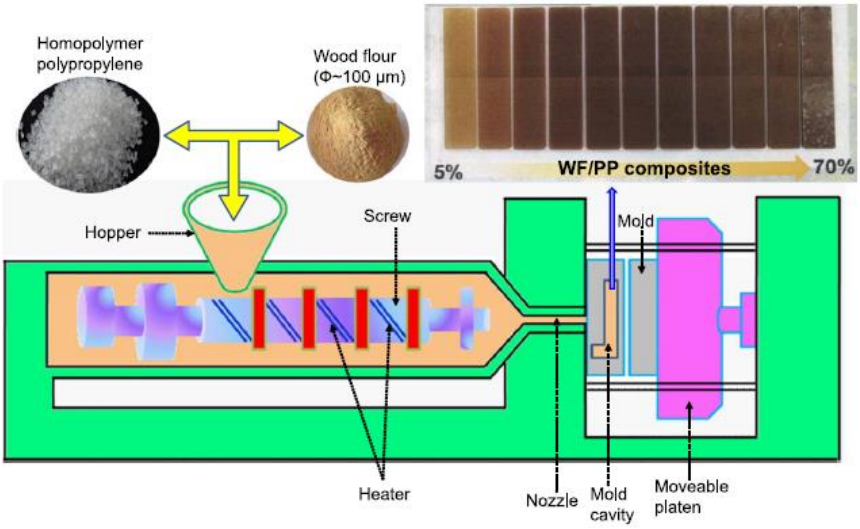

Figure 1.13 Fabrication of WF filled PP matrix by Ibrahim et al [56].

A linearly reciprocating ball-on-disk sliding test were used by Ibrahim et al as tribometer. Plate-shaped specimens shaped of 29 mm×23mm×3mm and a normal load of10 N was used. The specimens were slided under the counter face at a fixed sliding velocity of 20 mm s^{-1} for 1200 successive cycles. A Slider of stainless-steel of 12 mm diameter was used as the counter face, the specimens equipped with a surface roughness of Ra1=340.7 nm, Ra2=391 nm and Ra3=431 nm [56].

Figure 1.14 displays how the coefficient of friction (COF) changes with wear area across various wood flour (WF) contents. Under a radial load and sliding speed, 25 wt% wood filler (WF) in polypropylene (PP) composites reduced the coefficient of friction (COF) by 28% on certain abrasive surfaces, with COF decreasing as WF content increased. Lower WF content decreased COF due to the matrix's deformation, while higher content increased COF, likely from more wear. Wear patterns depended on the filler content and wear mechanisms, with optimal wear resistance at specific WF percentages. Pure PP showed poor wear resistance, and

wear areas under reciprocating motion on spherical surfaces showed minimal change during tests, with the most wear on the roughest surface [56].

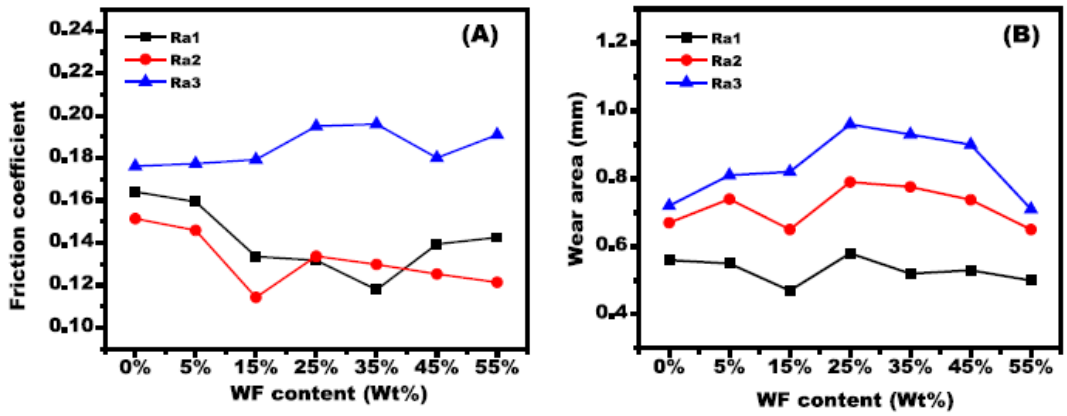

Figure 1.14. (A) The effect of WF content on the coefficient of friction under different abrasive surfaces. (B) The change in wear area at different WF content under different abrasive surfaces [56].

Figure 1.15 presents how the wear area varies with the geometry of friction surfaces Ra1, Ra2, and Ra3. The wear area on abrasive surfaces is influenced by their shape, with surface Ra3 showing more wear than Ra1 and Ra2 due to more debris, indicating three-body abrasive wear. This wear, where debris acts as a third body, is affected by the load and debris movement. Larger wear areas suggest higher friction, with the geometry of Ra3 causing more debris and wear. Wood flour (WF) increases fracture resistance, reducing grain pull-outs under stress. Overall, the load has a greater impact on wear than other factors, and WF composites show less damage than pure polypropylene (PP) under the same conditions [56].

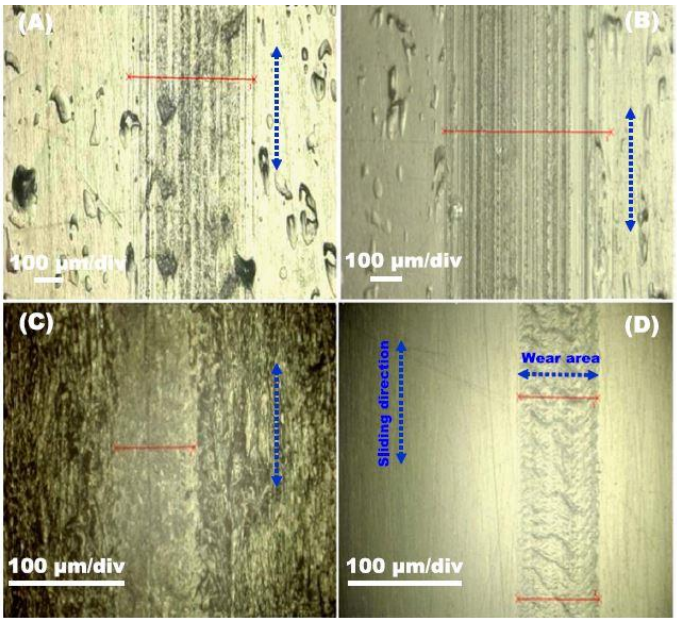

Figure 1.15. Microscopic micrographs for the wear surface of WF/PP composites tested using different abrasive surfaces [56].

This study achieved improved tribological outcomes, including reduced friction coefficients and wear rates. These improvements are likely due to the polymeric chains forming on the cellulosic reinforcement surfaces, enhanced by a coupling agent, leading to a strong bond between the two components. The findings offer deeper understanding of the tribological behavior of functionalized plastic/WF composite materials, highlighting their potential as effective bearing materials for widespread applications.

P. Jan et al [31] also treat the tribological behavior wood based composite on unrecycled and recycled polypropylene composites. Five wood-polymer composites were prepared with 5, 10, 20, 30, 40 wt % of wood fillers contents. Tribological tests were conducted on a reciprocating tribometer with a ball-on-disc configuration. The slider of 10 mm diameter of 100Cr6 steel. A fixed normal load of 3N and sliding speed of 0.15 m/s, during 3 hours.

The data in figure 1.16 shows that adding wood filler to polypropylene reduces the coefficient of friction, more so in recycled than in virgin polypropylene. Recycled polypropylene saw a 5% to 30% reduction in friction with 5% to 40% wood filler, while virgin polypropylene experienced up to a 15% reduction at 40% wood filler. Initially, recycled polypropylene had a higher friction coefficient than virgin, but both reached a similar level of 0.25 with 40% wood filler, minimizing the differences between them beyond 20% wood filler content.

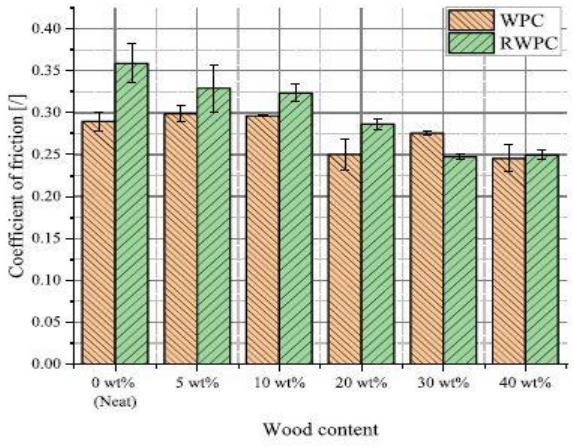

Figure 1.16. Steady state coefficient of friction [31].

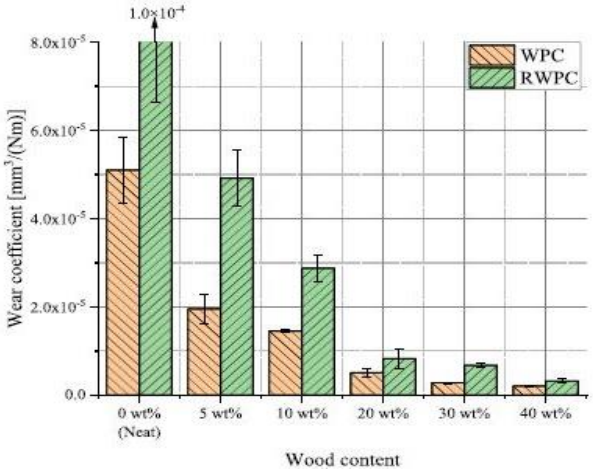

Figure 1.17. Wear coefficients [31].

Figure 1.17 shows that wood fillers significantly improve the wear resistance of polypropylene. Virgin polypropylene has a lower wear coefficient than recycled, but both benefit from wood fillers, with up to a 30% reduction in wear rate at 40 wt% filler. Even a small addition of 5 wt% wood filler greatly enhances wear resistance, demonstrating the effectiveness of wood fillers in both virgin and recycled polypropylene composites.

The SEM images in Figure 1.18 reveal the wear patterns of the materials tested. The main wear mechanisms for both new and recycled polymers are spalling and pit formation. Adding wood fillers up to 20% by weight didn't change these mechanisms, but it did increase the number of pits when wood particles came out. Recycled composites showed more wood particles and pits in the wear tracks compared to new composites.

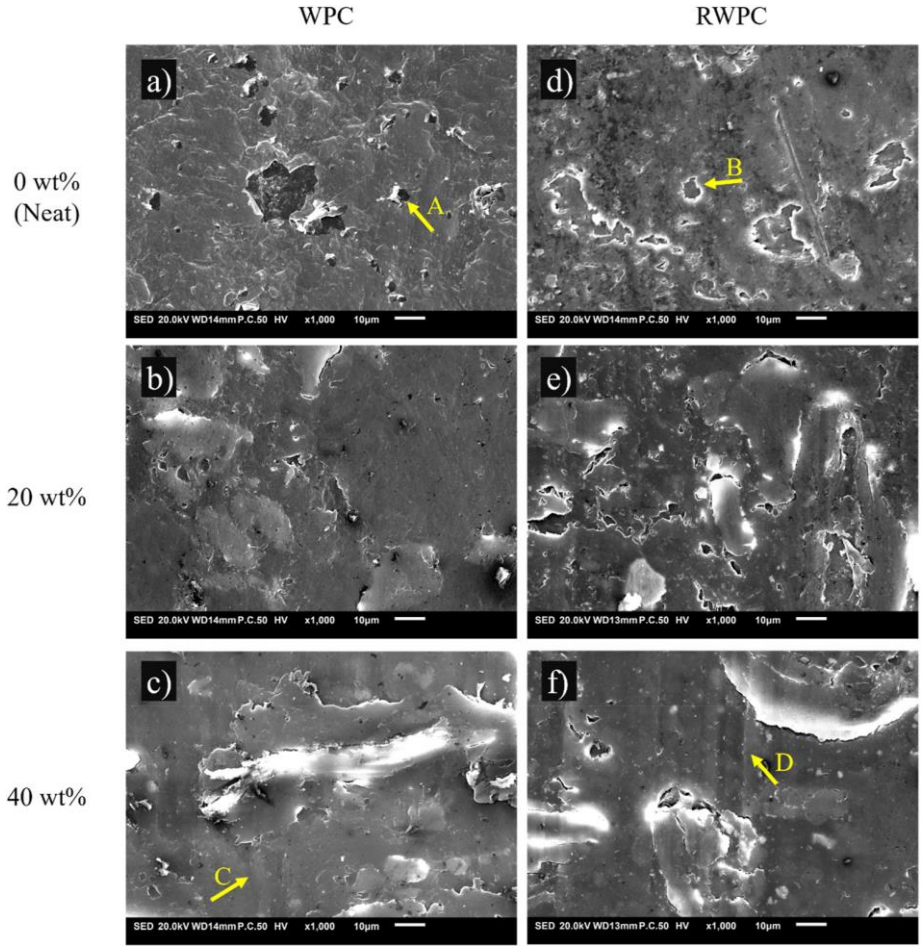

Figure 1.18. SEM images of unrecycled polypropylene wear scars [31].

In the recycled composite samples, the wood fillers were dislodged during sliding, for a sample with 10 wt% wood filler (Figure 1.19), leading to inferior wear resistance in comparison to the virgin composites. Furthermore, the wood particles in the recycled matrix were not firmly embedded. When the wood filler content was increased to 20 wt% or more, both virgin and recycled composites began to show signs of abrasion, especially as the wood content rose.

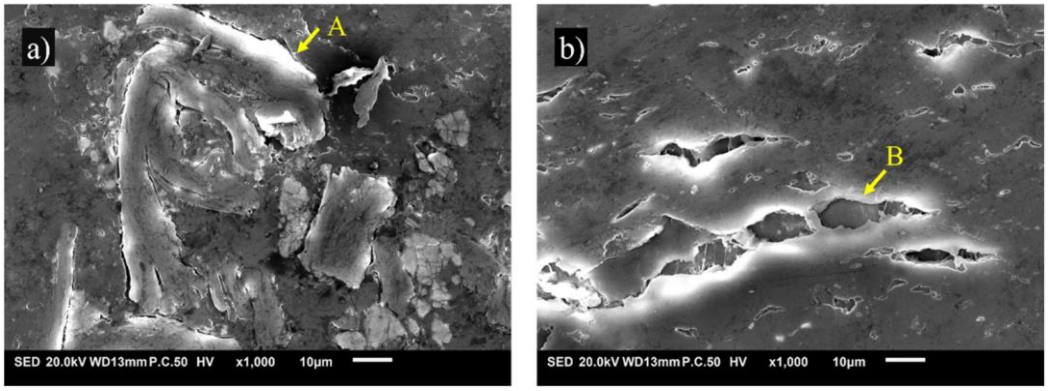

Figure 1.19. Example of 10 wt % filler-content recycled polypropylene [31].

Below 20% wood filler, wood particles tended to detach from the polymer base during friction, more so in recycled composites, leading to lower wear resistance than virgin composites. Above 20% filler, wood particles were better integrated into the composites, likely due to increased crystallinity, resulting in a more cohesive surface. Tensile strength was similar for both composite types, which may have improved wear resistance, as the wood fillers could reinforce the material more effectively, possibly because of better load distribution among the fibers. Figure 1.20 highlights the contrasting wear behaviors of composites with varying levels of wood filler content.

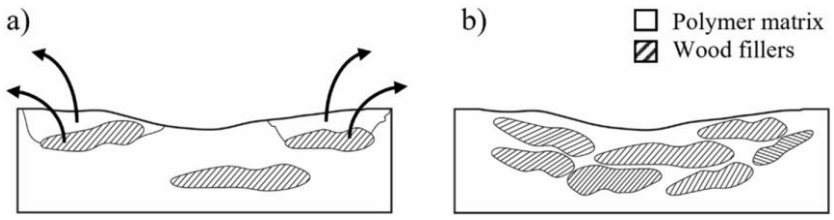

Figure 1.20. Schematically presented wear behavior for unrecycled (WPC) and recycled (RWPC) composites with wood-filler content: a) below 20 wt % and b) above 20 wt % [31].

Polypropylene (PP) wood composites, both virgin and recycled, exhibit superior tribological properties compared to neat PP. The addition of wood fillers reduces friction by 30% in recycled and 15% in virgin composites achieving a friction coefficient of 0.25 at 40% filler content. Wear resistance improves significantly with this level, increasing tenfold for virgin and a hundredfold for recycled composites. Up to 20% wood filler, spalling and pit formation are observed; above that, abrasion occurs. Higher filler content enhances particle embedding and performance due to increased crystallinity and better load transfer. Even a 5% addition boosts wear resistance by 63% in virgin and 43% in recycled composites, highlighting wood fillers as

a sustainable option for enhancing tribological properties and improving recycled material quality.

Overall, the addition of wood dust, such as pine, teak, mango, and babool, enhances mechanical properties and wear resistance, although the hydrophilic nature of wood can complicate bonding in hydrophobic polymers. Optimal filler content is crucial, as both insufficient and excessive amounts can negatively impact performance. The studies demonstrate that wood fillers reduce the coefficient of friction and improve wear resistance, especially in recycled polypropylene, showcasing their potential in eco-friendly materials. Techniques such as adding coupling agents and modifying filler characteristics can further enhance dispersion and bonding, leading to improved tribological behavior.

1.5. Applications of biodegradables fillers based polymers

1.5.1. Automotive and aerospace applications

Polymers reinforced with biodegradable fillers are increasingly used in structural automotive components by leading car manufacturers. For instance, the interior elements like dashboards and partitions in E-class vehicles are constructed from bio-composites [57]. Car doors' inner trim panels consist of a composite that blends 60% bio-fiber with 40% polyurethane [58]. Flax fiber-reinforced plastics, known for their high friction coefficient and low wear rate, are preferred materials for automobile brake linings and pads [59]. Many other interior automotive parts are also made from bio-fiber composites, as depicted in Figure 1.21. Over the past decade, various studies have investigated the performance of bio-fiber composites in automotive applications, some of which are summarized in Table 3.

Figure 1.21. Some interior automotive parts made from bio-fiber composites [57].

S. No	Fibres/Matrix	Application
1	Jute and glass/polyester	Seat backings, bumpers, luggage shelves in cars
2	Jute/polyester	Body panels of prototype cars
3	Hemp and flax/polypropylene and polyester	Floor-well panels in cars
4	Coconut/ rubber latex, Flax and sisal/ epoxy	Seats and door panels in in Mercedes Benz-A and E model cars
5	Flax and sisal mat/polyurethane	Door trim panels in Audi cars
6	Kenaf and flax/polypropylene	Door panels and floor trays in Ford cars
7	Flax/polypropylene	Rear shelf trim panels in Chevrolet cars
8	Roselle, banana and sisal/epoxy	Visor, side cover, indicator cover, billion sear cover in two wheelers
9	Flax / Polyester	High roof of cars
10	Coconut/rubber	Seat bottoms, heat restraints, inner trim, backrests
11	Recycled fibrowood/polypropylene	Retainer for seat back panel
12	Cotton/polypropylene	Sound proofing, insulations, trunk panel
13	Wood flour/polypropylene or polyolefin	Carrier for door panels, arm rest and covered inserts
14	Wool/leather	Seat covers and upholstery
15	Bamboo/polyurethane	Door panels

Table 1.3. Some application of bio fibers in automotive industry [57].

Aircraft components like spoilers, rudders, doors, elevators, keel beams, fan blades, wings, and rear bulkheads, along with various interior elements, are constructed using composites derived from bio-fibers [60]. In the aerospace industry, not only is the strength-to-weight ratio crucial, but so is flammability when designing aircraft parts. Developing bio-fiber composites with enhanced flame resistance is a key research focus [61]. Moreover, replacing traditional materials with ramie fiber-reinforced composites in aircraft wing boxes has resulted in a 14% weight reduction [62]. The components are illustrated in Figure 1.22.

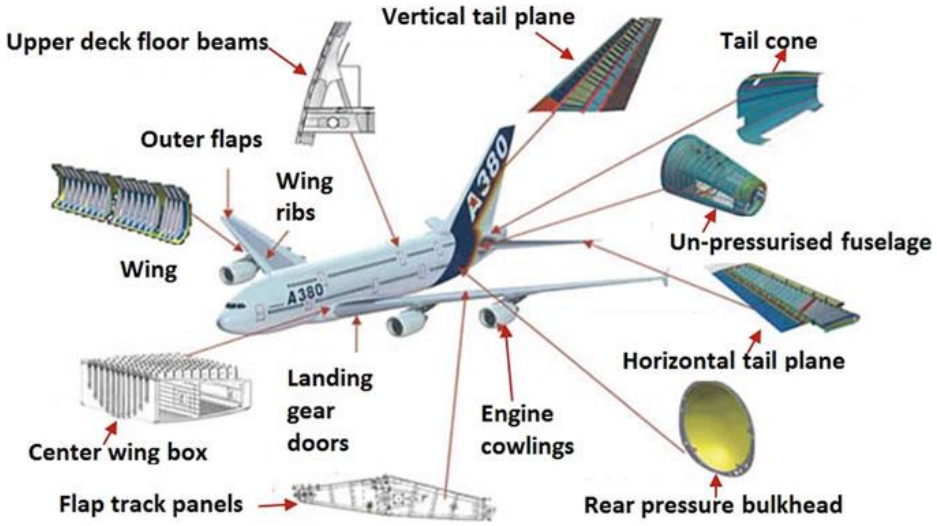

Figure 1.22. The airplane components made from natural fillers [57].

1.5.2. Biomedical applications

The success of bio-composites in the medical sector is influenced by various factors, including the surgical methods used, the patient's health status, immune response, and lifestyle. Before employing bio-composites in biomedical contexts, their compatibility is crucial [63]. This compatibility assesses the fiber's chemical, biological, and physical appropriateness. For implants, bio-composites need to maintain ideal stiffness under the highest load at the implant-tissue boundary [64]. Bio-fibers have been utilized in various biomedical applications, with pineapple leaf fiber proving versatile for drug delivery, medical implants, and tissue engineering [65, 66]. Nano-composites based on pineapple leaf fibers are employed in cardiovascular implants, joint cartilage, catheters, prostheses, tissue engineering scaffolds, and artificial skin [67]. Additionally, bio-fiber composites are alternatives for vascular grafts, pacemakers, biosensors, and more.

1.5.3. Environmental and economic impact of biocomposites

Globally, there is a growing emphasis on eco-friendly manufacturing and recycling to counteract the environmental damage caused by non-renewable materials, leading to stricter regulations. Consequently, researchers are turning their attention to the sustainable production of biocomposites (BCs). Plant fibers are integral to the life cycle of BCs, and employing life cycle assessment (LCA) is crucial for managing their end-of-life treatments [68]. In 2016, the European Union produced approximately 55 million tons of waste from plant-based forests and agriculture [69], which holds great potential for conversion into bio-based plastics, organic fertilizers, and food products. The production of natural fibers, requiring only 9.55 MJ/kg, is far more energy-efficient than that of synthetic materials like glass, which requires 54.7 MJ/kg [70]. BCs are considered environmentally friendlier than conventional petroleum-based plastics throughout their lifecycle, from fiber extraction to disposal. However, using solely bio-based materials may not always be economically feasible. A blend of natural and synthetic materials can be a more cost-effective solution for producing affordable products [71]. In 2014, the bioplastics market was valued at $3.94 billion [72]. Plastic production soared to 300 million tons in 2013, a 200-fold increase since 1950, and is projected to multiply further in the coming century [73]. By the end of this century, it's estimated that oil production might need to reach around 93 million barrels per day. Natural fibers have also significantly contributed to job creation and market growth.

1.6. Conclusion

The exploration of the tribology of polymers filled with biodegradable fillers highlights significant advancements and ongoing challenges in this field. Polymers offer unique advantages for tribological applications, such as their viscoelastic properties and low friction coefficients. However, their performance is notably influenced by factors like surface roughness, temperature, and the nature of fillers used. Biodegradable fillers, derived from plant, animal, and mineral sources, enhance the mechanical properties of polymers while maintaining their environmental sustainability. The successful integration of these fillers can lead to improved wear resistance and reduced friction, making them suitable for various applications, including automotive and aerospace components. Despite the benefits, the complexity of polymer tribology necessitates further research to fully understand the mechanisms of friction and wear, particularly under varying operational conditions. Continued innovation in processing techniques and filler treatments will be crucial for optimizing the performance of biodegradable polymer composites. As the demand for sustainable materials increases, the study of these composites will play an essential role in advancing both tribological performance and environmental responsibility.

References

[1] Jost, H.P., 1966. Lubrication (Tribology) - a Report on the Present Position and Industry's Needs. Department of Education and Science, H.M. Stationary Office, London, UK.

[2] Holmberg, K. and Erdemir, A., 2017. Influence of tribology on global energy consumption, costs and emissions. Friction, 5, pp.263-284.

[3] Hutchings, Ian, and Philip Shipway. Tribology: friction and wear of engineering materials. Butterworth-heinemann, 2017.

[4] Steiner, P.A. and Sandor, R., 1991. Polybenzimidazole prepreg: improved elevated temperature properties with autoclave processability. High Perform. Polym., 3, pp.139-150.

[5] Shooter, K.V. and Thomas, O.H., 1949. Research, 2, p.533.

[6] Archard, J.F., 1980. Wear theory and mechanisms. In: Wear Control Handbook. ASME, New York.

[7] El-Tayeb, N.S.M. and Mostafa, I.M., 1996. The effect of laminate orientations on friction and wear mechanisms of glass reinforced polyester composite. Wear, 195, pp.186-191.

[8] Watanabe, M., 1968. The friction and wear properties of nylon. Wear, 11, pp.379-388.

[9] Pihtili, H. & Tosun, N., 2002. Investigation of the wear behavior of a glass fiber-reinforced composite and plain polyester resin. Composites Science and Technology, 62, pp. 367-370.

[10] Santner, E. & Czichos, H., 1989. Tribology of polymers. Tribology International, 22, pp. 103-109.

[11] Stuart, B.H., Tribological studies of poly(ether ether ketone) blends. Tribology International.

[12] Mimaroglu, A., Unal, H. & Arda, T., 2007. Friction and wear performance of pure and glass fiber reinforced Poly-Ether-Imide on polymer and steel counterface materials. Wear, 262, pp. 1407-1413.

[13] Ilyas, R.A., Sapuan, S.M., Asyraf, M.R.M., Atikah, M.S.N., Ibrahim, R., Dele-Afolabi, T.T. & Hazrol, M.D., 2020. Introduction to Biofiller-Reinforced Degradable Polymer Composites. In: Biofiller-Reinforced Biodegradable Polymer Composites. 1st ed. CRC Press, pp. 1-23. eBook ISBN: 9780429322112.

[14] Gurunathan, T., Mohanty, S. & Nayak, S.K., 2015. A review of the recent developments in biocomposites based on natural fibres and their application perspectives. Composites Part A: Applied Science and Manufacturing, 77, pp. 1-25.

[15] Müssig, D.-I.J., Fischer, H., Graupner, N. & Drieling, A., 2010. Testing Methods for Measuring Physical and Mechanical Fibre Properties (Plant and Animal Fibres). In: Industrial

Applications of Natural Fibres: Structure, Properties, and Technical Applications. Berlin/Heidelberg: Springer, pp. 267-309.

[16] Ramamoorthy, S.K., Skrifvars, M. & Persson, A., 2015. A Review of Natural Fibers Used in Biocomposites: Plant, Animal and Regenerated Cellulose Fibers. Polymer Reviews, 55, pp. 107-162.

[17] Kock, J.W., 2006. Physical and Mechanical Properties of Chicken Feather Materials. Ph.D. Thesis, Georgia Institute of Technology, Atlanta, GA, USA.

[18] Chang, K.C., 1986. The Archaeology of Ancient China. 4th ed. New Haven, CT, USA: Yale University Press.

[19] Lucas, F., Shaw, J.T.B. & Smith, S.G., 1995. The silk fibroins. In: C.B. Anfinsen, ed. Advances in Protein Chemistry. London, UK: Academic Press.

[20] Engster, M.S., 1976. Studies on silk secretion in the trichoptera (F. Limnephilidae). Cell Tissue Research, 169, pp. 77-92.

[21] Feughelman, M., 1989. A note on the water-impenetrable component of α-keratin fibers. Textile Research Journal, 59, pp. 739-742.

[22] Chen, D., Tan, L., Liu, H., Hu, J., Li, Y. & Tang, F., 2009. Fabricating Superhydrophilic Wool Fabrics. Langmuir, 26, pp. 4675-4679.

[23] Idris, A., Vijayaraghavan, R., Rana, U.A., Patti, A.F. & Macfarlane, D.R., 2014. Dissolution and regeneration of wool keratin in ionic liquids. Green Chemistry, 16, pp. 2857-2864.

[24] Bouakkaz, A.O., Albedah, A., Bachir Bouiadjra, B., Khan, S.M.A., Benyahia, F. & Elmeguenni, M., 2018. Effect of temperature on the mechanical properties of polypropylene–talc composites. Journal of Thermoplastic Composite Materials, 31(7), pp. 896-912.

[25] Zolfaghari, S., Paydayesh, A. & Jafari, M., 2019. Mechanical and thermal properties of polypropylene/silica aerogel composites. Journal of Macromolecular Science, Part B, 58(2), pp. 305-316.

[26] Mazzanti, V., Malagutti, L. & Mollica, F., 2019. FDM 3D Printing of Polymers Containing Natural Fillers: A Review of their Mechanical Properties. Polymers, 11.

[27] Essabir, H., Nekhlaoui, S., Malha, M., Bensalah, M.O., Arrakhiz, F.Z., Qaiss, A. & Bouhfid, R., 2013. Bio-composites based on polypropylene reinforced with Almond Shells particles: Mechanical and thermal properties. Materials & Design, 51, pp. 225-230.

[28] Boujelben, M., Abid, M., Kharrat, M. & Dammak, M., 2021. Production and mechanical characterization of LLDPE biocomposite filled with almond shell powder. Polymers and Polymer Composites, 29(4), pp. 271-276.

[29] Ludueña, L., Vazquez, A. & Alvarez, V., 2012. Effect of lignocellulosic filler type and content on the behavior of polycaprolactone based eco-composites for packaging applications. Carbohydrate Polymers, 87(1), pp. 411-421. https://doi.org/10.1016/J.CARBPOL.2011.07.064.

[30] Agustin-Salazar, S., Ricciulli, M., Ambrogi, V., Cerruti, P. & Scarinzi, G., 2022. Thermomechanical Properties and Biodegradation Behavior of Itaconic Anhydride-Grafted PLA/Pecan Nutshell Biocomposites. Polymers, 14. https://doi.org/10.3390/polym14245532.

[31] Jan, P., Matkovič, S., Bek, M., Slemenik Perše, L. & Kalin, M., 2023. Tribological behaviour of green wood-based unrecycled and recycled polypropylene composites. Wear, 524, p. 204826.

[32] Guo, X., Yao, Y., Zhao, H., Chi, C., Zeng, F., Qian, F., Liu, Z., Huo, L. & Lv, Y., 2021. Environmental impacts of functional fillers in polylactide (PLA)-based bottles using life cycle assessment methodology. Science of the Total Environment, 788, p. 147852.

[33] Dilkes-Hoffman, L., Lane, J., Grant, T., Pratt, S., Lant, P. & Laycock, B., 2018. Environmental impact of biodegradable food packaging when considering food waste. Journal of Cleaner Production, 180, pp. 325-334. https://doi.org/10.1016/J.JCLEPRO.2018.01.169.

[34] Musioł, M., Jurczyk, S., Sobota, M., Klim, M., Sikorska, W., Zięba, M., Janeczek, H., Rydz, J., Kurcok, P., Johnston, B. & Radecka, I., 2020. (Bio)Degradable Polymeric Materials for Sustainable Future—Part 3: Degradation Studies of the PHA/Wood Flour-Based Composites and Preliminary Tests of Antimicrobial Activity. Materials, 13.

[35] Narancic, T., Verstichel, S., Chaganti, S., Morales-Gámez, L., Kenny, S., Wilde, B., Padamati, R. & O'Connor, K., 2018. Biodegradable Plastic Blends Create New Possibilities for End-of-Life Management of Plastics but They Are Not a Panacea for Plastic Pollution. Environmental Science & Technology, 52(18), pp. 10441-10452. https://doi.org/10.1021/acs.est.8b02963.

[36] Zhang, C., Wang, C., Cao, G., Wang, D. & Ho, S., 2019. A sustainable solution to plastics pollution: An eco-friendly bioplastic film production from high-salt contained Spirulina sp. residues. Journal of Hazardous Materials, p. 121773. https://doi.org/10.1016/j.jhazmat.2019.121773.

[37] Muniyasamy, S., Reddy, M.M., Misra, M. & Mohanty, A., 2013. Biodegradable green composites from bioethanol co-product and poly(butylene adipate-co-terephthalate). Industrial Crops and Products, 43, pp. 812-819. https://doi.org/10.1016/j.indcrop.2012.08.031.

[38] Anandjiwala, R.D. & Blouw, S., 2007. Composites from bast fibres-prospects and potential in the changing market environment. Journal of Natural Fibers, 4, pp. 91-109. https://doi.org/10.1300/J395v04n02_07.

[39] Ekundayo, G., 2019. Reviewing the development of natural fiber polymer composite: a case study of sisal and jute. American Journal of Mechanical and Materials Engineering, 3, p. 1. https://doi.org/10.11648/j.ajmme.20190301.11.

[40] Celebi, H. & Kurt, A., 2015. Effects of processing on the properties of chitosan/cellulose nanocrystal films. Carbohydrate Polymers, 133, pp. 284-293. https://doi.org/10.1016/j.carbpol.2015.07.007.

[41] Zhang, C.-L. & Yu, S.-H., 2016. Spraying functional fibres by electrospinning. Materials Horizons, 3, pp. 266-269. https://doi.org/10.1039/C6MH00045B.

[42] Francis, L., Venugopal, J., Prabhakaran, M.P., et al., 2010. Simultaneous electrospin–electrosprayed biocomposite nanofibrous scaffolds for bone tissue regeneration. Acta Biomaterialia, 6, pp. 4100-4109. https://doi.org/10.1016/j.actbio.2010.05.001.

[43] Drobota, M., Gradinaru, L.M., Vlad, S., et al., 2020. Preparation and characterization of electrospun collagen based composites for biomedical applications. Materials, 13, p. 3961. https://doi.org/10.3390/ma13183961.

[44] Singh, M.K., Tewari, R., Zafar, S., Mavinkere Rangappa, S. & Siengchin, S., 2023. A comprehensive review of various factors for application feasibility of natural fiber-reinforced polymer composites. Results in Materials, 17, p. 100355.

[45] Ma, Y., Liu, Y., Gao, Z., Lin, F., Yang, Y., Ye, W. & Tong, J., 2014. Effects of wool fibers on tribological behavior of friction materials. Journal of Thermoplastic Composite Materials, 27, p. 867.

[46] Oladele, I.O., Agbeboh, N.I., Omokafe, S.M. & Ibrahim, O.I., 2018. Effects of fiber fraction on the mechanical and abrasion properties of treated cow hair fiber reinforced polyester composites. Tribology in Industry, 40, pp. 254-262.

[47] Narendiranath Babu, T., Aravind, S.S., Naveen Kumar, K.S. & Sumanth Rao, M.S., 2018. Study on mechanical and tribological behaviour of Angora, kenaf and ramie hybrid reinforced epoxy composites. International Journal of Mechanical Engineering and Technology, 9, pp. 11-20.

[48] Rout, A. & Satapathy, A., 2012. Analysis of dry sliding wear behaviour of rice husk filled epoxy composites using design of experiment and ANN. Procedia Engineering, 38, pp. 1218-1232. https://doi.org/10.1016/j.proeng.2012.06.153.

[49] Debnath, K., Dhawan, V., Singh, I. & Srivatsan, T.S., 2019. Wear and frictional behaviour of composites filled with agro-based waste materials. Emerging Materials Research, 8, pp. 84-93. https://doi.org/10.1680/jemmr.18.00032.

[50] Ra, I., 2015. Effect of date palm seeds on the tribological behaviour of polyester composites under different testing conditions. Journal of Materials Science and Engineering, 4. https://doi.org/10.4172/2169-0022.1000206.

[51] Sydow, Z., Bula, K. & Gapiński, B., 2023. Friction and wear of polypropylene-based composites reinforced with cherry seed powder. Tribology International, 179, p. 108177.

[52] Sharma, H., Misra, J.P. & Singh, I., 2020. Friction and Wear behaviour of epoxy composites reinforced with food waste fillers. Composites Communications, 22, p. 100436. https://doi.org/10.1016/j.coco.2020.

[53] Kumar, S., Vedrtnam, A. & Pawar, S.J., 2019. Effect of wood dust type on mechanical properties, wear behavior, biodegradability, and resistance to natural weathering of wood-plastic composites. Frontiers of Structural and Civil Engineering, 13, pp. 1446-1462. https://doi.org/10.1007/s11709-019-0568-9.

[54] Zhou, Y., Fan, M., Chen, L. & Zhuang, J., 2015. Lignocellulosic fibre mediated rubber composites: an overview. Composites Part B: Engineering, 76, pp. 180-191. https://doi.org/10.1016/j.compositesb.2015.02.028.

[55] Güven, O., Monteiro, S.N., Moura, E.A.B. & Drelich, J.W., 2016. Re-emerging field of lignocellulosic fiber – polymer composites and ionizing radiation technology in their formulation. Polymer Reviews, 56, pp. 702-736. https://doi.org/10.1080/15583724.2016.1176037.

[56] Ibrahim, M.A., Hirayama, T. & Khalafallah, D., 2019. An investigation into the tribological properties of wood flour reinforced polypropylene composites. Materials Research Express, 7(1), p. 015313.

[57] Palanikumar, K., Thiagarajan, R. & Latha, B., 2022. Bio-Fiber Reinforced Composite Materials. Springer.

[58] Vinayagamoorthy, R., 2020. Influence of fibre pretreatments on characteristics of green fabric materials. Polymers and Polymer Composites. https://doi.org/10.1177/0967391120943461.

[59] Thiruchitrambalam, M., Alavudeen, A. & Venkateshwaran, N., 2012. Review on kenaf fiber composites. Review on Advanced Material Science, 32, pp. 106-112.

[60] Gupta, G., Kumar, A. & Tyagi, R., 2016. Application and Future of Composite Materials: A Review. International Journal of Innovative Research in Science, Engineering and Technology, 5, pp. 6907-6911.

[61] Szolnoki, B., Bocz, K., Soti, P.L., Bodzay, B., Zimonyi, E., Toldy, A., Morlin, B., Bujnowicz, K., Władyka-Przybylak, M. & Marosi, G., 2015. Development of natural fibre

reinforced flame retarded epoxy resin composites. Polymer Degradation and Stability, 119, pp. 68-76.

[62] Alexander, J. & Churchill, S.J.E., 2017. Mechanical characterization of basalt based natural hybrid composites for aerospace applications. IOP Conference Series: Materials Science and Engineering, 197(012008), pp. 1-8.

[63] Xia, C., Wang, K., Dong, Y., Zhang, S., Shi, S.Q., Cai, L., Ren, H., Zhang, H. & Li, J., 2016. Dual-functional natural-fiber reinforced composites by incorporating magnetite. Composites Part B: Engineering, 93, pp. 221-.

[64] Ramakrishna, S., Mayer, J., Wintermantel, E. & Leong, K.W., 2001. Biomedical applications of polymer-composite materials: A review. Composite Science and Technology, 61, pp. 1189-1224.

[65] Cherian, B., Leao, A., Souza, D., Thomas, S. & Pothan, L., 2010. Isolation of nanocellulose from pineapple leaf fibres by steam explosion. Carbohydrate Polymers, 81, pp. 720-725.

[66] Vinayagamoorthy, R., 2017. Parametric optimization studies on drilling of sandwich composites using the Box-Behnken design. Materials and Manufacturing Processes, 32, p. 645.

[67] Giri, J. & Adhikari, R., 2013. A brief review on extraction of nanocellulose and its applications. Nepal Journals Online, 9, pp. 81-87.

[68] Sommerhuber, P.F., et al., 2017. Life cycle assessment of wood-plastic composites: analysing alternative materials and identifying an environmental sound end-of-life option. Resources, Conservation and Recycling, 117, pp. 235-248.

[69] Ferri, M., et al., 2020. From winery waste to bioactive compounds and new polymeric biocomposites: a contribution to the circular economy concept. Journal of Advanced Research, 24, pp. 1-11.

[70] Joshi, S.V., et al., 2004. Are natural fiber composites environmentally superior to glass fiber reinforced composites? Composites Part A: Applied Science and Manufacturing, 35(3), pp. 371-376.

[71] John, M.J. & Thomas, S., 2008. Biofibres and biocomposites. Carbohydrate Polymers, 71(3), p. 343.

[72] AL-Oqla, F.M. & Omari, M.A., 2017. Sustainable biocomposites: challenges, potential and barriers for development. In: Green biocomposites. Berlin: Springer, pp. 13-29.

[73] Europe, P., 2015. An analysis of European plastics production, demand and waste data. Plastics-the facts.

Chapter 2: Experimental procedure for Polypropylene composites testing

2.1. Introduction

This chapter presents a comprehensive experimental procedure for characterizing two types of composite materials: PP-talc composites and PP-ASF biocomposites. For the PP-talc composites, the focus is on the microscratch test under the temperature effect and reciprocating sliding tests conducted to evaluate the coefficient of friction COF and wear rate W_r under various test conditions, such as normal load and different talc contents, number of cycles. Talc with an average particle size of 1 μm was added to the PP matrix at contents of 5%, 10%, and 50 wt.%. For studding the temperature effect on the PP-talc microscratch, a lab-made heating device was developed, tested and validated. The microscratch test was carried out under possible environmental temperature, four normal loads, the COF was evaluated. The reciprocating sliding tests were conducted on the PP-talc composite specimens using a steel slider under dry conditions at room temperature. The test conditions were: sliding speed of 30 mm/s, normal load of 10 N, and sliding distance of 15 mm per cycle. The coefficient of friction and wear rate were evaluated at 5,000, 10,000, and 15,000 cycles to study the tribological performance under different stages of the test. This information is essential for understanding the tribological performance of these materials and their potential applications. The second part of the study explores the preparation and characterization of PP-ASF biocomposites. Almond shells fillers were harvested from Ain Defla, Algeria, dried and grinded then characterized for filling PP for preparing PP-ASF biocomposites material. The ASF morphology and normal size distribution were examined, then a thermogravimetric analysis TGA was carried out for determining the biocomposite heating preparation cycles. The PP-ASF biocomposite was fabricated using two ASF size ranges, diameter 1 (D1) and diameter 2 (D2) of 600 μm ≤ D1 ≤ 900 μm and 400 μm ≤ D2 ≤ 600 μm. 0, 5, 10 and 15 weight proportions was used for each ASF size. The PP ASF biocomposite was well fabricated and their mechanical properties represented by Tensile test and Shore D hardness and the tribological properties were analyzed.

2.2. Polypropylene-Talc composite: Tribological caracterization methods

2.2.1. PP-Talc composite material

The used PP is Adstif HA840 R grade PP, a high-stiffness, high-gloss homo-polymer that is developed mainly for use in stiff molding injection. No nucleating agent was added to this PP. The following parameters are its principal physical characteristics: Density of 0.9 g/cm^3; melt flow rate (230°C/2.169 kg): 20 g/10 min. The Vicat softening temperature of neat PP is around

158 °C. The injection molding was used for the elaboration of the composite by a Romer injection machine. The used talc was of the chemical formula $Mg_3Si_4O_{10}(OH)_2$ and was ~1 µm in size that was added in different contents: 5, 10, and 50 wt.% with a fine powder obtained from the original talc powder (Figure 2.1). The talc has a density of 2.78 g/cm^3, and the sedimentation analyses displayed an average particle size of 1 µm [1].

Figure 2.1. PP-talc specimens.

2.2.2. Tribological test

2.2.2.1. Scratch test under temperature effect

The microscratch installation (Figure 2.2) comprises two stepper motors: one for vertical tip displacement and another for horizontal specimen displacement. During the scratching test, the installation records normal and tangential loads. To investigate the effect of temperature on the composite microscratch behavior, a heating device was integrated into the microscratch setup (Figure 2.2).

The heating device was designed for the following tasks:

- Fix four specimens movements simultaneously; their dimension was 3x11x110 mm.
- Heat, fix and controlling the four specimen's temperature in the range of 20°C to 100°C.

For those issues, the following solutions were chosen:

- A mechanism capable of simultaneously fixing four specimens it was developed.
- For the power alimentation, we opted for a laboratory power supply.
- For controlling and fixing the temperature, W1209 module was chosen; this device can control and fix the temperature.

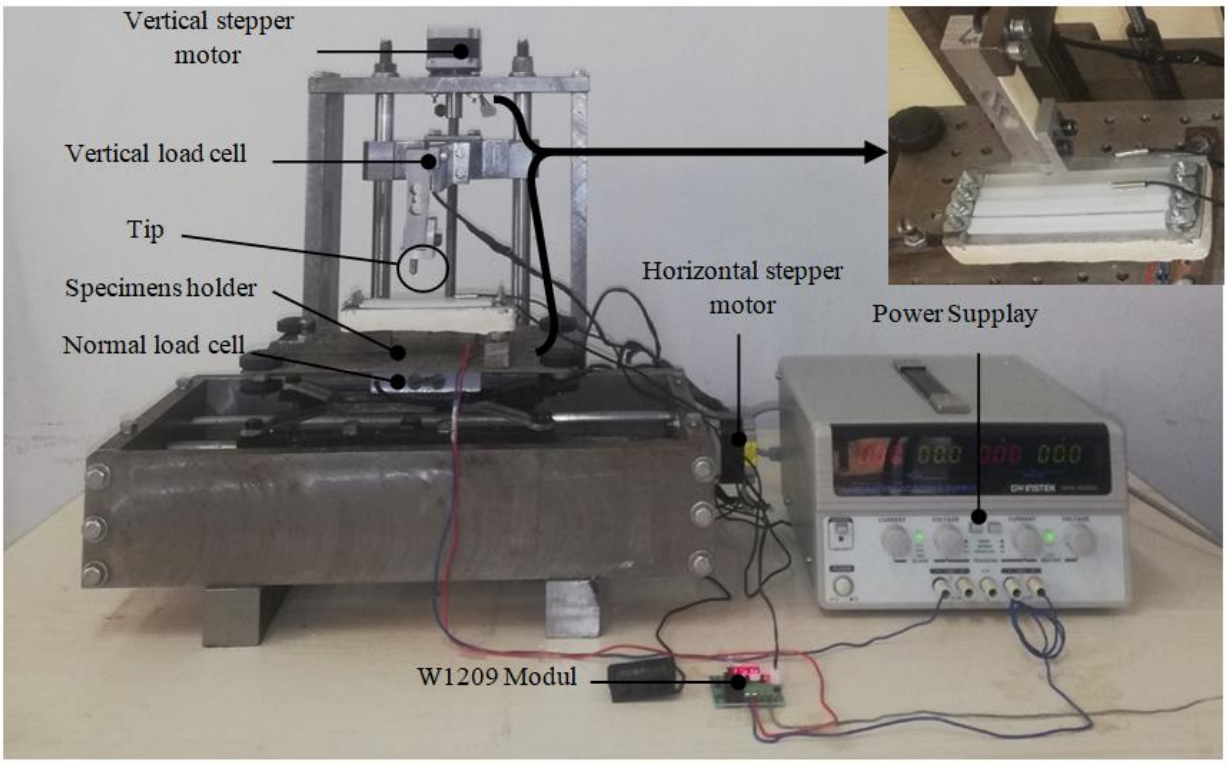

Figure 2.2. The microscratch installation with the heating device.

Hot plate design

The heating device that was made consists of an aluminum sheet, screws, nuts, rectangular rings, thermal electric resistance, body, Adhesive material, temperature sensor, and their dimensions as presented in figure 2.3.

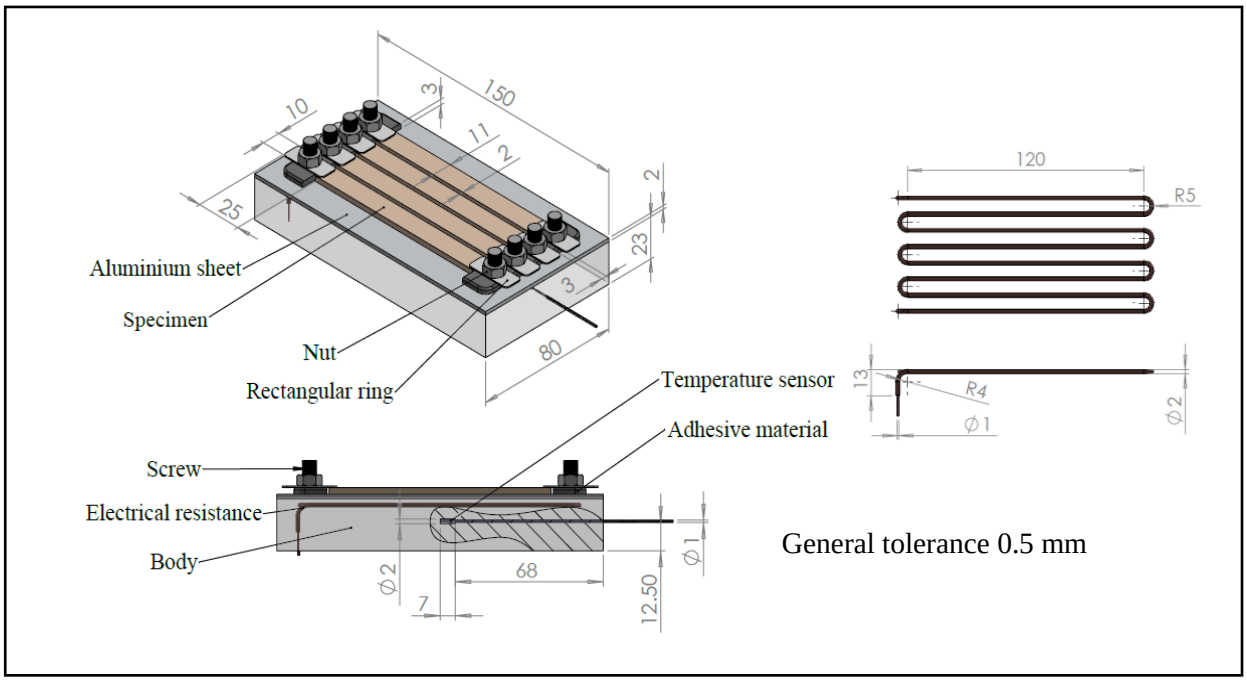

Figure 2.3. Schematic and dimensions of the heating device and its components.

The experimental setup consists of a hot plate, thermally energized by an electrical resistor. This process occur with the Joule effect, wherein electric current passing through a conductor generates heat. Consequently, the hot plate's temperature rises. Despite maintaining constant current and voltage, the temperature exhibits gradual escalation over time. To achieve temperature stability, W1209 thermostat module was employed for regulation. The temperature evolution can be divided into two distinct phases: transient and steady-state, as illustrated in figure 2.4. During the transient phase, the temperature ascends from ambient to the pre-set value determined by the thermostat. Subsequently, the steady-state phase ensues, characterized by ostensibly stabilized temperature. However, some fluctuation persists due to the thermostat's operational mechanism. It intermittently interrupts the power to the resistor upon reaching the target temperature, leading to initial overshoot before settling-a phenomenon constituting the control error.

Additionally, the assembly incorporates a fastening mechanism comprising four screws secured with a heat-resistant adhesive material (Epoxy Resin AB Hard Glue Epoxy Steel Glue). This adhesive withstands temperatures ranging from -60 °C to 230 °C and possesses a tensile shear strength of at least 16 MPa. These screws are strategically positioned on either side of the aluminum sheet (as shown in Figs 2 and 3). Finally, the specimens are affixed using a rectangular ring, tightened by nuts on each side.

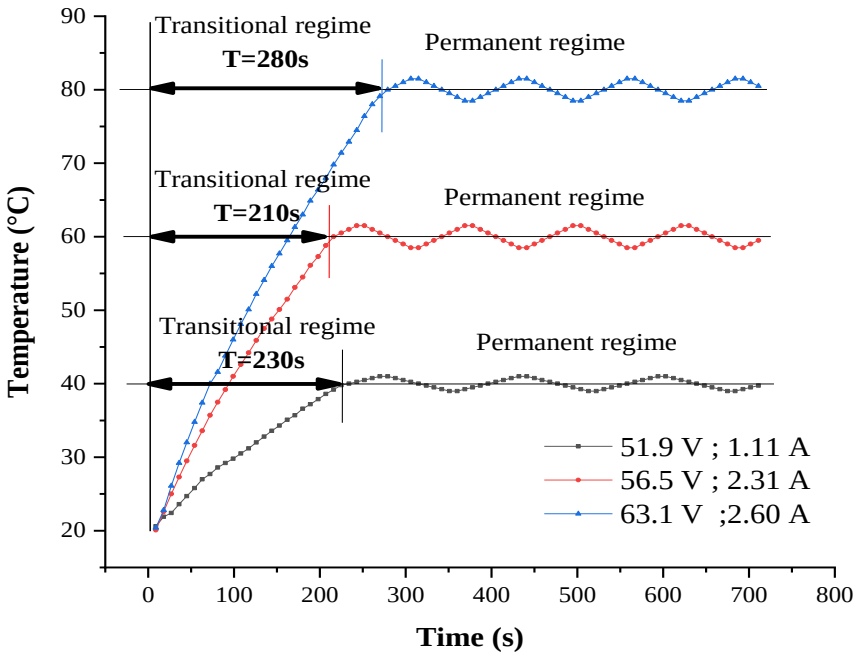

Figure 2.4. Heat temperature rise vs. time.

Control circuit

The control circuit equipped with a laboratory power Supply, GW INSTEK GPS-2303, that can generate the electrical current, it has two chains, CH1 and CH2, that can be used in series or in parallel, the maximum amperage and voltage is 3A and 32V for each chain (Figure 2.5). The circuit equipped also with module W1209, which controls and fixes the temperature, which is the approach utilized here. The W1209 is a thermostat controller with a lot of features. Various characteristics, such as on and off trigger temperatures, may be configured using three tactile switches. The on board relay is capable of switching up to 240V AC at 5A or 14V DC at 10A. A three-digit seven-segment display shows the current temperature in degrees Celsius, and an on board LED shows the current relay condition. The direct electrical current starting from the power supply and passing the hot plate via the thermal resistance that heat, then passing the W1209 module, finely for making a closed circuit the current return to the power supply from the W1209 module, the temperature sensor that situates inside the body of the hot plate is connecting to the Module

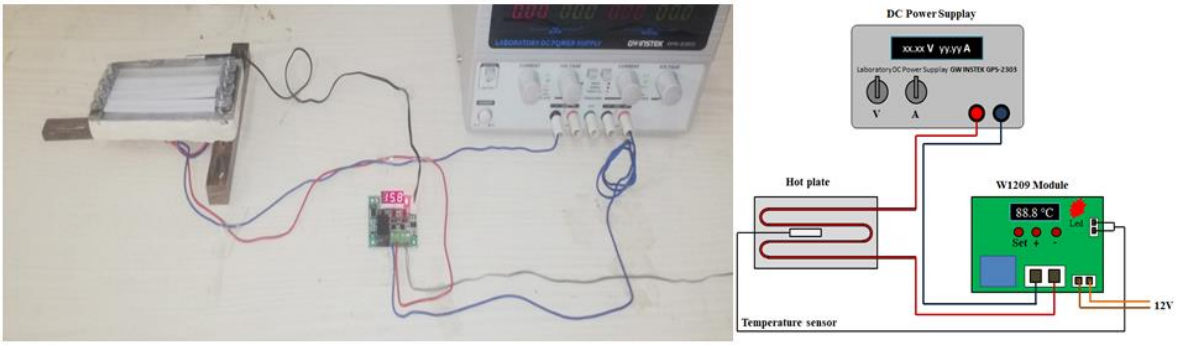

Figure 2.5. Control circuit and its schema.

Heat device testing for validation

Firstly, the W1209 module must be programmed by the following steps:

- **Setting the cooling or heating parameter P0:** The parameter P0 has two settings, C (Could) and H (Heat).
- **Setting the hysteresis parameter P1:** This sets how much change in temperature must occur before the relay will change state. For example if set to the default 2 °C and the trigger temperature has been set to 25 °C, it will not denergise until the temperature falls back below 23 °C. Setting this hysteresis helps stop the thermostat from continually triggering when the temperature drifts around the trip temperature.

- **Setting the upper limit of the thermostat parameter P2:** This parameter limits the maximum trigger temperature that can be set. It can be used as a safety to stop an excessively high trigger temperature from accidentally being set by the user.
- **Setting the lower limit of the thermostat parameter P3:** This parameter limits the minimum trigger temperature that can be set. It can be used as a safety to stop an excessively low trigger temperature from accidentally being set by the user.
- **Setting temperature offset correction parameter P4:** Should you find there is a difference between the displayed temperature and the actual temperature (for instance if the temperature probe is on a long run of cable).
- **Setting the trigger delay parameter P5:** This parameter allows for delaying switching of the relay when the trigger temperature has be reached. The parameter can be set in one minute increments up to a maximum of 10 minutes.
- **Setting the high temperature alarm parameter P6:** Setting a value for this parameter will cause the relay to switch off when the temperature reaches this setting. The seven segment display will also show '---' to indicate an alarm condition. The relay will not re-energise until the temperature falls below this value. The default setting is OFF.

After complete programming the W1209 module, now the power supply can be turned on, than the hot plate was ready to use. The temperature rise of this hot plate has been experimented under three values for the two electrical parameters are obtained and summarized in the table 1 as:

Table 2.1. Electrical parameters used for the temperature stability study.

Required temperature (°C)	40			60			80		
Domains	1	2	3	1	2	3	1	2	3
Tension (Volts)	31.6	32.8	40.7	41.7	46.7	51.3	56.3	63.1	67
Current (Amperes)	0.64	1.13	1.74	1.7	1.91	2.1	2.3	2.57	3.7

Device characteristics analysis

The Figure 2.6 presents the test of rate heat temperature vs. time for three different temperatures, this test was performed by choosing three different temperatures, 40, 60 and 80 °C, for each set temperature, it was choosing special values of voltage and amperage, (51.9 V ; 1.11 A for 40 °C, 56.5 V ; 2.31 A for 60 °C and 63.1 V ; 2.60 A), to analyses the rate of temperature. Each curve has two regimes, transitional (Figure 2.4) and permanent regime, the transitional regime show

the rise of the heat plate temperature, the other regime show the stability of its temperature, the high values of voltage and amperage shown the fast rise of temperature (63.1 V; 2.60 A), where the temperature reaches 80 °C (Figure 2.4), it takes 280 s (about 4 min and 40 s), and the low voltage and amperage shown a slow rise of the temperature (51.9 A ; 1.11 A), where the temperature reaches 40 °C, it takes 230 s (about 3 min and 50 s). Then for the hot plate temperature goes faster it was recommended to use high voltage and high current.

During this test the thermostat rely was make the circuit over when the temperature rich the set temperature, and make it closed when it was inferior, in order to the temperature reach the set temperature, the set temperatures were 40, 60 and 80 °C, each temperature were used for its stability analyses three different values of voltage and amperage. For each case, the high values of voltage and amperage shown the largest range and the more number of temperature cycles, the low voltage, and amperage shown smallest range and the low number of temperature, for example, in b case, the large range of temperature is (-0.5, -0.28 °C) for the high voltage and amperage used, the smallest range is (-0.13, 0.5 °C) for the low voltage and amperage, also in a domain of 160s, the high voltage and current (51.3 V, 2.3 A) correspondent of the high value of temperature cycles (four cycles) and the low values of the voltage and current (41.7 V, 1.7 A) correspondent to the small number of temperature cycles (3.5 cycles), the same for the other cases a and c.

So, for using this hot plate, it was recommended to use relatively small values of voltage and amperage in the used ranges, because it was correspondent to low rang and cycles of temperatures, also for the life of the W1209 that its life related to the number of cycles.

To analyze the temperature stability, the error must be calculated. Were taken the mean of the high and the low temperature values for each voltage and amperage used for each set temperature at an interval of 150 S for T= 40 °C, 150 s for T=60 °C and 170 s for T=80 °C, the relative error ($\Delta T/T$) where it is equal the variation in temperature divided by the set temperature and the variation equal the high temperature minus the lower temperature values, there is also the percentage error, that is equal ($\Delta T/T$) multiple by 100, the relative error mean every 1°C has an error with the relative error, but the percentage error mean that the measured temperature has an error in the form of a percentage. The calculated temperature errors ($\Delta T/T$) are shown in the table 2.

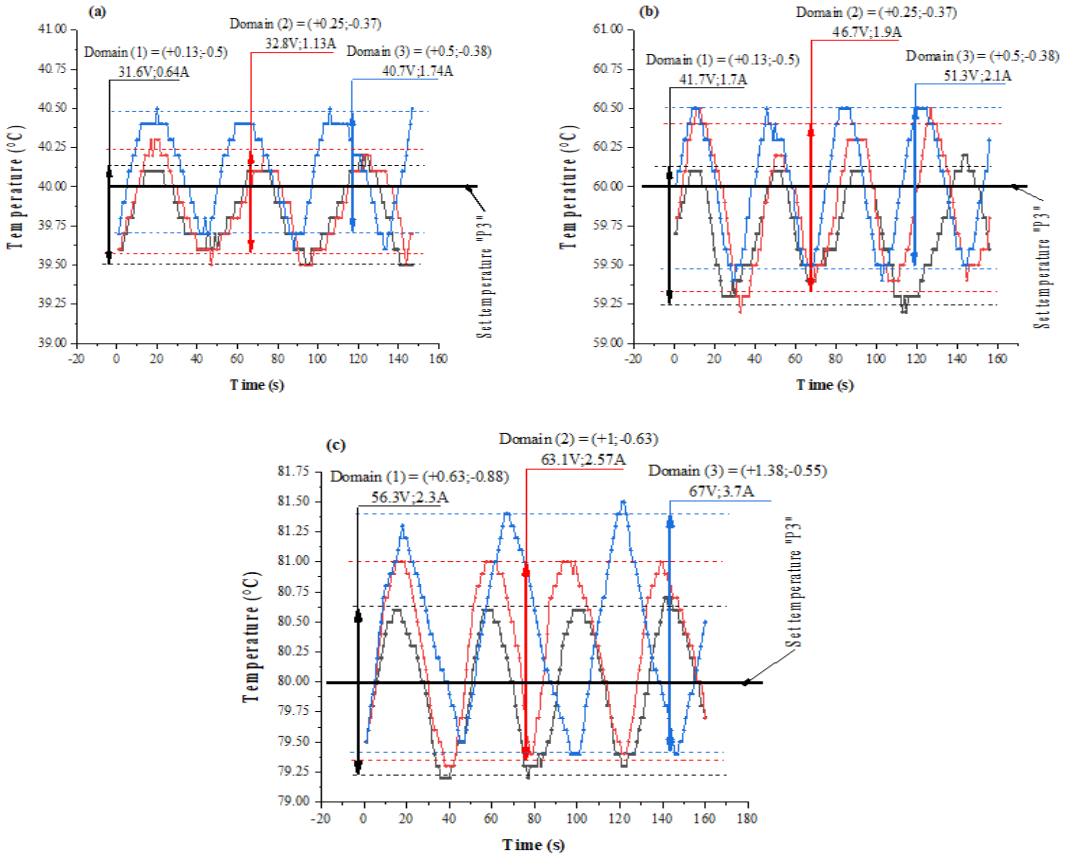

Figure 2.6. Temperature stability vs. Time at: (a) 40, (b) 60 and (c) 80 °C.

Table 2.2. Temperature errors ΔT/T in %.

	Heating temperature (°C)		
Domain	40	60	80
1	1.6 ±	1.05 ±	1.9 ±
2	1.5 ±	1.03 ±	2.04 ±
3	2.2 ±	1.5 ±	2.4 ±

The higher error value was observed at the 3^{ed} domain for T=80 °C, this is due to the high voltage and amperage values used where V=67 V and A=3.7 A, that was high values, and the low error value was observed at 2nd domain for T=60 °C, the temperature error was not related to the set temperature, but it was related to the voltage and amperage values, where the errors at T=40 °C are high then the errors at T=60 °C, then there is a proportionality between the error values and the voltage and amperage values used, where the error was high if there is great difference between the upper and the lower temperature values, for example at the 3rd domain for T=80 °C the error was 2.4 % and at the 1st domain for T=40 °C the error was 1.6 %, this mean the hot plate cannot balance between the set temperature and the ready temperature, either the voltage

and amperage cannot guarantee the needed power to the hot plate, then the hot plate lose power easily and it must has more time to get the set temperature, then the big hot plate temperatures range is inferior then the set temperature, or the power generated by the voltage and the amperage it is higher then what the hot plate needed, then the higher hot plate temperatures range are superior then the set temperature. The hot plate at this test show high performance, and the high error value was 2.4 %, this value is considered an acceptable value, and then the other values are also acceptable.

Figure 2.7 shown the measured tangential force and normal load vs. sliding distance at different temperatures of composite specimen, this test was performed by making microscratches by the microscratch installation on PP talc specimen heated by the heat plate. This scratch tests were carried out under ambient conditions (T≈20 °C) and using the hot plate at a temperature of 40 °C and 60 °C on a PP polymer, by imposed normal loads, the first is F_n= 10 N, the second is F_n=15N.

The components of the hot plate were designed, assembled, and programmed. The heating rate and the stability of the temperature was tested, The fixing specimens system showed good practicality, Scratch tests were also performed on PP talc specimens using the hot plate by fixing the temperature on 40 °C, 60 °C and 80 °C. The results showed a short time for its temperature to rise and showed an acceptable errors of its temperature stability, the hot plate need about 4 min and 40 s to its temperature reaches 80 °C, it takes 280 s, the high error value is 2.4 %. Now the incorporating hot plate is ready to use in the microscratch.

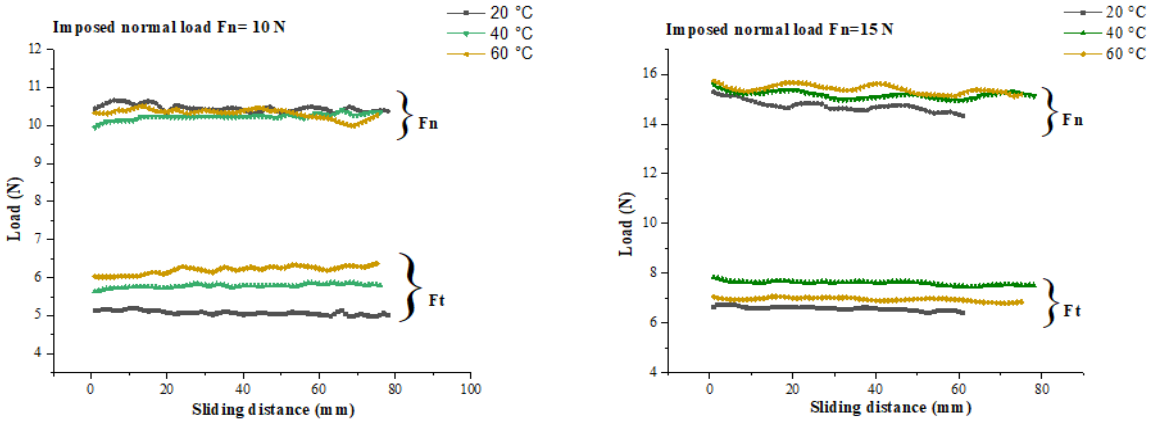

Figure 2.7. Tangential and normal loads vs. sliding distance at different temperatures for imposed normal load 10 N and 15 N.

2.2.2.2. Microscratch test

The four specimens with different talc proportions: 5, 10, 40, and 50 % were tested under microscratch sliding with a conical diamond indenter angle at the top θ = 120° with a spherical radius of 200 µm (Figure 2.8).

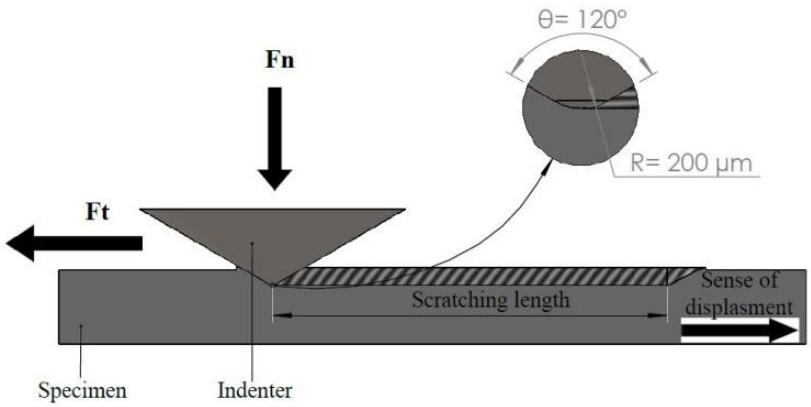

Figure 2.8. Scheme of the indenter-specimen contact geometry in microscratch test.

The tests are carried out at 8 mm/min steady speed. The used microscratch installation has a controlled temperature heating plate that simultaneously fixes and heats the tested specimens. This plate is connected to the electrical current using a laboratory power supply (GPS-2303 GW INSTEK). The W1209 module is used to command and control the temperature of both heater and used specimen. During the scratch test, the installation measures also the tangential F_t and normal F_n forces (Figure 2.2).

Normal loads F_n of 2, 5, 10, and 15 N were applied. This allows for scratching to occur not only in the hemispherical zone but also in the conical region of the indenter; moreover, the temperatures used were 20, 35, 50, and 65 °C. This allows the temperature influence on the microscratch qualities of the studied PP to be investigated. Because of the strong relationship between mechanical qualities and temperature, the temperature range chosen is 20°C to 65°C. During the scratch test, the apparent friction coefficient is defined as the observed tangential force F_t divided by the measured normal force F_n. A conventional analysis of the plowing phenomenon decomposed the friction force into two components: adhesive, μ_a, and plowing, μ_l components. Therefore the COF can be written as [2]:

$$COF=F_t/F_n = \mu_a + \mu_l \quad \text{(Eq 2.1)}$$

2.2.2.3. Reciprocating sliding test

The reciprocating sliding test was carried out on the PP-talc specimens of size 10 x 3 x 110 mm via a reciprocating tribometer (Figure 2.9) in dry and at room temperature (20 ± 2 °C) conditions. The slider has a spherical pin-shape of high-wear-resistant steel of grade 100Cr6 with a diameter of 10 mm. The slider material was chosen due to its high hardeness compared to the PP-talc specimens, inorder to ensor that the wear is caused only on the specimens and to reduce the temperature effect on the slider. The test conditions are a relativelly soft PP-talc specimen under a rigid and thermally stable indenter without any caused wear of its contact surface.

The sliding tests were conducted under speed, load, and sliding distance of 30 mm/s, 10 N, and 15 mm, respectively. One cycle is defined by two successive movements forward and backward on the tribometer table. The COF evolution was determined for all tested specimens until 15000 cycles. In addition, the tribological parameters COF and W_r were also determined at three levels: low, medium, and high number of cycles: 5000, 10000, and 15000, respectively. These numbers are chosen to guarantee that the tests were carried out under steady-state circumstances for each number of time cycles and that the test was in low, medium, and high number of cycles.

The chosen load (10 N) produces a mean contact pressure, calculated as a function of contact pressure, of 34.42 MPa, which is superior to all specimens' yield stress obtained by Bouakkaz et al. with the same material [1]. Each test was conducted three times with different specimens and for all talc proportions. The results were presented using the mean value and one standard deviation. As it is known, the Coulomb law of friction coefficient COF [3] during sliding is the ratio of the tangential load (F_t) to the normal load (F_n) as in equation (2.1).

The COF was calculated using equation1. Only the tangential force (F_t) was measured via the tribometer.

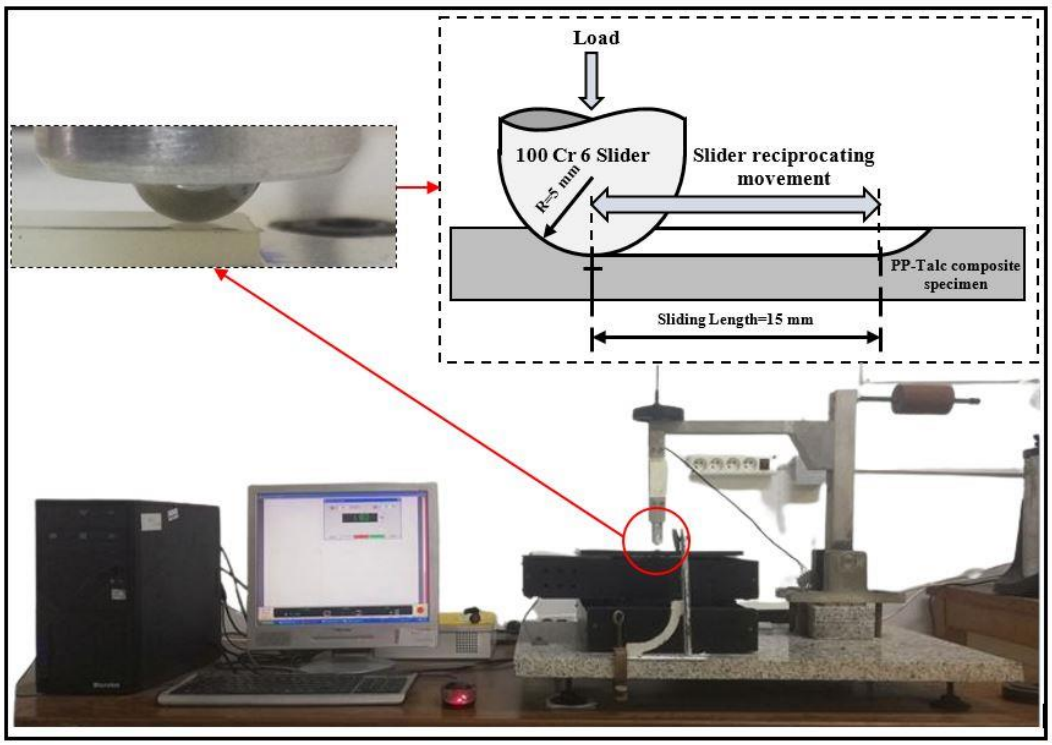

Figure 2.9. Reciprocating sliding tester and slider-specimen contact details.

2.2.2.4. Wear measurement

The wear rate, W_r, was obtained by measuring the wear track profile via the Taylor-Hobson Surtronic S series Profilometer. The measured track profile was used in the loss volume (V_m) determination using equation (2.2). The wear track profile and its standard deviation are calculated as a function of five values obtained by measuring five different positions. The wear rate can be obtained with equation (2.3) according to Archard's wear relation [4]:

$$V_m = S_m * D \quad \text{(Eq 2.2)}$$

$$W_r = \frac{V_m}{F_n.L} \quad \text{(Eq 2.3)}$$

Where: V_m is the measured loss volume, S_m, is the surface area of the measured wear track profile (Figure 2.10), D is the length of one sliding cycle fixed to 15 mm, F_n is the applied normal load, and L is the total sliding distance.

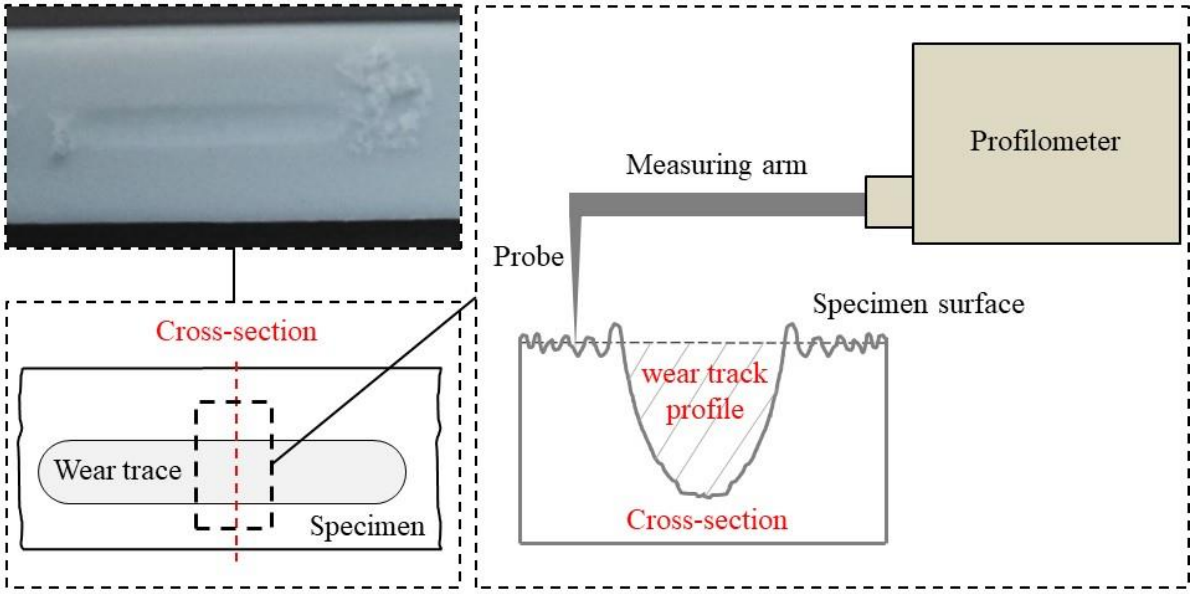

Figure 2.10. Wear track profile measurement.

2.2.2.3. Worn surfaces examination

The worn surfaces were initially coated with a gold layer by using a vacuum sputter chamber (Figure 2.11-a) and then analyzed via Q250 EDX Thermo Fisher Scanning Electron Microscopy (SEM) shown in figure 2.11-b.

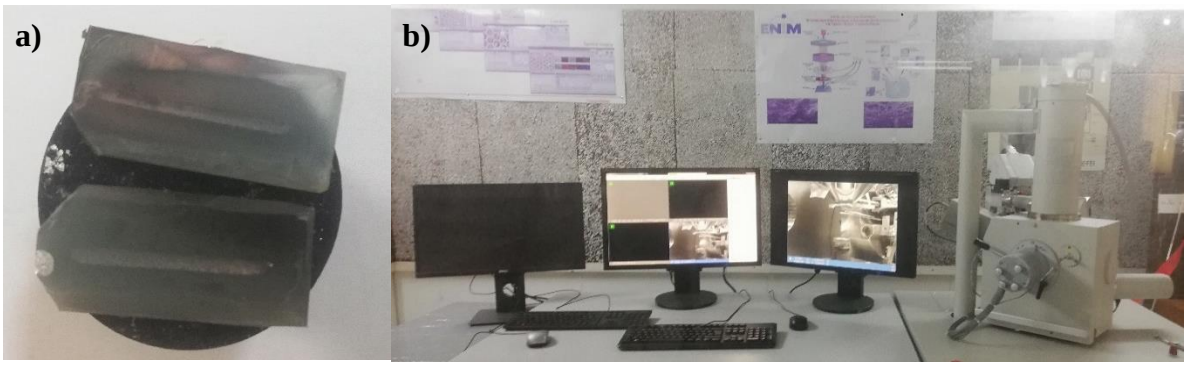

Figure 2.11. a) PP talc specimens coated with a gold layer and b) Q250 EDX Thermo Fisher Scanning Electron Microscopy (SEM).

2.3. Polypropylene-Almond Shells Particles: Biocomposite preparation

2.3.1. Matrix materials and Almond shells collection

Polypropylene (PP) homopolymer (HE125MO), Borealis Polymere, Burghausen, Germany. Which has a good flow, high stiffness and particularly used for high-speed injection. This PP has utilized as a matrix polymer for the biocomposites preparation by pressing and injection molding

techniques. The important characteristics of this polymer are density of 905 kg/m³, melt flow rate is 12 g/10 min at 230 °C under pressure of 2.16 kg, Young modulus of 1550 MPa and flexural modulus of 1350 MPa.

The used almond shells were extracted from almond fruits harvested in Ain Defla zone, Algeria (Figure 2.12-a)) during summer season, 2023. In its initial state, it contains soft outer and hard inner shell. The inner shell is distinguished by their solidity and integrity of their shape from cracks and openings during harvesting.

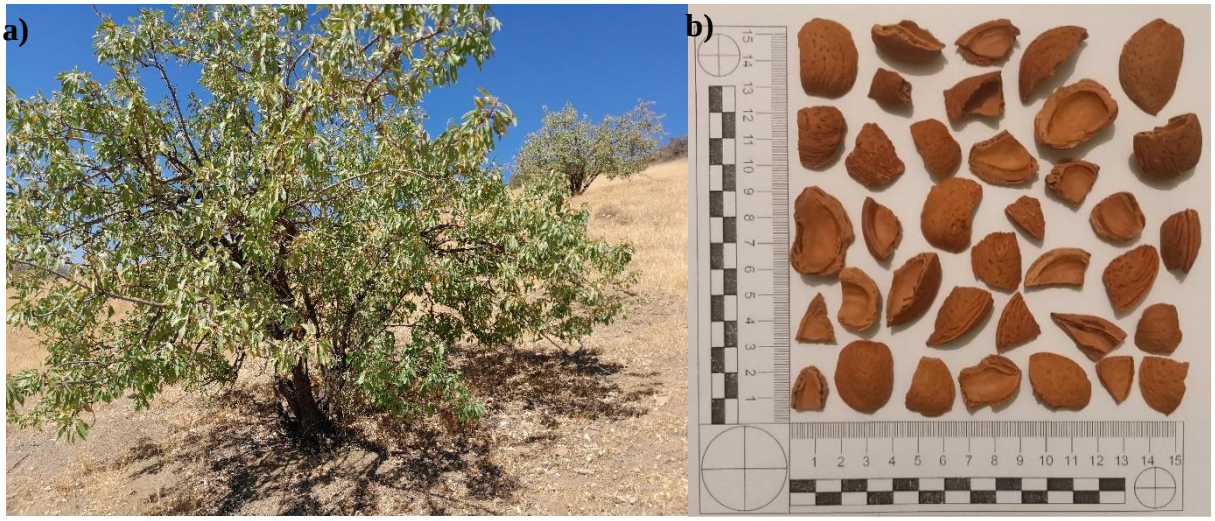

Figure 2.12. a) Almond tree (2023 summer season, Ain Defla zone, Algeria), b) Almond shells.

2.3.2. PP-Almond shells fillers biocomposite elaboration

Almond shell (Figure 2.12-b)) are harvested when the outer soft shell has fallen off. Only the hard inner shell were used. After that, the drying process was carried out by two steps. The first step was naturally under the sun (during the day) for 15 days in summer season when the average temperature in harvest zone is generally between 42 to 46 °C and low humidity. Thereafter, the residual moisture is removed by draying in Memmert (UN75pa), Memmert, Nuremberg, Germany, air circulating oven at 80°C for 4 hours before grinding for 5 min at a rotation speed of 7000 rpm. Resulting Almond shells fillers (ASF) passed with a sieve grade allowing two fillers size ranges, D1 and D2 of 600 µm ≤ D1 ≤ 900 µm and 400 µm ≤ D2 ≤ 600 µm. Thermogravimetric analysis was carried out on the almond shell fillers. The temperature of thermal degradation was obtained for determining the preparation heating cycles.

2.3.2.1. Almond shells fillers preparation

ASF morphology and normal size distribution

ASF morphology and particles size distribution were statistically determined by normal distribution using images obtained via SEM (JCM 6000 SEM) microscopy. Average number of 110 measurements were taken for each particle sizes ranges. Figure 2.13 shows the morphology of D1 and D2 particles ranges. It shows an agglomeration of the two ASF particles ranges, where it shows an irregular shape and define with flat surfaces. This is the result of the process of grinding the almond shells, which are characterized by their hardness, a similar observation was previously reported for almond shells collected from Spain [5]. A close observation on the ASF. Its surface appears like rod with pores, which makes the surfaces rough. The same morphology was reported in previous studies [6, 7].

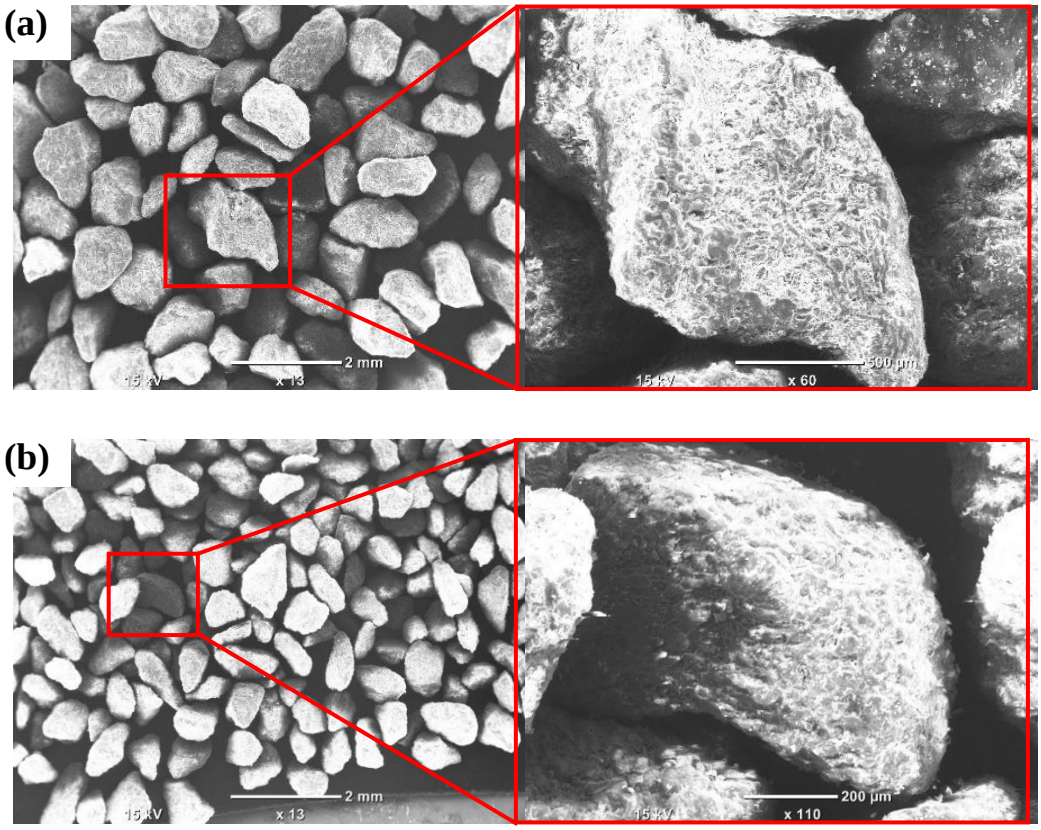

Figure 2.13. ASF Morphology, (a) D1 and (b) D2.

The statistical calculation of the normal size distribution is presented in Figure 2.14. The ASF average size calculation were obtained after sieving process with sieve openings of 600 µm ≤ D1 ≤ 900 µm and 400 µm ≤ D2 ≤ 600 µm. The particle average sizes were 905 ± 149 µm and 524 ± 134 µm for D1 and D2 respectively. Nevertheless, some ASF appear larger than the used sieve

openings, this is due to their irregular shape which facilitates its longitudinal infiltration into sieve meshes.

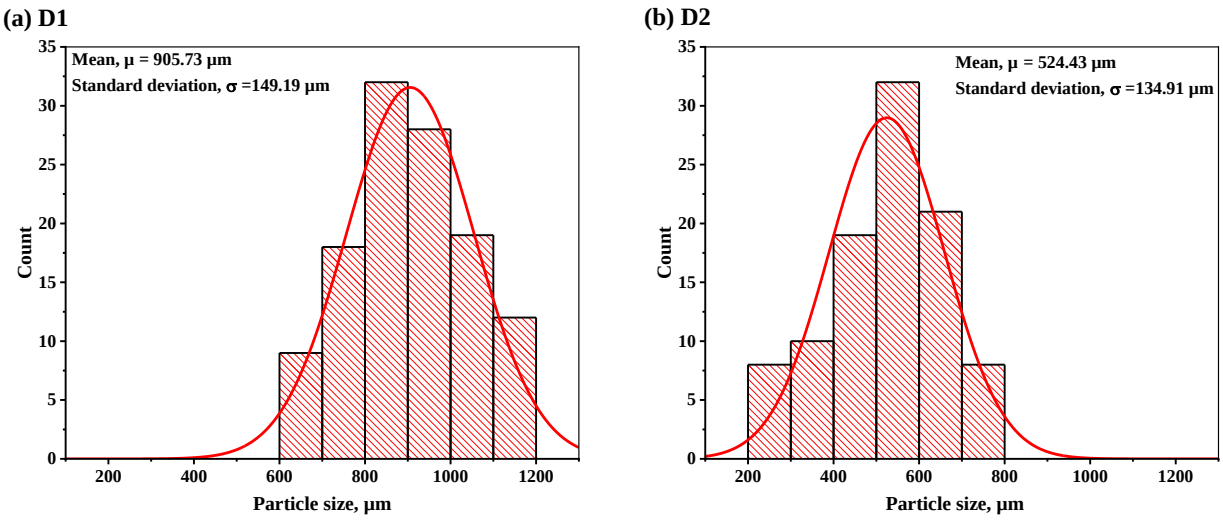

Figure 2.14. Particles size distributions of D1 and D2.

Thermogravimetric analysis TGA

The temperature of ASF degradation was performed via Perkin Elmer Pyris 6 TGA. A quantity of 6 mg was used for each size ranges. The tested particles were heated from 20 to 600 °C with heating rate of 10°C under inert atmosphere. Hemicelluloses, cellulose, lignin, and water moisture are known as the most different constituents of almond shells. However, TGA analysis was performed to determine the thermal stability and the thermal degradation of ASF and their constituents (Figure 2.15). Both D1 and D2 ranges, show almost the same thermal behavior TG and DTG and the used sizes had no effect on ASF thermal stability. The two ASF size ranges show three decomposition steps. Firstly, from room temperature to 100 °C, the small weight loss of about 5 % can be attributed to moisture losses

The Figure 2.15 shows thermal stability was observed between 100 to 242 °C. However, in the second step, it shows rapid weight loose peaks from 243 to 383 °C, at 293 and 363 °C. This weight loss is attributed to the decomposition of hemicellulose at the first peak. While, cellulose and lignin at the second peak, require high temperatures to degrade than hemicellulose due to their high degree of polymerization. Approximately the same two peaks were found at temperatures of 296 and 355 °C by Ramos et al. [8]. There is a slow weight loss at the third step, due to the devolatilization of biochar [9], and the carbonization phase [8]. In general, thermal and weight stability of ASF between 100 and 242 °C indicates their ability to perform a polymer process in this temperature range.

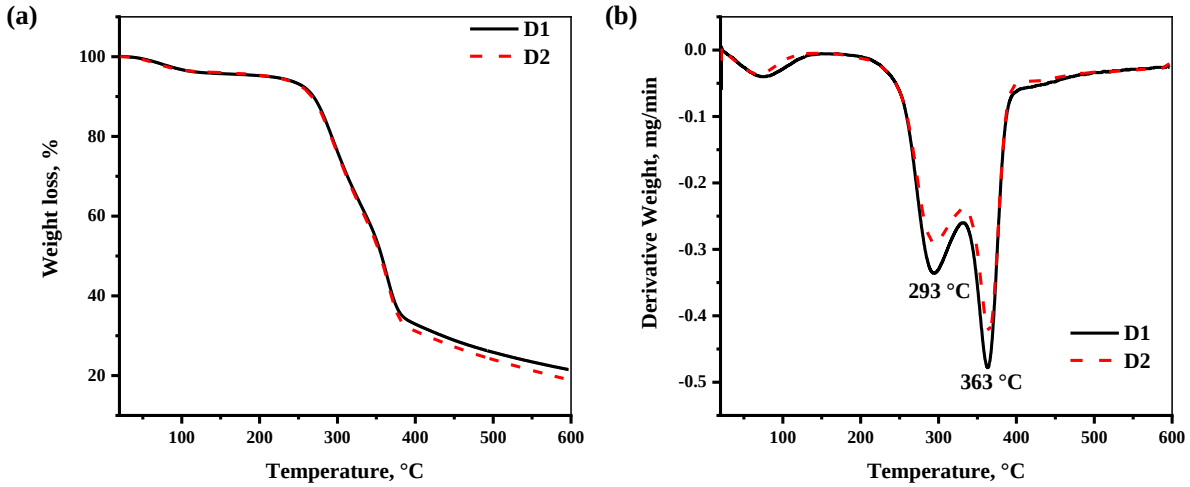

Figure 2.15. Thermogravimetric analysis of ASF (a) TG and (b) DTG for D1 and D2.

2.3.2.2. PP-ASF biocomposite preparation

Figure 2.16 summarized the preparation process of the PP-ASF biocomposite.

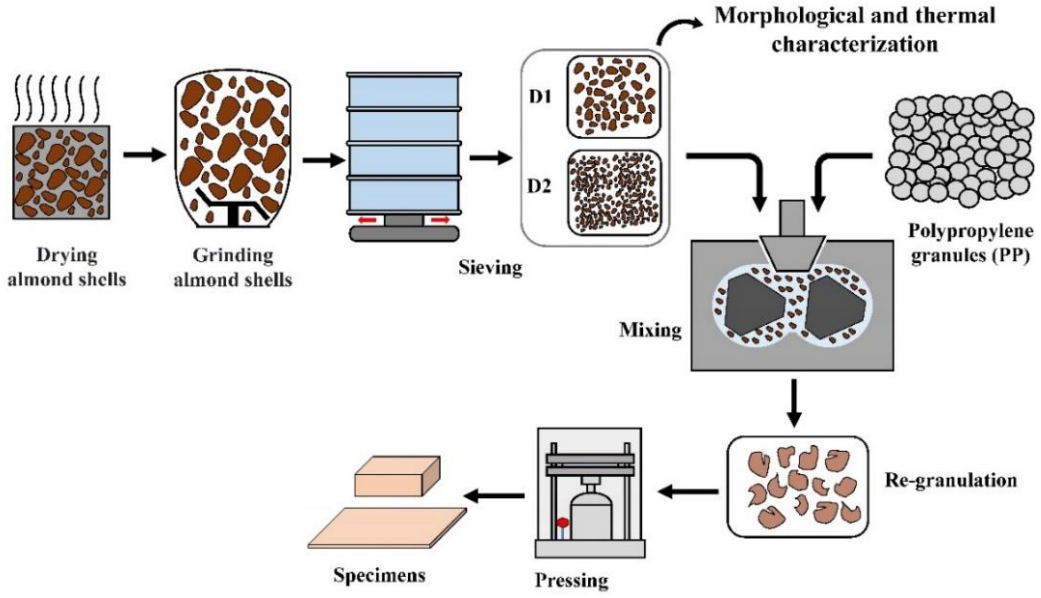

Figure 2.16. The biocomposite preparation process.

The biocomposite specimens were obtained using Polypropylene polymer as a matrix and ASF as fillers. Firstly, PP granules were introduced and melted in Brabender plastograph presented in figure 2.17-a (Plastograph EC & Mixer 50EHT – Brabender), Brabender, Duisburg, Germany. Equipped with a chamber of 50 cm^3 of volume. The used temperature was 180°C, with a mixing rotation speed of 40 rpm. Thereafter, the ASF are slowly added to the melted PP with weight proportions of 5, 10 and 15 wt% for each size range as it mentioned in Table 4. The mixed components are remained in the mixing chamber for 10 minutes, after that removed and let

cooled under room temperature. The obtained biocomposite material was molded by specimens of sizes 100x100x1 mm and 50x50x5 mm (Figure 2.17-b) under 180°C and 2 metric tons of pressure for 10 minutes in manual laboratory presses hydraulic unit Platen Carver (Model 3912, 12 metric tons), Carver, Indiana, United States (Figure 2.17-c). Finely, the obtained specimens were cooled under pressure for 10 minutes at room temperature.

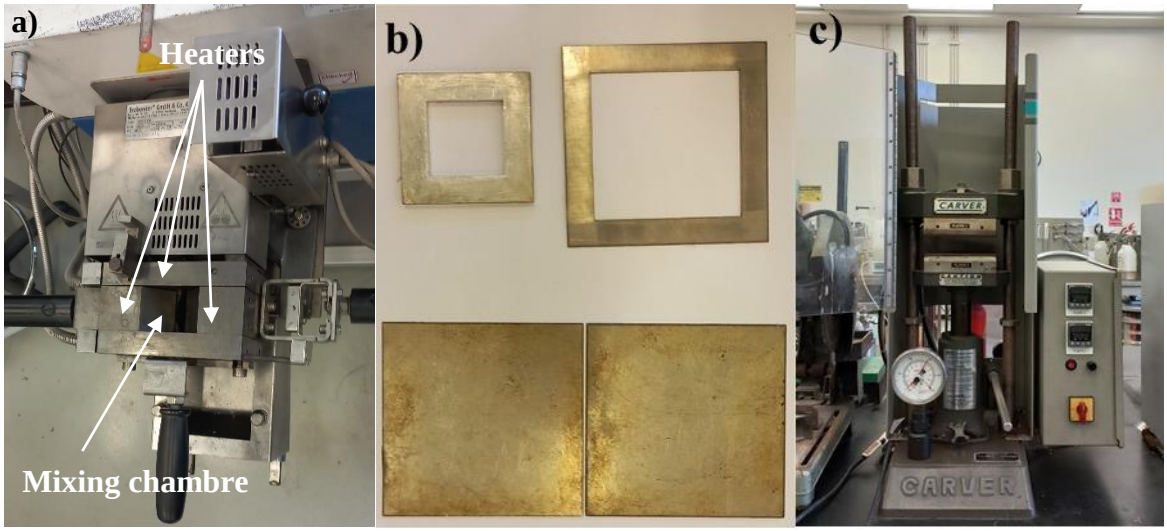

Figure 2.17. a) Brabender plastograph, b) The used molds and c) Laboratory presses hydraulic.

Table 2.4. PP-ASF biocomposite components proportions.

Specimen	Particle size µm	Particle wt%
Neat PP	-	0
PP-D1-5	$600 \leq D \leq 900$	5
PP-D1-10	$600 \leq D \leq 900$	10
PP-D1-15	$600 \leq D \leq 900$	15
PP-D2-5	$400 \leq D \leq 600$	5
PP-D2-10	$400 \leq D \leq 600$	10
PP-D2-15	$400 \leq D \leq 600$	15

2.3.3. PP-ASF biocomposite: Mechanical tests

The Shore D hardness tests were conducted according to ASTM D 2240 standard [10] on a Bareiss durometer (Germany) balance (Figure 2.18-a), on specimens as indicated in Figure 2.18-b, at room temperature of 23±2°C, five tests were realized for each specimen.

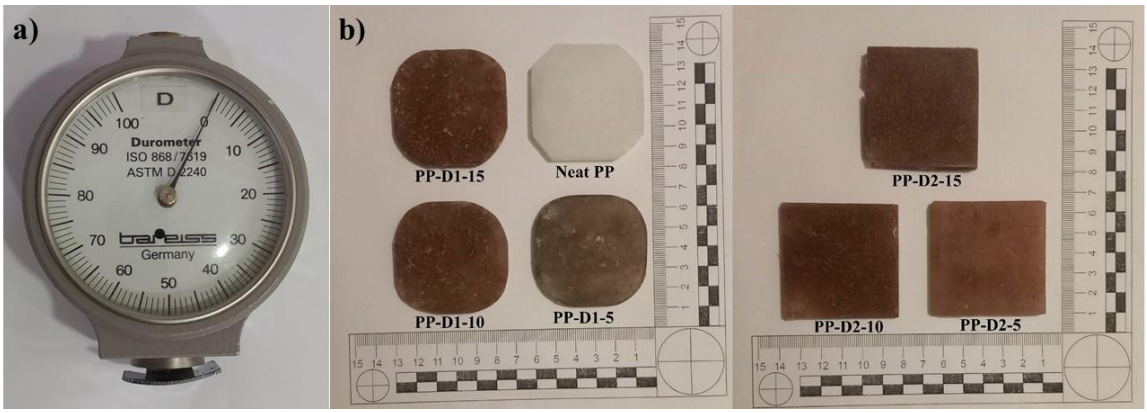

Figure 2.18. a) Bareiss durometer and b) PP-ASF specimens.

The tensile tests were performed according to ISO 37 Type II specimens [11] (Figure 2.19)), on a universal testing machine Lloyd LS 1K Plus Tensile instrument (Lloyd Instruments, UK) with a displacement speed of 5 mm/min (strain rate of 0.0025 s^{-1}) using a 1 kN load cell. Each test was repeated three times and the average values of mechanical properties and their standard deviations were reported.

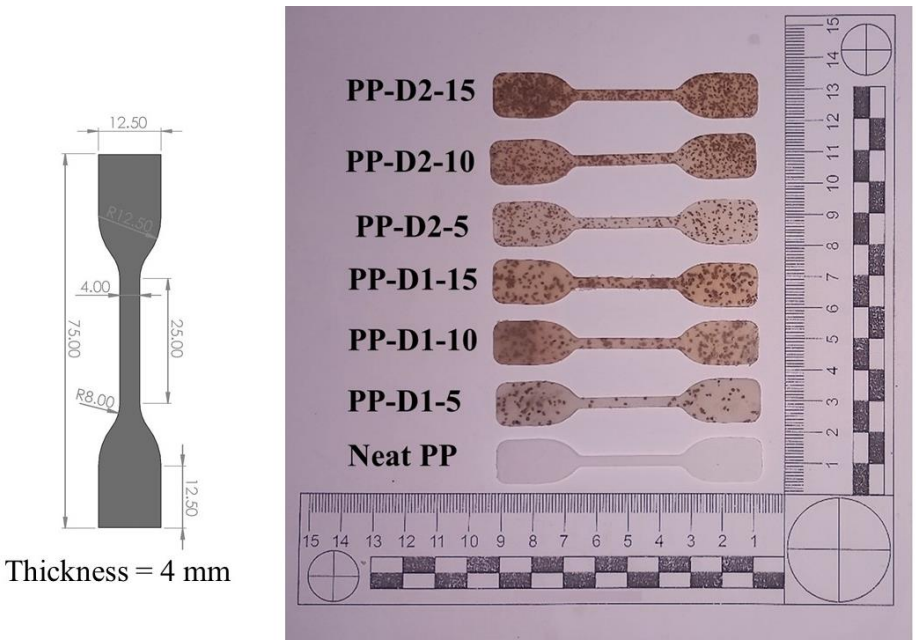

Figure 2.19. Tensile test specimens.

2.3.4. PP-ASF biocomposite: Tribological tests

The tribological experiments, on specimens of 50x50x5 mm in size, were performed via RTEC MFT-5000 (San Jose, California, U.S.A.) pin-on-disc rotary tribometer under dry conditions and room temperature of ~23±2°C. The used slider, of high wear resistance steel, has a spherical

shape of 6 mm diameter. This slider material was chosen to ensure that the wear occurs only on the specimens. The tests were under fixed normal load, Fn, of 10 N, constant rotational speed of 180 rpm following track radius, *R*, of 15 mm making a tangential speed of 0.28 m/s, during 90 minutes (Figure 2.20). The realized total wear distance, *L*, is thus ~1.5 km which ensures that the friction encompasses the running in and the steady state friction regimes. Both COF in the function of time and its average value accompanied by its standard deviation during the steady state were determined. In addition, the wear depths during the test were reported in function sliding distance.

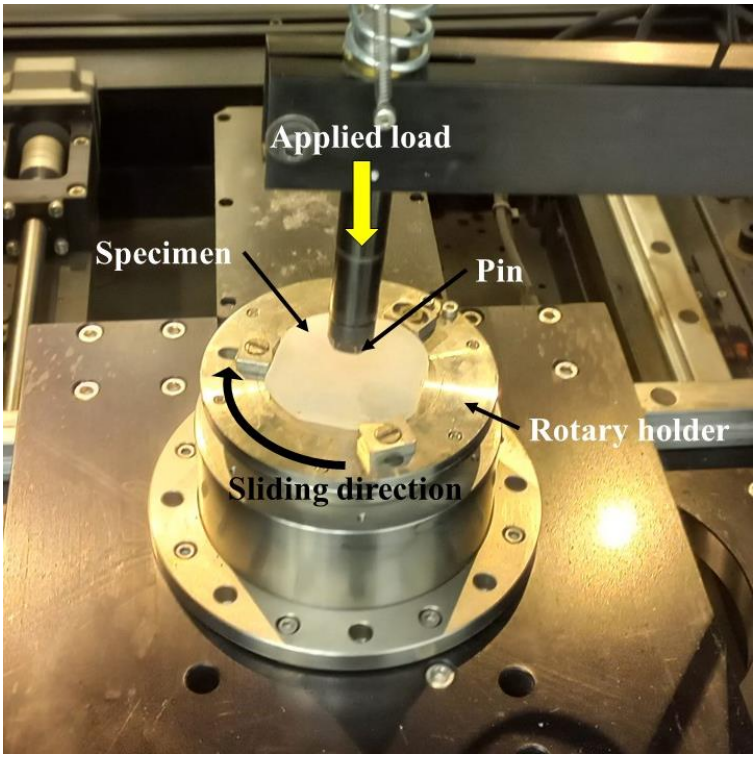

Figure 2.20. Tribological test settings.

The wear coefficient, W_c, (Eq 2.4) was determined using 3D topographic measurements via optical profilometer Leica DCM8 (Leica, Germany) on 3.51×2.64 mm^2 of area. The transversal wear track surfaces, *S*, were used in the loss volume, V_m, calculation (Eq 2.5). The two equations are as:

$$W_c = \frac{V_m}{F_n.L} \quad \text{(Eq 2.4)}$$

$$V_m = 2\pi RS \quad \text{(Eq 2.5)}$$

2.4. Conclusion:

The tribological characterization of PP-talc composites was realized. The PP matrix was a high-stiffness, high-gloss homopolymer grade. Talc fillers of around 1 µm size were added at 5 wt%,

10 wt%, and 50 wt% contents. The integration of a lab-made heating device into the microscratch test setup enables the investigation of the temperature-dependent tribological behavior of the composites. Reciprocating sliding tests were performed on the PP- talc composites under dry conditions at room temperature. The coefficient of friction (COF) and wear rate (W_r) were evaluated at different numbers of cycles (5000, 10000, 15000) to capture the steady-state behavior.

The preparation and characterization of polypropylene biocomposites reinforced with almond shell fillers PP-ASF was also presented. The almond shells were harvested, dried, and ground into two different particle size ranges (400-600 μm and 600-900 μm). The PP-ASF biocomposites were produced by melt mixing the PP matrix and the ASF fillers at 5 wt%, 10 wt%, and 15 wt% contents for each particle size range. The biocomposite specimens were then fabricated by compression molding.

References:

[1] Bouakkaz A, Albedah A, Bouiadjra BB, Khan SM, Benyahia F, Elmeguenni M. Effect of temperature on the mechanical properties of polypropylene–talc composites. J Thermoplast Compos Mater 2017;31:896–912. doi:10.1177/0892705717729016

[2] Sun, Wang, Guorong Sun, Junyan Liu, Xiang Huang, and Yang Wang. "Integration of MOF/COF core-shell composite material with wrinkled supramolecular hydrogel: A portable electrochemical sensing platform for noradrenaline bitartrate detection." Composites Part B: Engineering (2024): 112029.

[3] Ghatrehsamani S, Akbarzadeh S, Khonsari MM. Experimentally verified prediction of friction coefficient and wear rate during running-in dry contact. Tribol Int 2022;170:107508. doi:10.1016/j.triboint.2022.107508

[4] Archard JF. Contact and rubbing of Flat Surfaces. J Appl Phys 1953;24:981–8. doi:10.1063/1.1721448

[5] Quiles-Carrillo, L., Montanes, N., Sammon, C., Balart, R., & Torres-Giner, S. (2018). Compatibilization of highly sustainable polylactide/almond shell flour composites by reactive extrusion with maleinized linseed oil. Industrial Crops and Products, 111, 878–888.

[6] Debevc, S., HaftomWeldekidan, Snowdon, M. R., SingaraveluVivekanandhan, Wood, D. F., Misra, M., &Mohanty, A. K. (2022). Valorization of almond shell biomass to biocarbon materials: Influence of pyrolysis temperature on their physicochemical properties and electrical conductivity. Carbon Trends, 9, 100214–100214. https://doi.org/10.1016/j.cartre.2022.100214

[7] Ibáñez-García, A., Martínez-García, A., &Ferrándiz-Bou, S. (2021). Influence of Almond Shell Content and Particle Size on Mechanical Properties of Starch-Based Biocomposites. Waste and Biomass Valorization, 12(11), 5823–5836. https://doi.org/10.1007/s12649-020-01330-9

[8] Ramos, M., Dominici, F., Luzi, F., Jiménez, A., Garrigós, M. C., Torre, L., &Puglia, D. (2020). Effect of Almond Shell Waste on Physicochemical Properties of Polyester-Based Biocomposites. Polymers, 12(4), 835. https://doi.org/10.3390/polym12040835

[9] Li, X., Liu, Y., Hao, J., & Wang, W. (2018). Study of Almond Shell Characteristics. Materials, 11(9), 1782. https://doi.org/10.3390/ma11091782

[10] Palacios, Pedro A., et al. "Shore hardness of as-printed and dehydrated thermoplastic materials made using fused filament fabrication (FFF)." Materials Today Communications 35 (2023): 105971.

[11] Foltuţ, Daniel, et al. "Heat aging effect on tensile behavior at different strain rates of thermoplastic styrene elastomer." Materials Today: Proceedings 78 (2023): 257-262.

Chapter 3: Tribological properties of PP-talc composite

3.1. Introduction

The addition of minerals increases the Polypropylene (PP) stiffness and its heat distortion strength. Talc, glass beads, mica, silica, calcium carbonate, and others are the most commonly employed minerals as fillers for polypropylene composites [1-15]. Talc despite a low hardness, only Mohs hardness of one [16], and because of its capability of retaining fragrances, purity, and white color. The addition of talc to the PP increases its tensile strength [2,4] and its elastic properties [3]. However, it reduces its impact strength and its plastic deformation [1]. These mechanical property enhancements extend the application domains of this polymer under severe mechanical loading [1-7] as well as under tribological conditions [17-21]. Among these extending domains are pharmaceuticals, chemicals, agricultural and other automotive parts, as well as packaging [14, 15, 22, 23]. Some experimental works have treated the enhancement of not only the mechanical but also the wear resistance of many filled polymers simultaneously [17-21, 24, 25]. Among these polymers, there is the filled PP with several filler types [1-15]. The particles of talc, characterized by their low frictional coefficient [26], can be used as solid lubricants. It is used to enhance the tribological properties of lithium grease [27], oil qualities [28], and the tribological properties of PP composites with talc [19-21]. In this context, the optimization of PP composite content as a function of proportion, size, and type of fillers can be used to improve the PP's mechanical and tribological performances simultaneously. To do this, some experimental works have studied the wear resistance of talc-filled PP via several friction tests, such as pin on disc [19], using abrasive paper [20], and scratching [21]. However, in all these experimental works, the size of the used talc was between ~5 and ~22 µm. Furthermore, in the literature, there is a lack of understanding of tribological behavior under reciprocating sliding test of filled talc PP, which remains qualitatively and quantitatively insufficient and less explored. As a comparison, the wear mechanisms induced via reciprocating sliding differ from those induced in continued or non-repeated sliding [29, 30]. The formation of a third body in reciprocating conditions plays a major role in the wear resistance of material. The present chapter attempts to enhance the understanding of the talc proportion effects on the tribological behavior of PP-talc composite via dry reciprocating sliding tests.

3.2. Tribological properties of PP-talc composite

3.2.1. Scratch test

3.2.1.1. Friction coefficient vs. normal loads under different temperature degrees

Figure 3.1 presents the COF vs. normal loads under different used temperatures. For the low temperature T=20°C, all the COF of the all specimens are start from small values (0.42 to 0.48) correspondent to the low normal loads F_n=2N, and increase to reach its high values (0.52 to 0.58) correspondent to the medium normal loads used F_n=5 N, then goes decrease for the normal loads F_n=10 N and F_n=15 N (0.42 to 0.5), that those loads are considered high for the microscratch test of composites of PP.

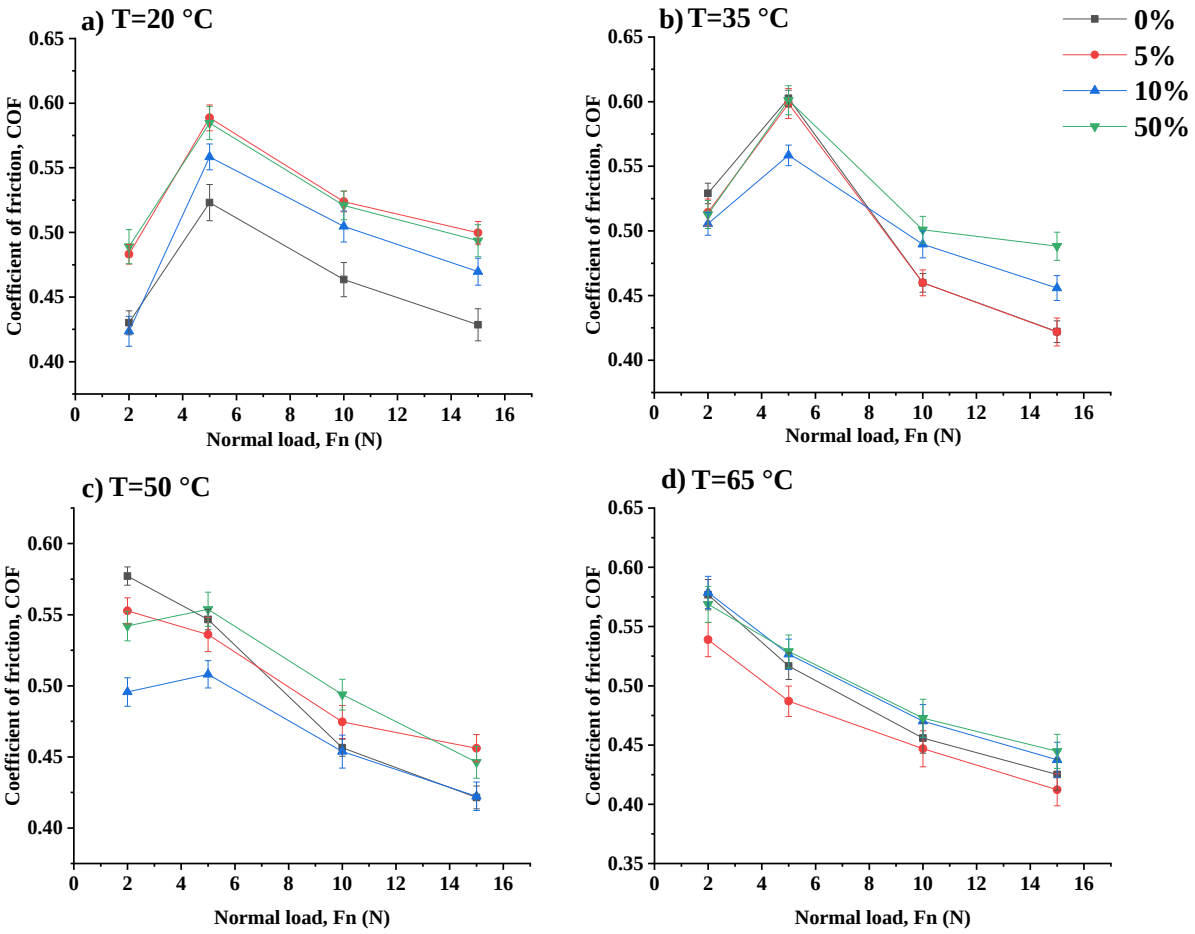

Figure 3.1. Friction coefficient *vs.* normal loads under different temperature degrees.

The COF are not linear vs. the normal loads, and its low values correspondent to the low normal loads, this is due to the relationship between the contact form between the diamond indenter and the scratched specimen surface and also to the mechanical properties of PP talc material

[31, 32]. At low temperatures and low normal loads, the contact is just superficial and the COF adhesive component dominates the friction and the deformation caused by the indenter it is mostly elastoplastic. In this situation, the PP and the talc fillers are just compressed in the scratch bottom, and the zones scratched are slips under the indenter [33, 34]. For the relatively medium normal loads F_n ~ 5N, the COF are in its high values due to the plowing deformation mode. The relatively medium scratch depth (in function of F_n) and material mechanical resistance which cause the stick-slip phenomenon [33, 34] and so too high COF (Figure 3.9 a and b) this explain the great resistance of the material where the PP chains are cut off [33, 34,35]. Therefore high normal loads, the plowing mode develops to wave mode of the scratched surface. So, the COF increases by increasing the continent of talc.

Generally, the increasing of specimen temperature (> 50 °C) conducts to a similar scratch behavior of the studied material and the COF decrease *vs.* the normal load and weak effect of talc proportion was observed.

3.2.2. Sliding test

3.2.2.1. Coefficient of friction (COF)

Figure 3.2 shows the evolution of the COF *vs.* the number of cycles until 15000 cycles and the specimen's talc proportion.

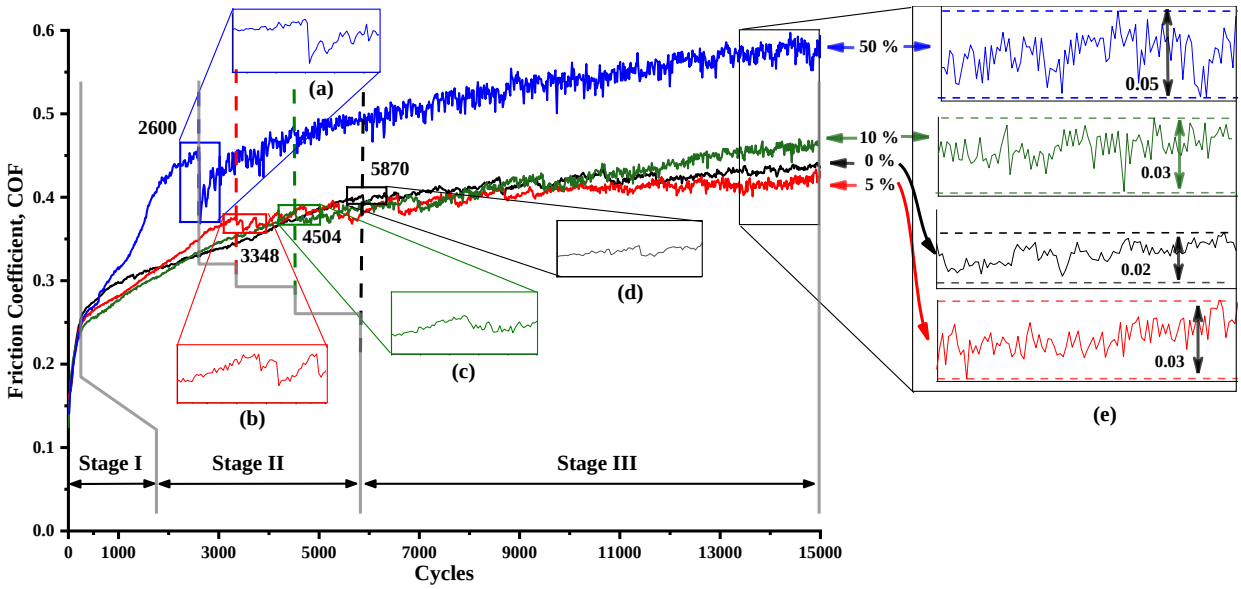

Figure 3.2. COF evolution vs. number of cycles and talc proportions.

For all specimens, the COF shows the same behavior *vs.* the number of cycles. The COF before 1000cycles goes through a stage of incubation, and it continues increasing smoothly as the number of cycle's increases until it reaches a certain specific number of cycles, each specimen has its specific correspondent number of cycles, then decreases suddenly for a few cycles, increase again but in a fluctuating manner. Then goes increases monotony until reaches 15000 cycles for talc proportions. Also the COF of the pure PP, 5 and 10% of talc are almost the same *vs.* number of cycles, where they are equal on many points, 2100, 4300, 6515, 8630, 9730 10915 and 11770 cycle, after the last point (11770 cycle), a marginal difference appears between the COF of these three talc proportions, where the COF is 0.47, 0.44, 0.42 for 10%, 0 % and 5 % respectively, the big difference between them is 0.05 (12 %), but for the specimen has 50 % of talc, show the biggest COF *vs.* number of cycles, where the difference between the COF of the specimen has 50 % of talc and the three others is increases with the number of cycles increase, where COF at 5000 cycle is 0.48 for 50 % of talc and it is about 0.38 for the others, so the difference between them is 26 %, also at 8500 cycle the COF is 0.54 for 50 % of talc and it is about 0.41 for the others, the difference between them is 31 %, until the number of cycles reach 15000, when the COF of the specimen has 50 % of talc show the biggest COF, where the difference between them is 0.34 %, the COF of 50% of talc is 0.6 and the COF of the others is about 0.44. Furthermore, the specific point that shows the change in the evolution of the COF is shown in Figure 3.2 (a, b, c, and d), from the smooth rice to the fluctuated rise, this point for 50 % of talc correspondent of 2600 cycles and COF=0.46, for 10 % of talc correspondent of 4505 cycles and COF=0.38, for 5% of talc correspondent of 3348 cycles and COF=0.38 a for 0% of talc correspondent of 5870 cycles and COF=0.40, so this point appears quickly for the specimen exhibit the higher talc content (2600 cycle) of talc (50%) compared to the net specimen (5870 cycles), where the number that correspondent to the specific point of cycles decrease with 55.7 % by adding 50 % content of talc, also it decreases with 23.25 % by adding 5% of talc and it decreases with 43 % by adding 10% of talc, also the COF correspondent of this point almost the same at 0 ,5 and 10 wt0 % of talc (0.40 for 0% and 0.38 for 5 and 10%), but for 50% of talc is 0.46, so the COF correspondent to the specific point increase with 13 % by adding 50% content of talc. For the last 1500 cycles, explain the amplitude of these fluctuations, for, 5 and 10% of talc, the amplitudes are about 0.02 for 0% of talc, 0.03 for 5 and 10% of talc, but for 50 % of talc it is 0.05, and this value represents about 9% of the COF, which is 0.58, so one out of ten of the COF is unstable.

Based on the COF results and the above section, the sliding behavior of the PP-talc composite was divided into three stages:

Stage I: The COF rapidly rises independently on the talc proportion vs. number of cycles, where the COF for all used talc proportions was almost the same. It increases until it reaches 0.25 after 250 cycles.

Stage II: Smooth sliding stage, it starts with ~250 cycles and reaches a limit depending on the talc proportion. This stage is characterized by a smooth increase in COF slope. For low talc proportions (0%, 5%, and 10%), the increasing slope was almost the same, but it was lower compared to the 50% talc proportion once.

Stage III: Rough sliding stage, it starts from the stage II limit and is occasioned by COF falling with different values (Figure 3.2-a, b, c and d) and by noticeable fluctuation evolution. This fluctuation increases with the talc proportion. During the stage III, the obtained COF is nearly the same when the talc proportion is under 10% and ranges from 0.3 to 0.4. However, when the talc proportion is 50%, high values of COF are registered, ranging from 0.38 to 0.55. The same findings were obtained when sliding on PP filled with wood flour [31].

The main differences between Stage II and Stage III are in the COF slop and COF fluctuation, whereas in Stage II the sliding does not generate any debris. Still, it begins to create at the beginning of the stage III.

3.2.2.2. Wear rate

The obtained wear rate result is presented in Figure 3.3 relative to 5000, 10000, and 15000 cycles. It can be seen that the wear rate of the PP talc composite increase with increasing talc proportion, also it was increase with increasing the number of cycles, the lowest ware rate was observed on the specimen has 0% of talc, it is 1.9 E-4 mm^2/N, and the highest ware rate was observed on the specimen has the highest talc content (50% of talc), it is 2.98 E-2 mm^2/N, and there is no big difference between the wear rate observed by adding 5% of talc, but by comparing the wear rate values of the pure PP, 10% and 50% of talc, it can be seen that by adding 10% of talc, the wear rate increase by 48 %, 294 % and 436 % after 5000 , 10 000 and 15 000 cycles respectively, so the wear rate increase by a half time, a three times and four times after 5 000 , 10 000 and 15 000 cycles respectively, also it can be seen that by adding 50 % of talc, the wear rate increase by 580 %, 1185 % and 3168 % after 5 000, 10 000 and 15 000 cycles

respectively, so the wear rate increase by a six times, a twelve times and thirty one times after 5 , 10 and 15 thousand cycles respectively.

Also by comparing the increase in the wear rate as a function of the number of cycles of each talc content, it can be seen that the wear rate of the pure PP increased by 1136 % (Eleven times) from 5 000 to 15 000 cycles, by adding 5 and 10 wt. % of talc, the wear rate increased by 1653 % (seventeen times) and 4368 % (forty-four times) respectively from 5 000 to 15 000 cycles, for 50 wt. % of talc it was observed the wear rate increased by 2192 % (twenty-two times) after 15 000 cycles from 5 000 to 15 000 cycles. As mentioned in the previous section, the specimen with 50 % talc exhibits the highest wear rate.

For all cycle numbers, the neat PP exhibits a low wear rate. However, after high numbers of cycles (15000 cycles), both the trace depth (Fig. 3-a) and the wear rate (Fig. 3-b) are remarkably affected by the talc proportion. During this time, this result is attributed to the combined effect of some phenomena such as plowing, fatigue, and delamination [32]. The low and medium talc proportions (5 and 10%) are occasioned by a low wear rate relative to the 50% once.

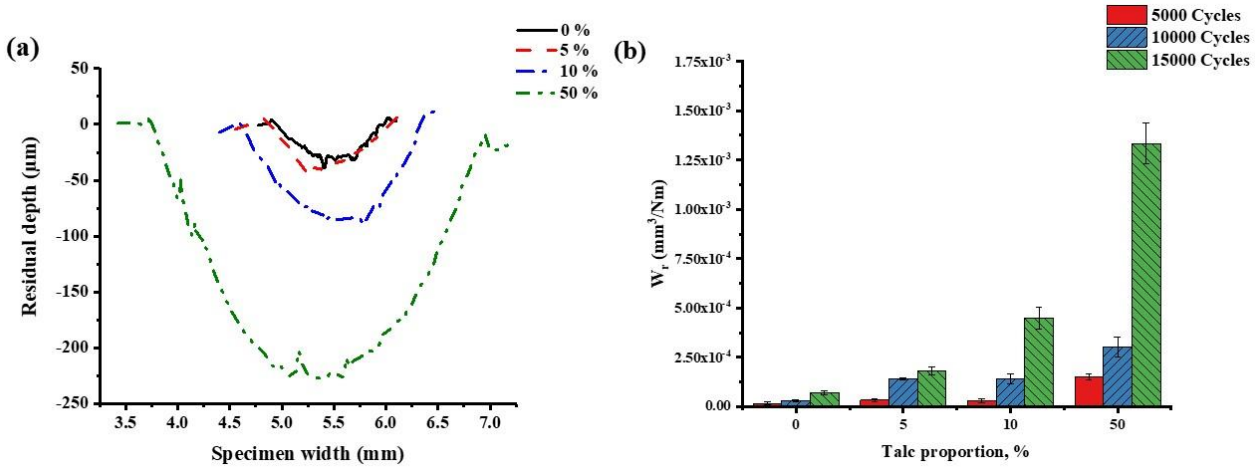

Figure 3.3. Track surface profile at 15000 cycles (a) and wear rate at 5000, 10000, and 15000 cycles vs. talc proportion (b).

Generally, in the initial stage of sliding, the wear of the PP-talc specimen is slightly affected by the talc proportion during the low time cycles under 10000 cycles. However, it strongly increases with the talc proportion, especially when the number of cycles increases. Thus, it is clear that both the high talc proportion and the time cycles accentuate the wear phenomena during the reciprocating sliding of the PP-talc composite.

3.2.2.3. Worn surfaces examination

Figure 3.4 shows the SEM micrographs of the worn surfaces of neat PP and the talc-filled PP obtained at a high number of cycles of 15000 cycles.

For the pure PP, the appearance of medium chips with their displacement on the sides of the friction groove, this chip was appeared after unmatched longitudinal micro-cutting of the material in the form of tracks, also some parts of this chip steel attached to the frictional surface, so the third body steel attached to the material, and the micro-cutting is more visco-plastic and just on the bottom, that caused by the adhesive wear, also small deep of the groove was observed.

But by adding 5% talc, the chips are larger and more numerous than in the case of pure PP. And adhere to each other at the bottom, and all of them were completely cutting from the frictional surface, unlike the previous case (pure PP), which contributes to their accumulation on top of each other, thus forming another surface for friction, so the third body was not attached to the frictional surface, which makes them gather in certain places at the friction track so that the friction track contains zones of accumulation of chips on top of each other and other zones specific to the material that not rubbed, also the micro-cutting turns to abrasive micro-cutting of the material, also there was adhesive wear, also it was more transverse micro-cutting than the pure PP, also a rolls formation was observed.

Unlike all of the above, in the case of 10% of talc, the chips come out completely outside the friction track and the appearance of regular longitudinal grooves formed from the accumulation of the removed material on top of each other to cover the entire friction track with the appearance of small holes in it to form a new friction surface by the third body, also there is an adhesive and abrasive wear, the abrasive wear that characterized by the longitudinal regular grooving along the frictional surface.

By adding 50% talc, the chips became smaller and a roll formation was observed, that caused by some of the abrasive and the adhesive wear, which caused the chips to shatter and crumble along the frictional surface. Like the other cases, the chips are stacked on top of each other to form the entire friction surface, the rolls are more appear, also the initiation of the rip of the material appears in the form of thin layers, that generate the chips which turn into rolls after remaining at the bottom of the friction track and friction with the counter body.

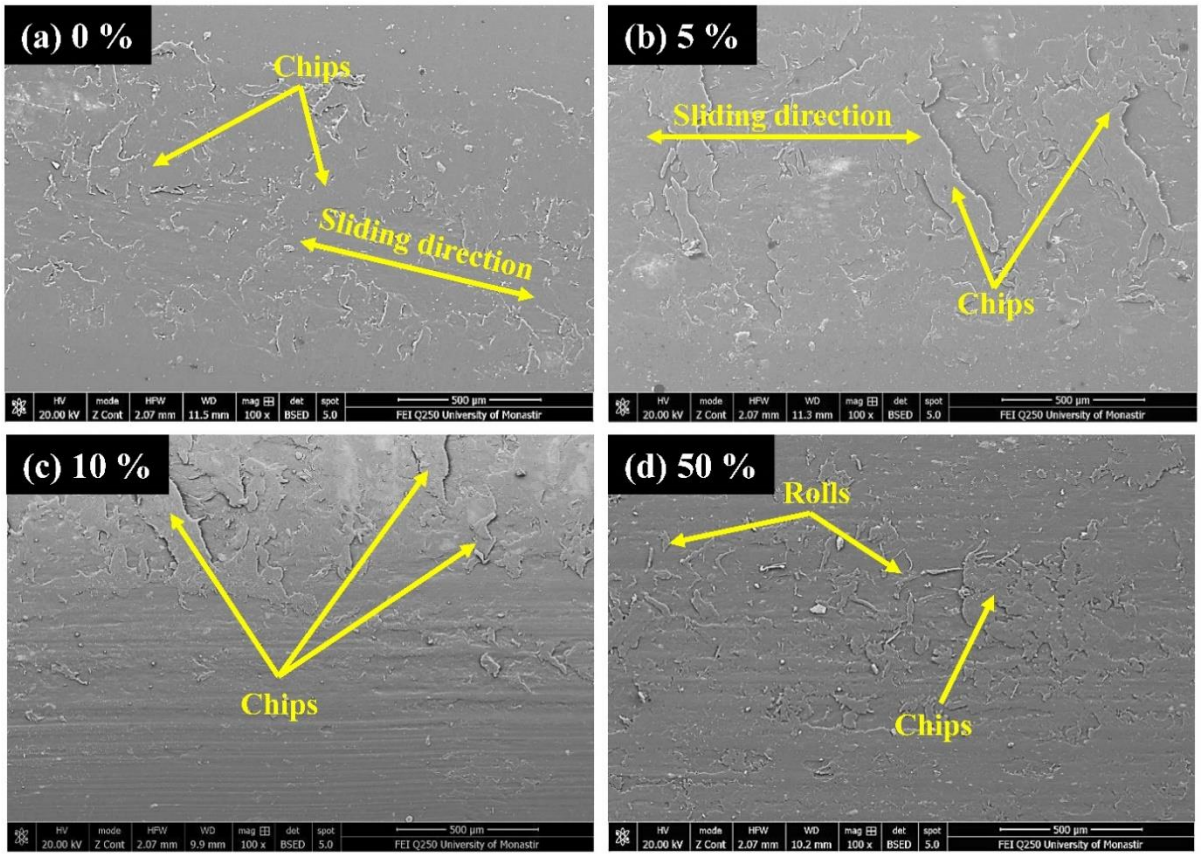

Figure 3.4. SEM micrographs of the worn surfaces vs. talc proportions or 15000 cycles.

The SEM analyses show that the sliding of neat PP leads to the formation of small chips without material displacement (Figure 3.4 a). However, these two phenomena accentuate the talc proportion (Figure 3.4 d). The size and displacement of the formed chips debris were higher when sliding the 5 and 10% proportions of talc than the other specimens. The chip displacement leads to the formation of grooves at the side and in the middle of the formed scratch (Figure 3.4 b c). In the case of 50% of talc, the sliding occurs with chips completely removed, crushed, and rolled under the slider (Figure 3.4 d).

Furthermore, the SEM micrographs show that at a high number of cycles, the specimen with a high talc proportion of 50% exhibits more small chips rolled and crushed on the worn surface (Figure 3.3 c d) than for the other studied cases. However, these damage phenomena weaken the surface beneath the slider and lead to the appearance of the stick-slip phenomenon and the formation of small and jointed micro-chips, causing high fluctuations in the COF (Figure 3.1). For neat PP and 5% talc proportion cases (Figure 3.3 a b), the micro-formed chips remain attached to the worn surface and form a layer attached to the bottom surface of the tracks.

3.2.2.4. Discussions

The distributed stress that was divided on the PP matrix and the talc fillers increase compared to the neat PP, due to the talc is has less hardness than the PP matrix, with a hardness of 1 on Mohs scale, than the stress distributed on the talc fillers can easily breaks up the talc fillers and in the same time contribute to increase the stress distributed on the PP matrix by exposing the PP matrix to more stress, this lead to increase the penetration of ball on the composite, this explain the increasing in the COF and the wear rate, also this can explain the total cut-off of the chips by increasing talc proportion, that generated due to the low attack angel, so the frontal and side pads formed by the ploughing mode, also the quantity of the material displaced depend on the normal load, that responsible to the total of the distributed on both of the matrix and the fillers, also this support that the penetration increase by increasing talc proportion. The damage observed is mainly caused by the stick-slip phenomenon and during the sticking cycle the material is plastically drawn along the scratch direction creating the damage pattern, also the stick-slip phenomenon becomes more pronounced when the tip penetrates deep into the polymer, so the stick-slip phenomenon has more effect by adding % wt. of talc.

Talc decreases the tensile strength of PP, so the scratch resistance also decreases [33], the temperature increasing during wear might cause a significant change in mechanical properties [1], that decrease the tensile strength of PP that contribute to an increase in the COF and wear. Also, talc contributed to the introduction of the brittle cracks [33] formation that accelerated the generation of the third body, these cracks were the initiation of the flaking of the composite, also talc was a soft material that contributed to change the ductile deformation of polymers to brittle deformation [33], so the talc gets the PP matrix more brittle.

The COF evolution under reciprocating sliding is characterized by three different stages. Initially, the adhesive mode dominates the sliding independently to the talc proportion. Its value can reach 0.23 (Figure 3.2 and Stage I) and is near the COF of almost all materials [34]. During this, the interfacial adhesion bonds develop and break to produce the adhesion component of friction, where the initial roughness of the surface can support the applied normal load. When this roughness becomes deformed, the sliding transfers to the plowing mode [32], and the sliding mode develops to stage II. During this second stage, the plowing mode dominates the sliding behavior of the material. This friction behavior is attributed to the changing of material mechanical properties [1], to the plastic deformation level under the relative hard slider, and also to the size of the formed chips. Under these conditions, the slider deforms the material's

initial cracks and chips of small size. Some contact interactions accompany the reciprocating sliding, which are more or less important relative to the talc proportion and the number of cycles. The chip and groove formation and chip displacements, as well as the stick-slip phenomenon, are the main observed phenomena creating damage patterns, which are also observed by Ammar et al. [20] and Jiang et al. [35].

The increasing number of sliding cycles and the temperature lead to surface fatigue [36]. Hence, it increases intense plastic deformation and surface cracking, causing chip fragmentation and displacement that become fixed on the slider surface (Figure 3.5). This material behavior is more observed in the 50% specimen than in the other specimens. Additionally, the talc contributes to brittle crack formation and contributes to changing the ductile deformation regime to a brittle deformation regime [33]. Therefore, this material behavior accelerates the generation of unattached wear particles of small size, which form the third body during the sliding.

The wear mechanism transforms from abrasive pure PP to both adhesive and abrasive wear by adding talc, due to the effect of incorporating fillers on the PP matrix [37] remaining chips of the third body adherent to the friction surface are caused by the PP molecular chains are remain attached by each other's for the pure PP, but by adding talc on the PP, it was completely freed from the frictional surface, so the talc contribute to facilitate the cutting of the chips, which leads to increase the wear rate, the residual depth and the generation of the third body, that also leads to increase the COF.

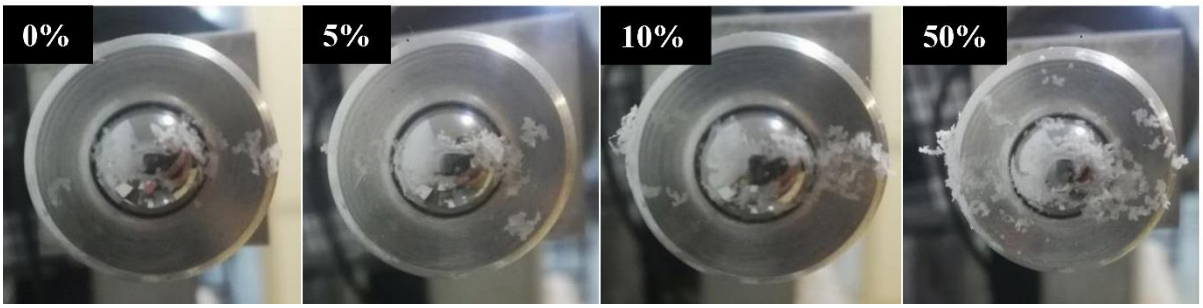

Figure 3.5. Material transfer on the slider after 15000 cycles vs. talc proportion.

The increase in the talc content leads to an increase in both of the wear rates, this means that the talc facilitates the penetration of the counter-body on the frictional surface of the composite, which increases the wear, also for the pure PP and its low talc content composites (5 and 10% of talc) compared to 50% of talc, the wear rate is almost the same, compared to the highest talc

content, this also due to the effect of the talc on the mentioned mechanical properties in the previous sections, the maximal elongation, maximal stress of the composite material [2,3,4, 36], and the shear resistance of the frictional surface of the PP-talc composite [33], which leads to getting frictional surface weak as the talc content increase, also the talc decrease the elastic recovery [23] which leads also to increase the residual depth that increases the wear rate.

However, the talc facilitates material fragmentation and, thus, the penetration of the slider into the specimens. This observation is noted for 50% of talc. The second stage is an intermediate stage between the initial wear mode, dominated by the plowing mode, and stage III, dominated by the combined effect of plowing with delamination phenomena. This latter stage is characterized by some wear particles entrapped between the slider and the worn surface. The amount of these particles increases with talc proportion (Figure 3.5). When both the number of cycles and the talc proportion are high, the formed chips increase in number and decrease in size (Figures 3.4 and 3.5). Take in the count of the COF and wear rate results and of the SEM analyses, and despite the fact that talc is known as a soft material, it did not act as a lubricant during the friction tests. To give a lubricant role to the talc, Zhan et al. [19] used modified talc coupled with a chemical agent and mixed with HDPP.

3.3. Conclusion

The study of the coefficient of friction (COF) in talc-filled polypropylene (PP) composites under varying normal loads and temperatures results indicate a distinct relationship between these parameters, revealing that at lower temperatures (20°C), COF values exhibit a non-linear response to increasing normal loads. Initially, a rise in COF was observed at low normal loads (2 N), attributed to superficial contact and adhesive friction. As the load increased to medium levels (5 N), COF reached its peak, primarily due to plowing deformation and the stick-slip phenomenon, highlighting the material's mechanical resistance and the influence of talc content. Furthermore, the behavior of the COF at high normal loads (10 N and 15 N) demonstrated a decrease in frictional resistance, suggesting a transition from a plowing mode to a wave formation on the scratched surface. This shift emphasizes the complex interplay between load, temperature, and material properties in determining tribological performance. Notably, as the temperature exceeded 50°C, the COF exhibited a consistent decrease with increasing normal loads, indicating a diminished effect of talc proportion on frictional behavior.

The reciprocating sliding tests on polypropylene (PP) composites filled with talc reveal significant insights into their tribological behavior. The study investigates the effects of varying talc proportions on the friction coefficient (COF) and wear rate, as well as the wear mechanisms involved.

Sliding Behavior and Wear Mechanisms

The sliding behavior of PP-talc composites transitions from adhesive mode to simple plowing and plowing with wear particle generation. This transition is influenced by the talc content in the composite. At low talc proportions (5% and 10%), the friction coefficient and wear rate exhibit small variations, indicating stable tribological properties. However, at a high talc proportion (50%), the COF becomes unstable and reaches high values, accompanied by a significant increase in wear rate.

Damage Patterns and Wear Behavior

The wear behavior of PP-talc composites is characterized by various damage patterns, including chip formation, displacement, rolling, and delamination. These damage patterns become more pronounced with increasing talc content and the number of sliding cycles. The high talc proportion (50%) accelerates the formation of brittle cracks and particles of different sizes, leading to a high stick-slip phenomenon and delamination wear process.

Efficiency of Low Talc Proportions

The study concludes that low talc proportions (5% and 10%) in PP composites are efficient in enhancing tribological properties. These proportions result in stable COF and wear rate values, making them suitable for applications requiring improved wear resistance and frictional performance.

Influence of Talc Proportion on Wear Mode

Under reciprocating friction, the talc proportion significantly influences the wear mode and its transition time. The high talc proportion (50%) leads to an unstable COF, high wear rate, and pronounced damage patterns, while low talc proportions (5% and 10%) contribute to stable tribological properties.

References

[1] Bouakkaz A, Albedah A, Bouiadjra BB, Khan SM, Benyahia F, Elmeguenni M. Effect of temperature on the mechanical properties of polypropylene–talc composites. J Thermoplast Compos Mater 2017;31:896–912. doi:10.1177/0892705717729016.

[2] Lapcik L, Jindrova P, Lapcikova B, Tamblyn R, Greenwood R, Rowson N. Effect of the talc filler content on the mechanical properties of polypropylene composites. J Appl Polym Sci 2008;110:2742–7. doi:10.1002/app.28797.

[3] Khoury Moussa H, Challita G, Badreddine H, Montay G, Guelorget B, Vallon T, et al. Enhancement of mechanical properties of high modulus polypropylene grade for multilayer sewage pipes applications. J Appl Polym Sci 2022;140. doi:10.1002/app.53314.

[4] Nga PT, Nguyen V-T. Experimental study on mechanical behavior of polypropylene-based blends with talc fillers. Adv Sci Technol Eng Syst j 2020;5:571–6. doi:10.25046/aj050669.

[5] Castillo LA, Barbosa SE. Influence of processing and particle morphology on final properties of polypropylene/talc nanocomposites. Polym Compos 2020;41:3170–83.

[6] Castillo LA, Barbosa SE, Capiati NJ. Influence of talc morphology on the mechanical properties of talc filled polypropylene. J Polym Res 2013;20. doi:10.1007/s10965-013-0152-2.

[7] Lee J, Ha C-S. Mechanical properties of polypropylene/talc composites prepared via solid-state extrusion. J Adhes Interface 2016;17:131–5. doi:10.17702/jai.2016.17.4.131.

[8] Jahani Y. Comparison of the effect of mica and talc and chemical coupling on the rheology, morphology, and mechanical properties of polypropylene composites. Polym Adv Technol 2009;22:942–50. doi:10.1002/pat.1600.

[9] Lee D, Kim S, Kim B-J, Chun S-J, Lee S-Y, Wu Q. Effect of nano-caco3 and talc on property and weathering performance of PP Composites. Int J Polym Sci 2017;2017:1–9.

[10] Samsudin MS, Ishak ZA, Jikan SS, Ariff ZM, Ariffin A. Effect of filler treatments on rheological behavior of calcium carbonate and talc-filled polypropylene hybrid composites. J Appl Polym Sci 2006;102:5421–6. doi:10.1002/app.25054.

[11] Azizi H, Faghihi J. An investigation on the mechanical and dynamic rheological properties of single and hybrid filler/polypropylene composites based on talc and calcium carbonate. Polym Compos 2009;30:1743–8. doi:10.1002/pc.20685.

[12] Putfak N, Larpkasemsuk A. Wollastonite and talc reinforced polypropylene hybrid composites: Mechanical, morphological and thermal properties. J Met Mater Miner 2021;31:92–9. doi:10.55713/jmmm.v31i3.967.

[13] Bakar MB, Leong YW, Ariffin A, Ishak ZA. Mechanical, flow, and morphological properties of talc- and kaolin-filled polypropylene hybrid composites. J Appl Polym Sci 2007;104:434–41. doi:10.1002/app.25535.

[14] Nofar M, Ozgen E, Girginer B. Injection-molded PP composites reinforced with talc and Nanoclay for automotive applications. J Thermoplast Compos Mater 2019;33:1478–98.

[15] Syed SF, Chen JC, Guo G. Optimization of tensile strength and shrinkage of talc-filled polypropylene as a packaging material in injection molding. J Package Technol Res 2019;4:69–78. doi:10.1007/s41783-019-00077-6.

[16] Dokmai V, Sinthiptharakoon K, Phuthong W, Pavarajarn V. Anisotropic robustness of talc particles after surface modifications probed by atomic force microscopy force spectroscopy. Particuology 2021;58:308–15. doi:10.1016/j.partic.2021.04.008.

[17] Daniel DJ, Panneerselvam K. Abrasive wear of polypropylene/cloisite 30B/elvaloy AC 3427 nanocomposites. J Compos Mater 2017;52:1833–43. doi:10.1177/0021998317734624.

[18] Satti AJ, Molinari EC, de Freitas AGO, Tuckart WR, Giacomelli C, Ciolino AE, et al. Improvement in abrasive wear resistance of metallocenic polypropylenes by adding siloxane based polymers. Mater Chem Phys2017;188:100–8. doi:10.1016/j.matchemphys.2016.12.007.

[19] Zhan F, Chen NC. Studies on friction and mechanical properties of high density polypropylene (HDPP) filled with modified talc. Adv Mater Res 2012;624:279–82.

[20] Ammar O, Bouaziz Y, Haddar N, Mnif N. Talc as reinforcing filler in polypropylene compounds: Effect on morphology and mechanical properties. PolymSci2017;03.

[21] Świetlicki M, Chocyk D, Klepka T, Prószyński A, Kwaśniewska A, Borc J, et al. The structure and mechanical properties of the surface layer of polypropylene polymers with talc additions. Mater 2020;13:698. doi:10.3390/ma13030698.

[22] Kuroda S, Mizutani A, Ito H. Effect of talc size on surface roughness and glossiness of polypropylene injection molding application to automotive plastics. Polym Eng Sci 2019;60:132–9. doi:10.1002/pen.25266.

[23] Râpă M, Matei E, Ghioca PN, Cincu C, Niculescu M. Structural changes of modified polypropylene with thermoplastic elastomers for medical devices applications. J Adhes Sci Technol 2016;30:1727–40. doi:10.1080/01694243.2015.1132103.

[24] Palanikumar K, AshokGandhi R, Raghunath BK, Jayaseelan V. Role of calcium carbonate(caco3) in improving wear resistance of polypropylene(pp) components used in automobiles. Mater Today Proc 2019;16:1363–71. doi:10.1016/j.matpr.2019.05.237.

[25] Zolfaghari S, Paydayesh A, Jafari M. Mechanical and thermal properties of polypropylene/silica aerogel composites. J MacromoLSci B 2019;58:305–16.

[26] Vasić B, Czibula C, Kratzer M, R A Neves B, Matković A, Teichert C. Two dimensional talc as a van der waals material for solid lubrication at the nanoscale. Nanotechnology 2021;32:265701. doi:10.1088/1361-6528/abeffe.

[27] Kumar N, Saini V, Bijwe J. Exploration of talc nanoparticles to enhance the performance of lithium grease. TribolInt2021;162:107107. doi:10.1016/j.triboint.2021.107107.

[28] Saini V, Bijwe J, Seth S, Ramakumar SSV. Potential exploration of nano-talc particles for enhancing the anti-wear and extreme pressure performance of oil. Tribol Int 2020 ;151:106452.

[29] Hsia F-C, Elam FM, Bonn D, Weber B, Franklin SE. Wear particle dynamics drive the difference between repeated and non-repeated reciprocated sliding. TribolInt2020;142:105983.

[30] Ward R. A comparison of reciprocating and continuous sliding wear. Wear 1970;15:423 34. doi:10.1016/0043-1648(70)90237-1.

[31] Jan P, Matkovič S, Bek M, Perše LS, Kalin M. Tribological behaviour of green wood based unrecycled and recycled polypropylene composites. Wear 2023;524–525:204826.

[32] Rigney DA. Fundamentals of friction and wear of materials: Papers pres. at the 1980 ASM materials science seminar, 4-5 Oct. 1980, Pittsburgh, PA. ; spons. by the Seminar Committee of the Materials Science Div. of the American Soc. for metals. 1981.

[33] Kurkcu P, Andena L, Pavan A. An experimental investigation of the scratch behaviour of polymers – 2: Influence of hard or soft fillers. Wear 2014;317:277–90.

[34] Friedrich K. Friction and wear of polymer composites. Elsevier; 1986.

[35] Jiang H, Cheng Q, Jiang C, Zhang J, Yonghua L. Effect of stick-slip on the scratch performance of Polypropylene. Tribol Int 2015;91:1–5. doi:10.1016/j.triboint.2015.06.024.

[36] Zhu X, Zhang S, Zhang L, He Y, Zhang X, Kang X. Frictional behavior and wear mechanisms of AG/mos2/WS2 composite under reciprocating microscale sliding. Tribol Int 2023;185:108510. doi:10.1016/j.triboint.2023.108510.

[37] Peng S, Luo L, Wu R, Yi Z, Wuliu Y, Shi P, et al. Study on Scratch Behavior and application of a novel cardanol-based additive in polypropylene. TribolInt2023;180:108243.

Chapter 4: Mechanical and tribological properties of PP Almond shells biocomposite

4.1. Introduction

The effect of biofillers on the mechanical and tribological properties of polymers constitutes an important and potential solution to be studied [1,2] in the involvement of its mechanical resistance and green tribological applications [3-6] as well as its impositions for other industrial production. Several studies have investigated the mechanical properties of polypropylene filled with various natural sources fillers, such as almond shell particles (ASF) [7-11]. These studies have shown that the incorporation of these particles into polypropylene can enhance its mechanical properties, especially, its flexural and Young modulus [7, 11]. Besides the mechanical properties, several works have focused on the tribological behavior investigating biofilled polymers. Barari et al. [12] found that the Coefficient of Friction (COF) decreases with increasing volume fraction of nanocellulose fillers in the epoxy and only 1.4 wt% of nanocellulose enhances the tribological. Sharma et al [13] exploited the Citrus limetta peels as a biofillers for developing an epoxy composite specimens. They found that the COF decreases with decreasing the fillers size. The filling of PP with wood flours decreases the COF with a drop of 15% [14] at 40 wt% of these fillers accompanied by improvement of the wear resistance. Furthermore, tribological properties such as low friction coefficients and low abrasion rates were obtained by Ibrahim et al [15] with these flours. Other studies involved that the addition of coir fiber [16] and cherry seed powder [17] into PP has also led to a remarkable drop with 9% of the COF and an enhancement of 40% of wear resistance [15]. The high content of cherry seed powder in PP shows also a positive effect on frictional behavior compared to the neat PP [17]. However relative to the above mentioned works, the tribological behavior of these polymer-based biocomposites is associated not only with the filler type but also with its proportion and size. In addition, the particle size effect on the COF is not clear and it is linked to the used filler type [17]. For low cherry seed filler contents, abrasion mode is the dominant wear mechanism, while for all cherry seed filler sizes of high content [17].

In addition to above and on the other hand, there are few, if not non-existent, studies in the existing literature that investigate and exploit the almond shell fillers effect, regarding the size and proportion of particles, on the mechanical and tribological properties of polymer based composites, particularly with polypropylene.

4.2. Polypropylene Almond shells fillers biocomposite: Mechanical properties

4.2.1. Shore D hardness

Figure 4.1 presents a comprehensive summary of the Shore D hardness results for polypropylene (PP) specimens reinforced with almond shell particles (ASF). The data clearly indicate that the neat PP exhibits the lowest hardness value among all the tested specimens. This observation is consistent across both particle sizes, D1 and D2.

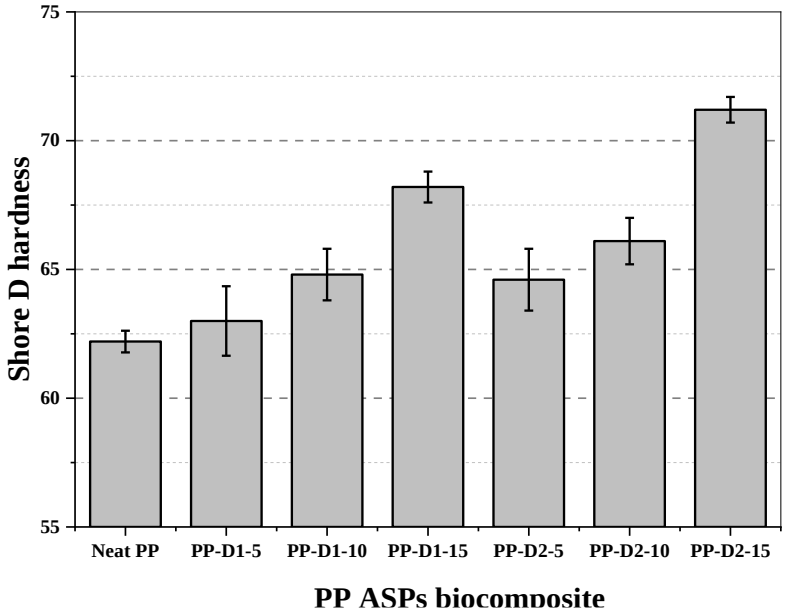

Figure 4.1. PP-ASF specimens Shore D hardness.

As the proportion of ASF increases, there is a notable enhancement in the hardness of the PP composites. Specifically, the hardness values show a positive correlation with the increasing ASF content for both D1 and D2 particle sizes. This trend suggests that the incorporation of ASF significantly improves the mechanical properties of the PP matrix. A comparative analysis of the two particle sizes reveals that the D2 ASF specimens exhibit higher hardness values than the D1 ASF specimens. This finding underscores the influence of particle size on the mechanical performance of the composites. The larger D2 particles contribute to a more pronounced reinforcement effect, resulting in higher hardness values compared to the smaller D1 particles. These results clearly demonstrate the impact of particle size on the hardness of PP composites reinforced with ASF. It is noteworthy that this effect is not observed in the case of cherry seed powder [17], which does not exhibit a similar influence on the hardness of polypropylene. This distinction highlights the unique reinforcing capabilities of ASF and their potential for enhancing the mechanical properties of PP composites.

4.2.2. Tensile test properties

Figure 4.2 presents the PP-ASF properties obtained via tensile test. The neat PP correspondent to the lower tensile modulus comparing to the other PP ASF biocomposite which was 1530 MPa, and the tensile modulus increase by increasing the ASF proportion in the PP matrix. For 5% proportion of ASF regardless of size, the tensile modulus was almost the same, but for 15% proportion of ASF, the tensile modulus for D1 was 1766 MPa, and for D2 was 2013 MPa, so there is an increasing in the tensile modulus of 15% for D1 and an increasing of 32% for D2. Consequently, ASF D2 was more efficient than ASF D1 for enhancing the PP ASF tensile modulus.

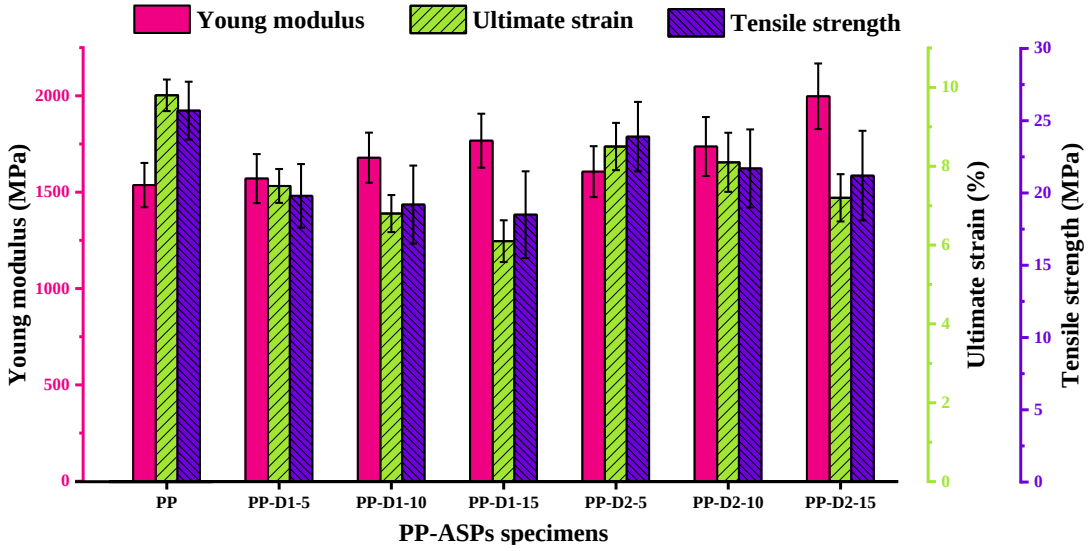

Figure 4.2. PP-ASF specimen's tensile properties.

For the tensile strain of the PP ASF biocomposite. The neat PP correspondent to the highest tensile strain value which was 9.8%, and this value decreasing by increasing the ASF proportion regardless its size, but regard the size, the D1 ASF exhibit the lower tensile strain values compared to D2, where this value was decreased by 38% by adding ASF with 15% for D1 and it was decreased by 26% but adding the other ASF D2, so the higher ASF size, D1, weaker the PP ASF biocomposite tensile strain compared to the higher ASF size D2.

For the tensile strength of the PP ASF biocomposite. Neat PP exhibited the highest tensile strength, which was about 26.7MPa, while adding ASF to PP matrix contribute to the reduction of this tensile property. Furthermore, regardless the PP ASF size, the biocomposite tensile strength decrease by increasing the added ASF proportion to PP matrix, while the lowest values

of tensile strength were observed on the PP ASF biocomposites to which high ASF size D1 were added, which were about 19MPa for all ASF proportions, so there is no noticeable change in the tensile strength property of the biocomposite with adding high ASF size D1 with different proportion, whilst the PP ASF biocomposites that were filled with small ASF size D2 occupied the middle values, where it was decrease by 10% by adding 5% and decrease by 20% by adding 15%.

As a conclusion we can say that the Young modulus of neat PP was 1530 MPa lower than for all other specimens. Furthermore, this modulus increases with increasing ASF proportion for both D1 and D2 sizes. Regardless of its sizes, the Young modulus was almost the same for 5 and 10 %, except for 15 % the Young moduli were 1766 MPa and 2013 MPa for D1 and D2 respectively slightly greater than of neat PP. Globally, the specimens with D2 size are characterized by Young moduli slightly higher than specimens with D1 size. There is a rise of Young modulus by 15 % s and by 32 % for D1 and D2 size respectively at 15 % of ASF.

In addition, the neat PP exhibits the highest ultimate strain relative to the other specimens. The ultimate strain decreases with increasing the ASF proportion for both used ASF sizes. Comparatively, the D1 size exhibits lower ultimate strain values than the D2 size. Thus, the increasing ASF content increases the biocomposite rigidity. However, the neat PP exhibits the highest tensile strength, while adding ASF to the PP matrix contributes to the reduction of tensile strength. Furthermore, for both D1 and D2, the tensile strength decreased with increasing ASF proportion, while the lowest values of tensile strength were obtained with ASF size D1 of ~19MPa for 15 % of content.

4.3. Polypropylene Almond shells fillers biocomposite: Tribological properties

4.3. 1. Friction coefficient (COF)

Figure 4.3 presents the friction coefficient (COF) evolution as a function of sliding distance. The average friction coefficient (COF_m) and its standard deviation are presented in Figure 4.5 relative to the steady stage period. All tested specimens go through the running in process to the steady state regimes before about 200 meters of sliding which corresponds to about 10 minutes of sliding. During the steady state period and relative to the COF evolution of neat PP, the obtained results permit to distinction two COF groups. The group of PP-ASF filled with D2 size exhibits almost the highest COF, and the other one with D1 size exhibits the lowest COF. This ascertainment shows the effect of particle size on the evolution of friction coefficient.

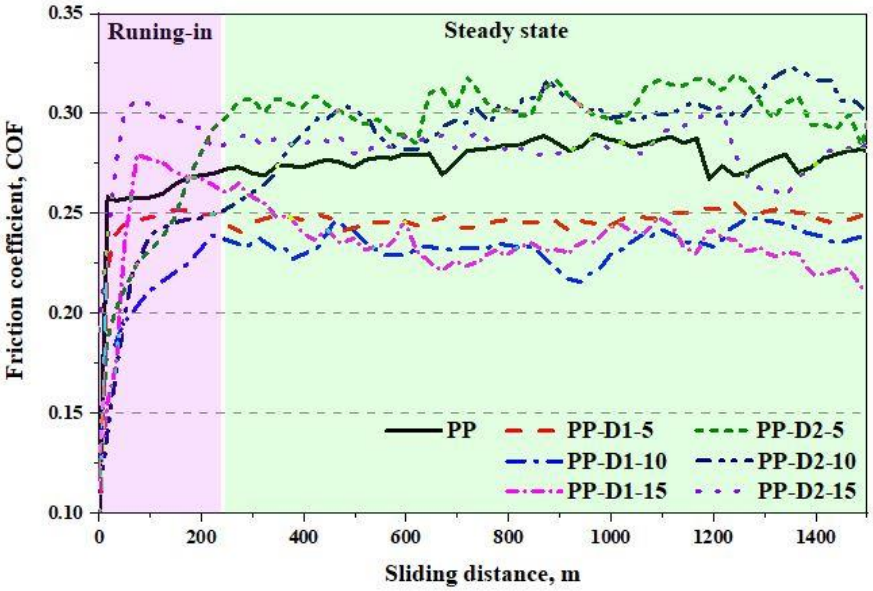

Figure 4.3. Friction coefficient vs. test duration.

During the steady state and for all tested specimens, the COF_m values are between 0.2 and 0.3 (Figure 4.4). The obtained COF_m values with D1 size are close and ranging between 0.23 and 0.25 lower than obtained with neat PP and with D2 size. Furthermore, the COF_m decreases by increasing ASF proportion for both D1 and D2 sizes. The same findings were previously obtained in the case of wood filler or cherry seed as filler in the PP matrix [14, 15, 17]. Nevertheless, the low COF was observed with D1 size for 10% and 15% that makes a reduction of 20 % than of the neat PP. This COF reduction, obtained with 10 % of ASF, was more important than that obtained with 40 % and 55 % of wood powder which make a COF reduction of 15 % and 20 % respectively [14, 15]. The reduction of COF, in the case of the present work, can be attributed to the presence of high stiffness ASF particles. However, regarding the obtained results, the COF is not directly related to the particle size, but it can be connected to the filler source being used [17]. It previously observed that the high cherry seed fillers size was more efficient for reducing the COF compared to the low fillers size [17], in contrast, for Citrus limetta peels fillers of epoxy the lower fillers size leads to the lower COF relatively to the neat epoxy.

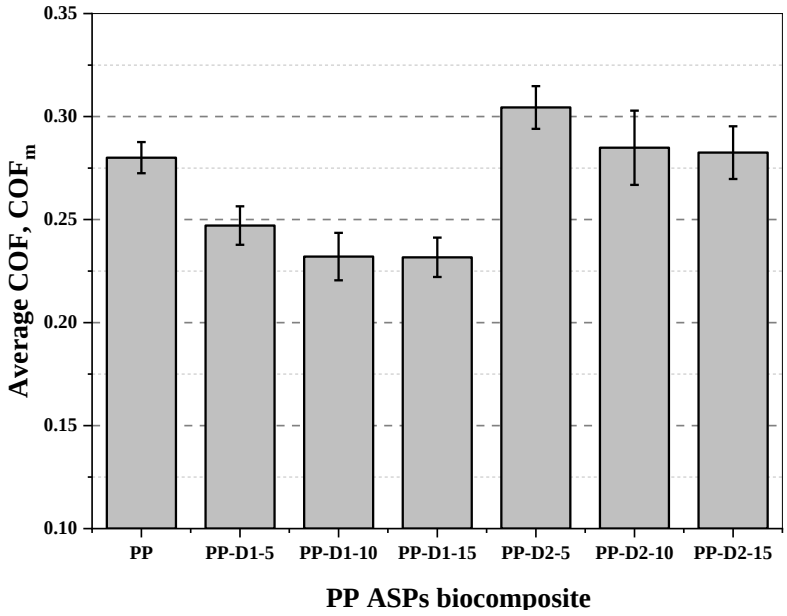

Figure 4.4. Steady state average COF.

4.3.2. Wear coefficient (W_c)

The tribological properties of thermoplastic composites have a considerable link with their mechanical properties [18], especially their viscoelastic behavior. The wear coefficient, W_c, results are presented in Figure 4.5. The neat PP and PP-D2-15 exhibit the lowest W_c of ~2.10^{-4} mm^3 Nm^{-1}, while for both 5 and 10 % proportions, the obtained Wc values are almost closer to ~$3.5.10^{-4}$ mm^3 Nm^{-1} for both D1 and D2 sizes. The wear of PP-D1-15 was occasioned by the highest W_c value. This result implies that for both 5 and 10 % low proportions, the particle size has a minor effect on the wear coefficient, while for high particle proportion, the size is a decisive factor in determining the wear coefficient. The high W_c values for D1 can be attributed to its high size causing the rupture of a brittleness ASF and made more material removal than D2 size specimens. The observed ASF filler size effect on the W_c was similar to the Citrus limetta peels fillers size effect, where the high fillers size produces voids leading to a poor composite miscibility [13]. It should be noted that these results were obtained at the end of the friction test.

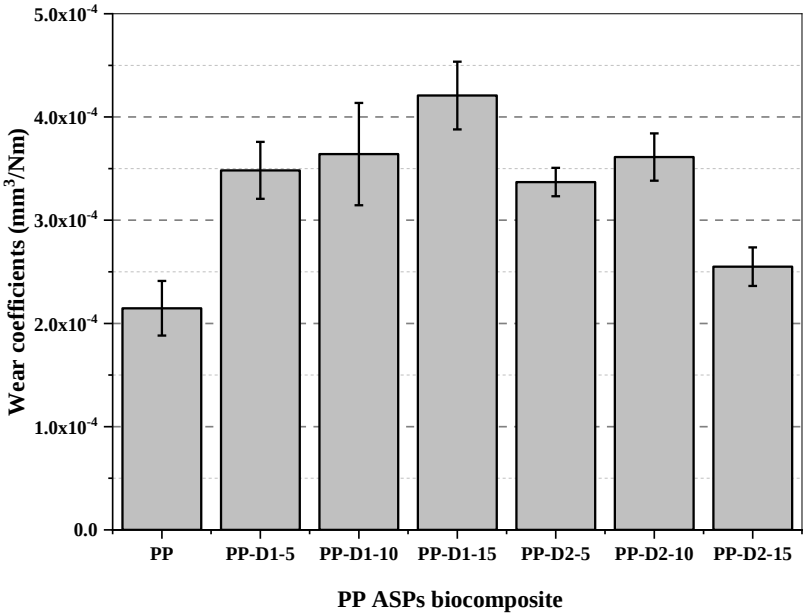

Figure 4.5. Wear coefficient, W_c vs the size and proportion of particle at the end of wear tests.

The friction behavior at the end of testing does not give a comprehensive overview of the wear coefficient. To achieve an analysis of the W_c, the wear depth was evaluated during the test (Figure 4.6). The wear depth (WD), as a function of sliding distance, evolved according to three stages. The first presents the running in process where the depth slightly increases due to the surface asperities being removed for the first 200 meters of distance. After that, the WD shows a pseudo-stability along the second stage that corresponds to regular wear, during which the material shows a relative wear resistance. Along the third stage, the WD evaluates in the same manner as in the second stage but it drops rapidly. There is a similarity between the WD evolution of neat PP and PP-D2-15 during all sliding distance showing less depths compared to the other specimens. However, the PP-D1-15 shows the deepest track wear along the overall distance traveled. At the end of the test, neat PP and PP-D2-15 biocomposites exhibit the lowest WD, while PP-D1-15 exhibits the highest WD. These results are in good concordance with the findings of the wear coefficient, W_c, (Figure 4.5).

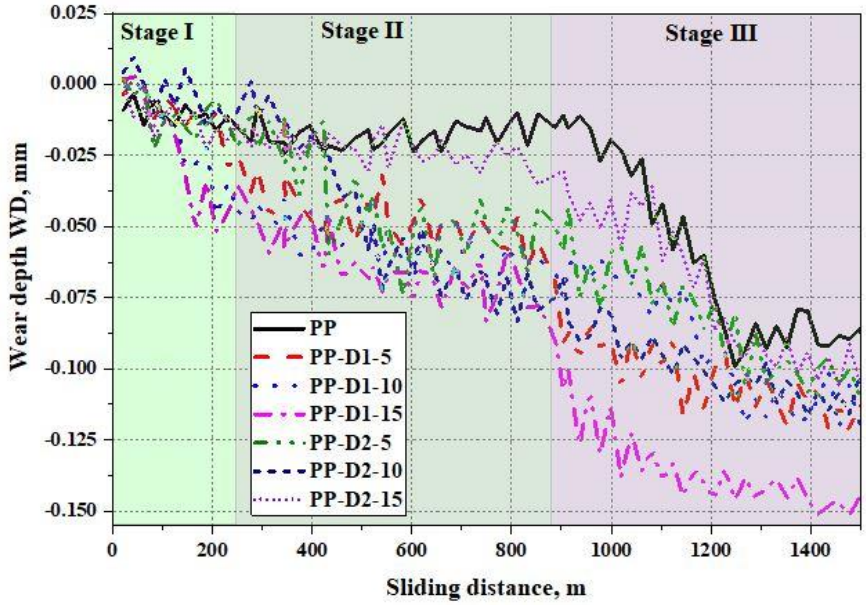

Figure 4.6. Wear depth (WD) vs. sliding distance.

4.3.3. Wear mechanisms

To analyze the wear mechanisms of the studied biocomposites, the Optical 3D micrographs of wear tracks at the end of wear tests, were exposed in Figure 4.7. The neat PP exhibits a wear track profile of the smallest width and containing voids (Figure 4.7 a). The addition of ASF has contributed to the formation of pile up on the track sides more pronounced for D2 size than for D1 size. For the filled PP, the wear tracks in the case of D1 are occasioned by rough and deep surfaces more noticeable (Figure 4.7 b, c and d) than in the case of D2 size of smooth grooves (Figure 4.7 e, f and g), for all ASF proportion. Sharma et al [13] found the same above phenomenon where the lower, the fillers size, the smother, the wear track surfaces. The wear of both sizes occurs with the formation of microscratches, these microscratches resulted from the crushing and displacement by the slider of ASF during the continued sliding, which indicates the presence of the wear with the formation of third body, which leads to the formation of tribofilm between contact surfaces.

The occurred wear mechanisms are principally due to the effect on sliding history, environment, surface topography changes, and the material subsurface damage, which accentuate the wear leading to the wear by delamination phenomenon and formation of wear debris. However, the neat PP filled PP with D2 size shows better resistance compared to PP-ASF filled with D1. As clearly shown, the neat PP wear mechanism exhibits voids formation caused by removed parts that are sticking on the slider and tearing off from the track surface (Figure 4.7 a). The observed voids on neat PP can be attributed to the stick slip phenomenon [19]. These voids were absent

in the case of filled PP. However, comparing the damage forms observed for both sizes, we can deduce that the formation of tribofilm is more noticeable for D2 than for D1 affecting the wear coefficient (Figs. 4 and 5). This wear behavior was similar to the cases of incorporation of wood flour [15], and coir fiber in PP [17]. Hence, the presence of ASF on the wear tracks led to an increase in the abrasion by third body debris [13-15, 17]. The filling of PP with ASF and cherry seed powder led to a similar effect on the wear mechanism [17].

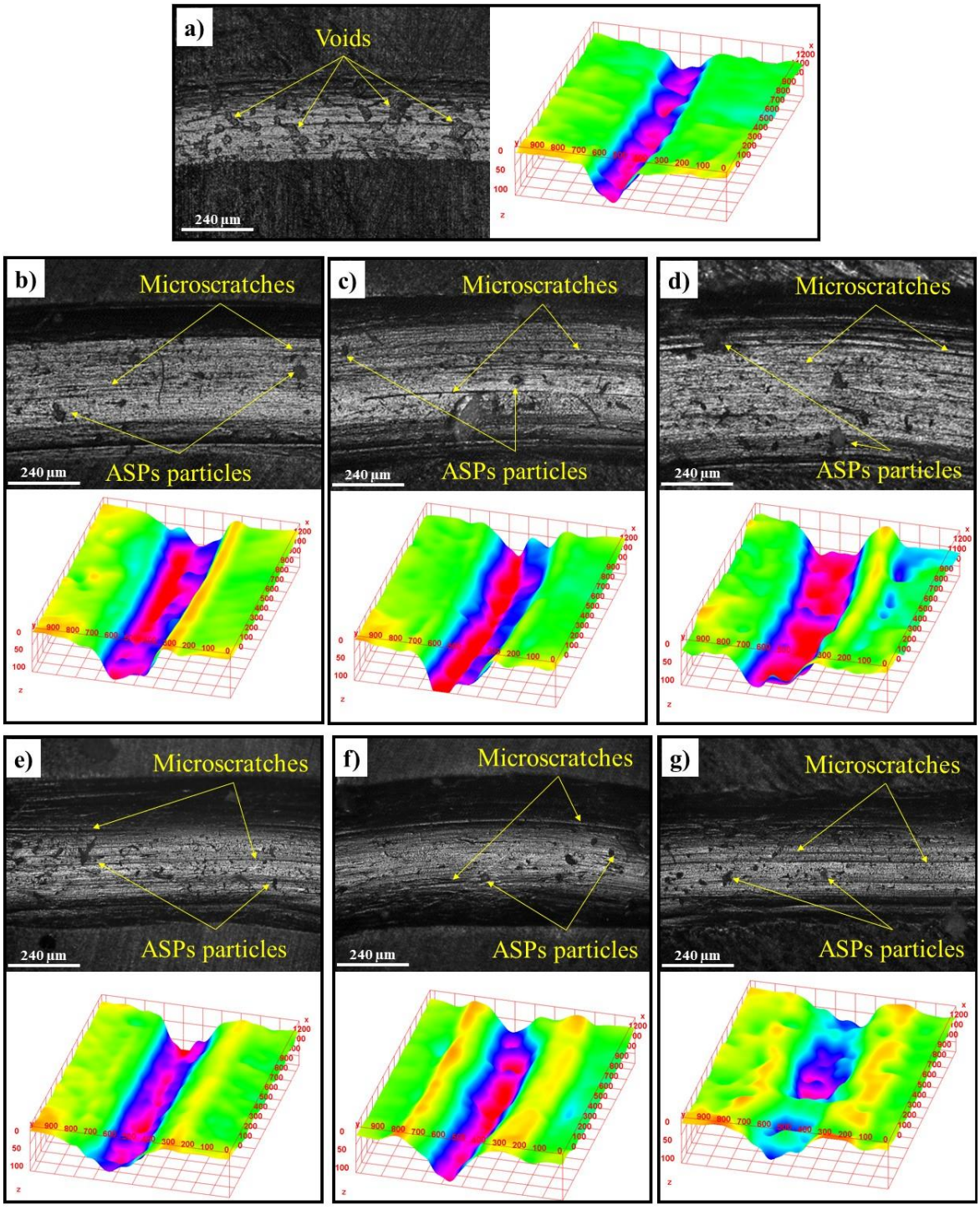

Figure 4.7. PP-ASF wear tracks micrographs and Optical 3D, a) PP, b) PP-D1-5, c) PP-D1-10, d) PP-D1-15, e) PP-D2-5, f) PP-D2-10 and g) PP-D2-15.

Based on the presented findings, our study contributes to the comprehension of the effect of ASF on the mechanical and tribological properties of filled PP. Both properties are connected and evaluated differently in the function of filling parameters such as the particle size and their proportions. The filling of PP with ASF gives better hardness and Young modulus and can reduce the COF. Nevertheless, the wear coefficient can be optimized with an adequate choice of size and proportion of the ASF, which can enhance the mechanical and tribological behavior of the obtained composite compared to the neat PP. These results show the requirements and objectives of sustainable materials for industrial applications have proved that the filling of PP with ASF, of low cost, can be a suitable and sustainable choice for green tribology reducing the environmental impact of polymers.

4.3.4. Discussion

For the mechanical properties, there is an enhancement of the tensile modulus by the addition of ASF to the neat PP matrix, where it was increased by 15% by adding 15% of ASF D1 and by 32% of ASF with the same proportion, there is a notable enhancement of this mechanical property for the low ASF size D2 compared to the high ASF size D1. So, the low ASF size was the efficient than the high ASF size for enhancing the tensile modulus of the PP matrix. But for the tensile strain and tensile strength there is a reduction in this two later by the addition of ASF in the PP matrix, where the tensile modulus decreased by increasing ASF proportion on the PP matrix, where ASF D1 decreased it by 38%, and ASF D2 decreased it by 15%. Also, tensile strength decreased by increasing ASF in the PP matrix, where it was decreased by 28.8 % by adding 15% of the high size ASF (D1) and by 20% by adding the low ASF (D2) with the same proportion. This behavior results from the adhesion between the ASF and the PP matrix. Specifically, the ASF-PP interface is the main determinant of this behavior, so the interface is a crucial factor in determining tensile properties of the PP ASF biocomposite, where at the tensile test the loading is distributed on the matrix and the fillers and in the same time also at the interface between them, where by filling PP with ASF that considered harder than PP matrix due to the distribution of loads on the fillers and the matrix and the interface, the tensile modulus increase, tensile strain and tensile strength. Many research report the same behavior and a batter mechanical behavior by adding ASF to PP matrix with and without compatibilizer [7, 8, 10, 11], because the mechanical properties of polymer composites strongly depend on the fillers size, degree of dispersion, interfacial adhesion and fillers proportions [7]

The tribological testing of PP ASF biocomposite indicate that the addition of ASF to PP matrix can maintains its COF and can noticeably reduce its COF with about 18%. The average COF

indicate a wobbly frictional behavior by adding ASF to PP matrix, in the same time there is no correlation between the added ASF size and its proportion in the PP matrix. The reduction of the COF can be attributed to that the ASF was more soft compared to the PP matrix, especially with PP-D1-15 where the ASF are larger and more proportional in the PP matrix, which by its softness make the sliding easiest than in the other cases, so, the biocomposite with higher ASF size, the lower COF, which mean that the highest ASF size and highest ASF proportion the more efficient on the COF reduction. The same effect was reported with cherry seed powder [17]. However, a reduction on the COF was previously reported, where the addition of wood fillers on PP matrix can reduce the COF by 44% with 30% proportion [20], the same with the wood fibers, where it was can reduce the COF with 20% with 55% proportion.

But for the wear, neat PP exhibit the low wear coefficient that was in the order of 2.10^{-4} mm^3/Nm, and this property increase by adding ASF to PP, in the same time its size was a decisive factor in the determination of the wear coefficient of the biocomposite. For the high ASF size wear coefficient increase by increasing ASF proportion, this is can be attributed to that the ASF was more brittle than PP matrix, where those fillers by the continues sliding were consume especially with PP-D1-15 that exhibit the larger ASF and the high ASF proportion, which its W_c was exceed 4.10^{-4} mm^3/Nm. But for low ASF size there is no correlation between its proportion ant the wear coefficient, where it was increase from 5% to 10% then decrease in the case of 15% that exhibit the lower PP filled with ASF, this may be can attributed to the size effect, where for this ASF size and this distribution, the PP-D2-15 biocomposite exhibit the best PP filled wear resistance. Since the tribological properties of thermoplastic composites has a considerable link with their mechanical characteristics [7], the increasing in the wear coefficient by the addition of ASF can be attribute to the brittleness of the PP ASF biocomposite that increases by increasing ASF proportion, so this effect was previously reported by the addition of mediterranean lignocellulosic fiber on PP matrix [21].

The dominate wear mechanism was the adhesive wear that turned to abrasion by filling PP with ASF especially with high proportions, where PP is known for this behavior. The observed voids on neat PP can be attributed to the effect of stick slip phenomenon [19], those voids were absent by the addition of ASF on PP matrix. This change attributed to that the ASF was more brittle then PP matrix that by continues sliding it was crushed than divided into two parts, one of them sink in the wear track the other contribute on the abrasion wear mechanism. So the presence of ASF on the wear tracks led to an increasing in the abrasion by three body abrasion [14, 15, 17]. For neat and lower ASF proportions the adhesive wear mechanisms was dominate and it was tuned to the abrasive wear mechanism, this effect during sliding can be attributed to the ASF

fillers was more harder than PP matrix but in the same time it was less harder than the slider steel, so, through sliding, the fillers crushed and part of them sinks into the PP matrix, and the other part contributes to abrasion of material. Which makes ASF fillers and cherry seed powder similar in their effect on the wear of PP matrix [17].

Based on the presented findings, filling PP matrix with ASF demonstrates a sustainable and cost-effective approach to substantially enhance the mechanical and tribological properties of the resulting biocomposite. The PP ASF biocomposite exhibit a maintained COF and wear coefficient, which was an improvement in the mechanical and tribological properties of the PP matrix. This remarkable improvement in composite properties, thereby significantly impacting the sustainability of these polymers. Consequently, the resulting PP ASF biocomposite prove to be a suitable and sustainable choice for tribological applications.

4.4. Conclusion

Based on the experimental results, analyses, and observations presented in this study, the following conclusions can be drawn:

The hardness of PP-ASF composites increased with the proportion of ASF, with the smallest particle size, D2, being more effective in enhancing the hardness of PP. The addition of ASF to PP also increased the Young's modulus. A high proportion of ASF (15%) and smaller particle size resulted in a higher Young's modulus, with a significant increase of 32% observed for D2 at 15% ASF. Tribological findings indicate that the addition of larger ASF (D1) and a higher proportion (15%) was more effective in terms of the coefficient of friction (COF). The wear coefficient increased with the addition of ASF regardless of their size and proportion, except for PP filled with D2 particles at 15% proportion, which showed a minor effect on the wear coefficient compared to neat PP. Adhesive wear dominated the wear mechanism for neat PP and low ASF proportions, but transitioned to abrasion with the addition of higher proportions of ASF. The presence of ASF on the wear tracks caused wear by three-body abrasion, with PP filled with smaller ASF (D2) showing better wear resistance compared to D1.

The requirements and objectives of sustainable materials for industrial applications have demonstrated that filling PP with ASF can be a suitable and sustainable choice for green tribology, reducing the environmental impact of polymers.

References

[1] A.S. Grenadyorov, A.A. Solovyev, N.M. Ivanova, M.O. Zhulkov, A.M. Chernyavskiy, V.V. Malashchenko, I.A. Khlusov, Enhancement of the adhesive strength of antithrombogenic and hemocompatible aC: H: SiOx films to polypropylene, Surf. Coat. Technol. 399 (2020) 126132. https://doi.org/10.1016/j.surfcoat.2020.126132

[2] A. Alsabri, F. Tahir, S.G. Al-Ghamdi, Environmental impacts of polypropylene (PP) production and prospects of its recycling in the GCC region, Mater. Today. Proc. 56 (2022) 2245-2251. https://doi.org/10.1016/j.matpr.2021.11.574

[3] Z. Bai, Y. Xu, Z. Zhang, J. Zhu, C. Gao, Y. Zhang, H. Jia, J. Guo, Highly flexible, porous electroactive biocomposite as attractive tribopositive material for advancing high-performance triboelectric nanogenerator, Nano. Energy. 75 (2020) 104884. https://doi.org/10.1016/j.nanoen.2020.104884

[4] B.P. Chang, H. Md Akil, M.H. Zamri, Tribological Characteristics of Green Biocomposites, In: M. Jawaid, S. Sapuan, O. Alothman (Eds.), Green Biocomposites, Green Energy and Technology, Springer., Cham, 2017, pp. 149–179

[5] R.A. Ilyas, M.Y.M. Zuhri, M.N.F Norrrahim et al, Natural fiber-reinforced polycaprolactone green and hybrid biocomposites for various advanced applications, Polymers. 14 (2022) 182. https://doi.org/10.3390/polym14010182.

[6] S.W. Zhang, Green tribology: Fundamentals and future development, Friction. 1 (2013) 186–194. https://doi.org/10.1007/s40544-013-0012-4

[7] H. Essabir, S. Nekhlaoui, M. Malha, M.O. Bensalah, F.Z. Arrakhiz, A. Qaiss, R. Bouhfid, Bio-composites based on polypropylene reinforced with Almond Shell particles: Mechanical and thermal properties, Mater. Des. 51 (2013) 225–230. https://doi.org/10.1016/j.matdes.2013.04.031

[8] Z. McCaffrey, L. Torres, S. Flynn, T. Cao, B.S. Chiou, A. Klamczynski, G. Glenn, W. Orts, Recycled polypropylene-polyethylene torrefied almond shell biocomposites, Ind. Crops. Prod. 125 (2018) 425–432. https://doi.org/10.1016/j.indcrop.2018.09.012

[9] R. Lewis, H. Weldekidan, A.U. Rodriguez, A.K. Mohanty, D.F. Mielewski, M. Misra, Design and engineering of sustainable biocomposites from ocean-recycled polypropylene-based polyolefins reinforced with almond shell and hull, Composites Part C: Open Access. 12 (2023) 100373. https://doi.org/10.1016/j.jcomc.2023.100373

[10] B. Chiou, D. Valenzuela-Medina, M. Wechsler et al, Torrefied biomass-polypropylene composites. J. Appl. Polym. Sci. 132 (2014). https://doi.org/10.1002/app.41582

[11] F.Z. El Mechtali, H. Essabir, S. Nekhlaoui, M.O. Bensalah, M. Jawaid, R. Bouhfid, A. Qaiss, Mechanical and thermal properties of polypropylene reinforced with almond shell particles: Impact of chemical treatments. J. Bionic. Eng. 12 (2015) 483–494.

[12] B. Barari, E. Omrani, A. Dorri Moghadam, P.L. Menezes, K.M. Pillai, P.K. Rohatgi, Mechanical, physical and tribological characterization of nano-cellulose fibers reinforced bio-epoxy composites: an attempt to fabricate and scale the 'Green' composite, Carbohydr. Polym. 147 (2016) 282–293. https://doi.org/10.1016/j.carbpol.2016.03.097

[13] H. Sharma, J. P. Misra, I. Singh, Friction and wear behaviour of epoxy composites reinforced with food waste fillers, Compos. Commun. 22 (2020) 100436. https://doi.org/10.1016/j.coco.2020.100436

[14] P. Jan, S. Matkovič, M. Bek, L. Slemenik Perše, M. Kalin, Tribological behaviour of green wood-based unrecycled and recycled polypropylene composites, Wear 524-525 (2023) 204826. https://doi.org/10.1016/j.wear.2023.204826

[15] M.A. Ibrahim, T. Hirayama, D. Khalaf, An investigation into the tribological properties of wood flour reinforced polypropylene composites, Mater. Res. Express. 7 (2019) 015313.

[16] L. Liu, Z. Wang, Y. Yu, S. Fu, Y. Nie, H. Wang, P. Song, Engineering Interfaces toward High-Performance Polypropylene/Coir Fiber Biocomposites with Enhanced Friction and Wear Behavior, ACS. Sustain. Chem. Eng. 7 (2019) 18453–18462. https://doi.org/10.1021/acssuschemeng.9b04381

[17] Ł. Wojciechowski, Z. Sydow, K. Bula, B. Gapiński, Friction and wear of polypropylene-based composites reinforced with cherry seed powder, Tribol. Int. 179 (2023) 108177–108177. https://doi.org/10.1016/j.triboint.2022.108177

[18] L.M. Kneissl, G. Gonçalves, R. Joffe, M. Kalin, N. Emami, Mechanical properties and tribological performance of polyoxymethylene/short cellulose fiber composites, Polym. Test. 128 (2023) 108234. https://doi.org/10.1016/j.polymertesting.2023.108234

[19] H. Jiang, Q. Cheng, C. Jiang, J. Zhang, L. Yonghua, Effect of stick-slip on the scratch performance of polypropylene, Tribol. Int. 91 (2015) 1–5.

[20] O. Mysiukiewicz, T. Sterzy´nski, Influence of water on tribological properties of wood-polymer composites, Arch. Mech. Technol. Mater. 37 (2017) 79–84, doi.org/10.1515/amtm-2017-0013.

[21] AL-Oqla, F. M., Hayajneh, M. T., & Aldhirat, A. (2021). Tribological and mechanical fracture performance of Mediterranean lignocellulosic fiber reinforced polypropylene composites. Polymer Composites. https://doi.org/10.1002/pc.26241.

General conclusion and perspectives

General conclusion and perspectives

This thesis has comprehensively investigated the tribological behavior of filled polypropylene (PP) composites with biodegradable particles, specifically talc and almond shell particles (ASF). This study explores the mechanical and tribological properties of these composite materials, emphasizing their potential for sustainable applications in various industries. The findings reveal critical insights into how the incorporation of biodegradable fillers can enhance the performance of polymers while addressing environmental concerns. The general conclusions are:

The exploration of tribology in polymers filled with biodegradable fillers has highlighted significant advancements, particularly in the context of sustainable materials. Polymers possess unique viscoelastic properties and low friction coefficients, making them suitable for a variety of tribological applications. The integration of biodegradable fillers, derived from natural sources, not only enhances the mechanical properties of these polymers but also contributes to their sustainability. The study demonstrated that the right choice and proportion of fillers can lead to improved wear resistance and reduced friction, making these materials suitable for applications in automotive, aerospace, and other sectors.

The experimental procedures outlined in this thesis provided a thorough characterization of two types of composite materials: PP-talc composites and PP-ASF biocomposites. The microscratch tests and reciprocating sliding tests conducted on PP-talc composites under various conditions (temperature, normal load, and talc content) revealed a clear relationship between these parameters. The development of a lab-made heating device allowed for a nuanced understanding of how temperature affects tribological performance.

The study of COF in talc-filled PP composites showed a non-linear response to increasing normal loads, particularly at lower temperatures. At low talc proportions (5% and 10%), the COF and wear rates remained stable, indicating effective tribological performance. However, at higher talc content (50%), the COF became unstable, leading to increased wear rates and pronounced damage patterns, including chip formation and delamination. This shift underscores the importance of optimizing talc proportions to enhance material performance.

The incorporation of almond shell fillers into PP matrices was found to significantly enhance the hardness and Young's modulus of the composites. The tribological tests indicated that while higher proportions of ASF generally increased the COF, the smallest particle size (D2) demonstrated superior friction performance and better wear resistance compared to larger

particles (D1) and pure PP. The transition from adhesive to abrasive wear mechanisms with increasing ASF content further emphasizes the need for careful selection of filler size and proportion to achieve desired performance characteristics.

The findings of this research underscore the critical role that biodegradable fillers can play in the development of sustainable polymer composites. As industries increasingly prioritize environmental responsibility, the use of materials that fulfill both performance and sustainability criteria becomes paramount. The successful integration of biodegradable fillers not only enhances the mechanical and tribological properties of polymers but also contributes to reducing the overall environmental impact associated with plastic use.

Future Perspectives

1) Despite the advancements presented in this study, further researches are needed to deepen the understanding of the mechanisms underlying friction and wear in polymer composites. This includes investigating the effects of different environmental conditions, such as humidity and varying temperatures, on the tribological performance of these materials.

2) Continued innovation in processing techniques will be essential for optimizing the performance of biodegradable polymer composites. Future studies could explore various methods of filler treatment, compounding techniques, and composite fabrication processes to enhance the compatibility between fillers and polymer matrices.

3) The exploration of other biodegradable fillers, such as cellulose, chitosan, or natural fibers, could provide new avenues for improving the performance of polymer composites. Investigating the synergistic effects of combining different fillers may also yield composites with superior mechanical and tribological properties.

4) Long-term wear studies are crucial for understanding the durability and longevity of biodegradable composites in real-world applications. Research should focus on simulating actual service conditions to assess how these materials perform over extended periods and under varying loads and temperatures.

5) Future research should also consider application-specific studies to tailor the properties of biodegradable polymer composites for particular uses in industries such as automotive, aerospace, and consumer products. Understanding the specific requirements and challenges faced in these applications will guide the development of more effective and efficient materials.